EXPERIMENTAL AND NUMERICAL STUDY OF PULSE CHARGING STRATEGIES ON LITHIUM-ION BATTERY PERFORMANCE AT BOTH LOW AND ROOM TEMPERATURES

by

JIAHAO LIU

A dissertation submitted in partial fulfillment of the
requirements for the degree of

DOCTOR OF PHILOSOPHY IN MECHANICAL ENGINEERING

2025

Oakland University
Rochester, Michigan

Doctoral Advisory Committee:

Xia Wang, Ph.D., Chair
Laila Guessous, Ph.D.
Hongwei Qu, Ph.D.
Ankun Yang, Ph.D.

© Copyright by Jiahao Liu, 2025
All rights reserved

To Changnan, Wenyang and my grandparents

No words could adequately convey the profound gratitude

I hold for the love, care, support, and motivation

you have so generously bestowed upon me.

ACKNOWLEDGMENTS

I would like to express my sincere thanks to those people who have helped me with love and kindness.

First, I would like to express my deepest gratitude to my advisor, Professor Xia Wang for her continuous support, guidance, and inspiration throughout my doctoral studies and research. In fact, Professor Wang has also helped me in life. During the times when I felt most confused and lost, she was a patient listener. Her kindness and scholarly wisdom helped me survive that difficult period- something I will never forget.

Second, I would also like to thank Professor Laila Guessous, Professor Ankun Yang and Professor Hongwei Qu for serving on my advisory committee and offering valuable comments and suggestion in shaping this dissertation.

Third, I would like to thank my host family in the United States, Ziyan Zhu, Andrea Mo, Mrs. & Mr. Mo for their care and support during my doctoral journey. Because of them, I have spent a fulfilling and happy time in a foreign country.

Finally, I would like to give my greatest appreciation to my family in China. Their unconditional love and support have been the biggest driving force pushing me forward in life. While the completion of my doctoral journey marks the end of my academic career, it also signifies a new starting point in my life. It is because of your care that my life shines in so many meaningful ways.

Jiahao Liu

ABSTRACT

EXPERIMENTAL AND NUMERICAL STUDY OF PULSE CHARGING STRATEGIES ON LITHIUM-ION BATTERY PERFORMANCE AT BOTH LOW AND ROOM TEMPERATURES

by

JIAHAO LIU

Advisor: Xia Wang, Ph.D.

Lithium-ion batteries are widely used in power electronic devices, electric vehicles, and large energy storage devices, which demand faster, safer and more durable charging methods.

Compared with the conventional constant current and constant voltage charging method, pulse charging can both improve battery performance and shorten charging time. This dissertation investigates how pulse charging can shorten charging time under different temperature conditions and mitigate capacity loss over multiple cycles. This study combines experimental testing and numerical simulation.

Firstly, this study designed experiments to evaluate pulse charging at different temperatures. Using the Taguchi method, we treated protection capacity ratio and pulse discharge current rate as control parameters. At low temperature, pulse charging with a 25% protection capacity ratio and a 12C pulse discharge rate reduced total charging time by approximately 11% compared to the conventional constant current and constant voltage charging strategy. At room temperature, three fundamental pulse modes (C-C, C-

R and C-D) and several derived strategies were studied. Their effects on internal resistance and battery cycle life were then measured. The experimental results show that, under the same average input current, pulse charging yields an average internal resistance reduction of 15% compared to the constant current and constant voltage charging strategy, and shows a slower capacity decay rate over 800 charge and discharge cycles. These findings are also confirmed across lithium-ion batteries with various chemistries.

Secondly, an electrochemical and thermal coupled model was developed in COMSOL Multiphysics to reveal the mechanisms of pulse charging. After validation, the model was used to study lithium-ion concentration and electrode lithium distributions inside the battery under different pulse charging protocols. The model results show that pulse charging, particularly the C-D mode, promotes a more uniform lithium-ion distribution within the battery, thereby improving charging performance of lithium-ion battery by reducing cell resistance. These findings are consistent with the experimental results.

Finally, a multi-objective optimization method was used to find the optimal parameters for pulse charging at room temperature. The objectives were to minimize total charging time, minimize temperature rise and maximize charging efficiency. The resulting optimal pulse charging strategy can reduce charging time by 6.8% per cycle and lower temperature rise by more than 8% compared to conventional constant current and constant voltage charging.

This research studied pulse charging of lithium-ion batteries at different temperatures through experimental design, numerical simulation, and optimization. Pulse charging improves the performance of lithium-ion batteries by saving charging time and

reducing capacity loss. Numerical simulation provides deeper insight into lithium migration and diffusion dynamics under pulse conditions. This research lays a solid foundation for future charging protocol development.

TABLE OF CONTENTS

TABLE OF CONTENTS—Continued

TABLE OF CONTENTS—Continued

TABLE OF CONTENTS—Continued

LIST OF TABLES

LIST OF FIGURES

NOMENCLATURE
GREEK LETTER ABBREVIATIONS

c_l	Electrolyte concentration ($mol \cdot m^{-3}$)
c_p	Heat capacity ($J \cdot Kg^{-1}K^{-1}$)
c_s	Concentration of lithium in active material particles ($mol \cdot m^{-3}$)
c_l	Electrolyte concentration ($mol \cdot m^{-3}$)
D_l	Diffusion coefficient of electrolyte ($m^2 \cdot s^{-1}$)
D_s	Diffusion coefficient of lithium in active material ($m^2 \cdot s^{-1}$)
E_{act}	Activation energy ($J \cdot mol^{-1}$)
$f_{\pm}$	Average molar activity coefficient
F	Faraday's constant ($C \cdot mol^{-1}$)
h	Heat transfer coefficient ($W \cdot m^{-2}K^{-1}$)
j_0	Exchange current density ($A \cdot m^{-2}$)
j_{loc}	Local charge transfer current density ($A \cdot m^{-2}$)
k_0	Reaction rate constant ($m^{2.5} \cdot mol^{-0.5} \cdot s^{-1}$)
q	Heat generation rate ($W \cdot m^{-3}$)
$\bar{R}$	Gas constant, 8.314 ($J \cdot mol^{-1}K^{-1}$)
R_s	Radius of electrode particles (μm)
S_a	Specific surface area (m^{-1})
t_+	Transference number of lithium ions
T	Temperature (K)

GREEK LETTER ABBREVIATIONS

U_{eq}	Open circuit potential of the electrode (V)
$\forall_{cell}$	Cell volume (m^3)
α_a	Anodic transfer coefficient
α_c	Cathodic transfer coefficient
β	Bruggeman porosity exponent
δ	Thickness of each battery component (μm)
ε_l	Electrolyte volume fraction or porosity
ε_s	Active material volume fraction
κ_l	Ionic conductivity of electrolyte ($S\ m^{-1}$)
λ	Thermal conductivity ($W \cdot m^{-1}K^{-1}$)
η	Local surface overpotential (V)

NOMENCLATURE
SUBSCRIPTS, SUPERSCRIPTS AND ACRONYMS

0	Initial or equilibrated value
s	Solid phase
l	Electrolyte phase
eff	Effective value
neg	Negative electrode
pos	Positive electrode
sep	Separator
ref	Reference value

CHAPTER ONE

INTRODUCTION

1.1 Background

Lithium-ion batteries are rechargeable batteries that are widely used in a variety of fields due to their high energy density and high power density. Products using lithium-ion batteries include but are not limited to: consumer electronics, electric vehicles, energy storage systems used for renewable energy storage such as solar and wind energy, and medical equipment such as pacemakers and hearing devices. Among these applications, the electric vehicle industry has undoubtedly been the most popular and fastest growing industry in recent years. In 2022, the US government planned to invest $369 billion, focusing on supporting the development of clean energy industries such as electric vehicles and photovoltaics [1]. Based on a $2.3 billion investment in 2021, the GM battery plant will begin converting to lithium iron phosphate (LFP) battery production at the end of 2025, with commercial production expected to begin at the end of 2027 [2]. Ford is currently planning its next generation of electric vehicles and has invested $3 billion in the Blue Oval Battery Park in Michigan [3]. Many internationally renowned car companies such as BYD and Geely have received government subsidies for electric vehicles [4]. The electric vehicle industry has driven the development of the battery industry. The new lithium-ion battery designed by CATL increases the battery pack volume utilization from 55% to 72% and supports fast charging [5].

The United States Advanced Battery Consortium (USABC) is a non-profit organization jointly established by the three major American automakers General Motors,

Ford Motor Company and Fiat Chrysler Automobiles (FCA, now Stellantis). The goal of the USABC is to promote the development and application of advanced battery technology, especially in the fields of electric vehicles and hybrid vehicles. In their vision, electric vehicles will gradually replace traditional internal combustion engine vehicles [6].

At present, lithium-ion batteries are playing an important role in transitioning from traditional fossil energy to clean energy. As the energy density of lithium-ion batteries continues to increase and their cost gradually decreases, the range and economy of electric vehicles have improved significantly.

Lithium-ion batteries are widely used in electric vehicles, but their long charging time is a common complaint. A Level 1 charger typically takes 8-12 hours to fully charge an electric vehicle, while a Level 2 charger takes about 4-8 hours. The voltage required for a Level 2 charger is 240V, which is twice that of a Level 1 charger. Fast charging technology can reduce charging time. However, high current involved in fast charging causes the battery temperature to rise, which may lead to battery safety issues. At the same time, the high heat loss resulting from the high current will reduce charging efficiency. Furthermore, people must consider how to charge the battery at different ambient temperatures. For example, high current charging at low temperatures can lead to the formation of lithium dendrites, which may damage the lithium-ion battery.

Given the market expansion of electric vehicles in recent years, lithium-ion batteries currently play a pivotal role. However, due to the long charging time of electric vehicles and the safety risks of lithium-ion batteries when charging, people still have

concerns about buying electric vehicles. In summary, the research on lithium-ion battery charging strategies is very necessary and urgent.

1.2 Lithium-ion Batteries Basics

1.2.1 Basic Components of Batteries

In general, a typical lithium-ion battery consists of the following major components as shown in Figure 1.1:

1. Positive electrode. The most common positive electrode materials are lithium nickel oxide, lithium cobalt oxide, lithium cobalt manganese and lithium iron phosphate [7,8]. The key parameters of a lithium-ion battery are energy and power density, safety, temperature dependence, and cost [9]. These factors must be taken into consideration when selecting a positive electrode material.

2. Negative electrode. At present, the most common negative electrode material for a lithium-ion battery is graphite. The use of selected carbon and graphite materials as negative electrode materials has enabled the development of lithium-ion secondary batteries [10-16]. Lithium titanate (LTO) is another negative electrode material that has excellent thermal stability and fast charging capability compared to graphite [10], but it has lower energy density compared to graphite. Silicon-based materials can store more lithium ions than graphite [14], leading to a much higher capacity but poor cycle life due to volume changes of silicon during the charging process.

3. Separator. The separator is a polymer film with a microporous structure which allows lithium ions to pass freely. Electrons cannot pass through the separator. Polyethylene or polypropylene materials with higher melting points are suitable materials for use as a separator [9].

4. Electrolyte. There are two main types of electrolytes: one is a liquid electrolyte, and the other is a solid electrolyte. During the operation of a lithium-ion battery, the electrolyte acts as a carrier of lithium ions, and it exists in the separator and the electrode. The liquid electrolyte in a lithium-ion battery consists of lithium salts (such as LiPF6, LiBF4, and LiCIO) in an organic solvent [17]. Solid electrolytes use solid materials as the electrolyte. Compared to liquid electrolytes, solid electrolytes have no risk of leakage. Solid polymer electrolytes (SPEs) and ceramics can be used as solid electrolyte materials [18].

5. Current Collector. Typically, the positive electrode current collector is made of aluminum while the negative current collector is made of nickel or copper.

6. Battery Case. The battery case is generally made of aluminum (for prismatic batteries), nickel-plated iron (for cylindrical batteries) or the aluminum plastic film (for pouch cells with soft packaging).

1.2.2 General Technical Specifications

Lithium-ion battery technology involves many specialized terms. Table 1.1 shows some common lithium-ion battery technical specifications and their brief explanations.

1.2.3 Working Principles

Lithium-ion batteries are secondary batteries (rechargeable batteries) that rely on lithium ions to move between the positive and negative electrodes to work. During charging, Li-ions are deintercalated from the positive electrode and transported into the negative electrode through the electrolyte, so that the negative electrode is in a lithium-rich state. During discharging, Li-ions are deintercalated from the negative electrode and inserted into the positive electrode through the electrolyte, and the positive electrode is in

a lithium-rich state. Figure 1.1 describes the typical structure of a lithium-ion battery and its charging and discharging process [19]. Taking a lithium iron phosphate battery as an example, the reaction formulas during the charge-discharge process are:

For the positive electrode:

$$LiFePO_4 \leftrightarrow Li_{1-x}FePO_4 + xLi^+ + xe^- \tag{1.1}$$

For the negative electrode:

$$xLi^+ + xe^- + C_6 \leftrightarrow Li_xC_6 \tag{1.2}$$

During the charging process, lithium-ion batteries form solid electrolyte interphase (SEI) and lithium plating on the surface of the negative electrode (typically graphite). The SEI is a thin passivation layer that forms during the first few charging cycles which protects the negative electrode from continuous reaction with the solvent molecules in the electrolyte [20]. The SEI, however, grows over time during lithium-ion battery cycling, consuming more lithium and thickening, which increases battery resistance and reduces battery performance [21]. Fast charging uses high current during the charging process, which forces lithium ions to move at a faster rate and accumulate on the surface of the negative electrode, making it impossible for them to be effectively intercalated, resulting in lithium plating [22]. At lower temperatures, the kinetics of lithium-ion intercalation slow down, increasing the likelihood of lithium plating. Lithium plating leads to a loss of active lithium, reducing the battery's capacity over time [23].

Both SEI growth and lithium plating lead to capacity fade and reduced cycle life of lithium-ion batteries. Since they are mainly formed during the charging process, various charging strategies for lithium-ion batteries can be studied and selected to reduce their impact on battery performance.

Table 1.1 General technical specifications of Li-ion batteries

Items	Unit	Definition
Charging rate (C-rate)	C	C-rate is a measure of the rate at which a battery would be theoretically fully discharged or charged. 1C means that the battery can theoretically be fully discharged or charged in 1 hour.
State of Charge (SOC)	%	Indicates the percentage of the battery's current capacity relative to its maximum capacity. SOC is a key parameter for battery management.
Depth of Discharge (DOD)	%	The percentage of a battery's discharged capacity relative to its total capacity. *DOD = 1 – SOC*
State of Charge (SOH)	%	Indicates the health of a battery, defined as the ratio of the maximum charge capacity of an aged battery to the maximum charge capacity when the battery was new.
Cycle Life	#	The number of charge and discharge cycles a battery can complete before its capacity drops to 80% of its initial capacity.
Nominal Voltage	V	The voltage of the battery under normal working conditions. The nominal voltage is measured at 50% SOC under specified conditions.
Discharge Capacity	Ah	The total charge that can be discharged from a fully charged battery.
Internal Resistance	mΩ	The overall equivalent resistance within the battery. The measured voltage output is lower than the no-load voltage; the difference is the voltage drop caused by the internal resistance: $r_{ir} = (V_{OCV} - V_{cell})/I$
Energy Density	Wh $/m^3$	The amount of energy stored per unit volume of a battery.
Specific Energy	Wh /Kg	The amount of energy stored per unit mass of a battery.
Specific Power	W /Kg	The peak power per unit mass of a battery.

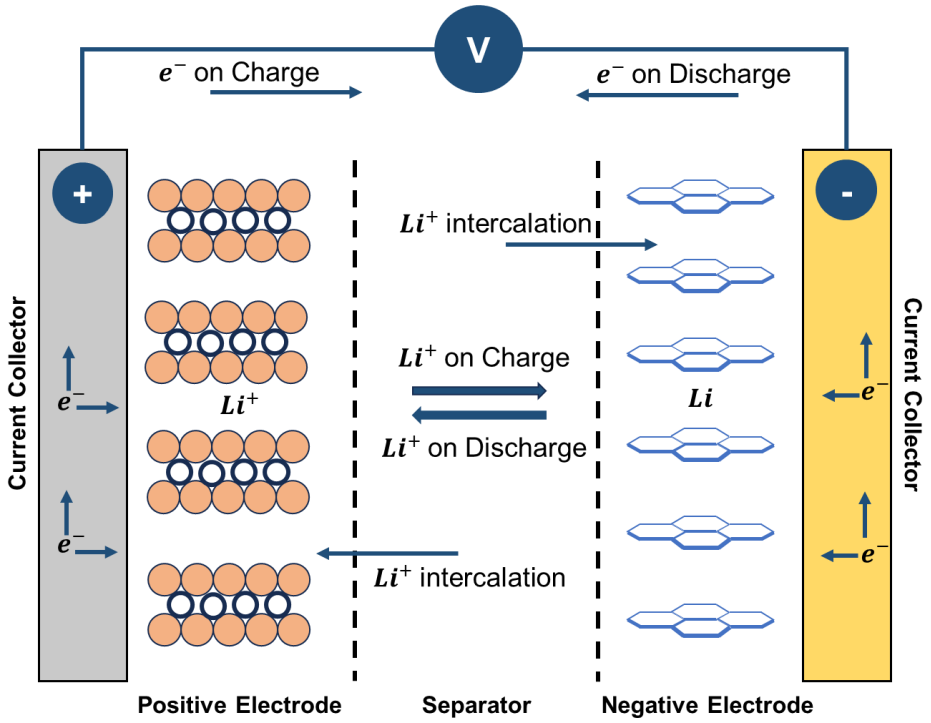

Figure 1.1: Schematic of electrochemical process in a Li-ion battery.

1.3 Battery Charging at Different Temperatures

When charging lithium-ion batteries in low temperature environments, special attention should be paid to the following strategies. The first one is to preheat the battery. Before charging at extremely low temperatures, the battery can be heated to a suitable temperature range (usually 10°C to 30°C) using a battery self-heating or preheating device before charging. The second one is to reduce the charging current. Under low temperature conditions, the electrochemical reaction rate of lithium-ion batteries decreases and the ion diffusion rate slows down [24]. In order to prevent lithium plating at the negative electrode, it is usually necessary to reduce the charging current (C-rate). In

addition, the charging cutoff voltage can also be reduced: when charging at low temperatures, the charging cutoff voltage can be appropriately decreased to reduce the risk of lithium plating at the negative electrode.

In room temperature environments, the charging strategy of lithium-ion batteries can be more flexible, but there are also a few points that need to be noted. First, one must select a suitable charging current and limit the voltage. A very high charging current will cause the battery to overheat and shorten its cycle life. Generally, the cutoff voltage of lithium-ion batteries is between 3.6V and 4.2V [21-23]. When charging, the voltage must be kept below this voltage to avoid overcharging. At the same time, temperature monitoring is also required. Although room temperature is ideal for charging lithium-ion batteries, it is still necessary to monitor the battery temperature to ensure that the temperature is within a reasonable range to prevent overheating or other abnormal conditions.

When charging lithium-ion batteries in high temperature environments (such as above 35°C), special care must be taken to prevent overheating and avoid safety issues [25]. First, the charging current should be reduced at high temperatures. A high temperature tends to result in low internal resistance and fast electrochemical reaction, but it will also accelerate the decomposition of the electrolyte and other side reactions. Properly reducing the charging current can reduce heat generation and mitigate the risk of battery overheating. Second, the battery temperature must be monitored in real time when charging in a high temperature environment. If the cell temperature exceeds a certain threshold (such as 45°C), battery performance will degrade, and therefore charging

should be stopped or cooling measures should be taken. This can be effectively achieved using a battery management system (BMS).

1.3.1 CC-CV Charging Strategy and High Current Charging Strategy

A common charging method for lithium-ion batteries is the constant current and constant voltage (CC-CV) charging strategy [26]. Figure 1.2(a) shows the charging profile of a lithium-ion battery. First, the battery is charged with a constant current. When the voltage reaches the cutoff voltage, the voltage is kept constant and the input current is reduced until the battery is fully charged. This charging method is slow and does not take into account changes in the battery's internal state during the charging process.

High current charging uses an extremely high current to charge the battery in a short period of time. Once the cutoff voltage is reached, it transitions to constant voltage (CV) charging as shown in Figure 1.2(b) or continues with low current CC-CV charging. Notten et al [27] found that compared to 1C CC-CV charging, high current charging saves charging time by 30%-40% without apparent capacity fade. In contrast, Keil and Jossen [28] found that high current charging results in a higher capacity decay rate than CC-CV for a similar charging duration.

1.3.2. Multi-stage Charge Strategy

Since CV stage takes a lot of time in CC-CV charging strategy, a multi-stage charging strategy has been proposed to overcome this problem. The multi-stage charging strategy as shown in Figure 1.2(d) usually uses a high current for constant current charging as the first stage, and then gradually reduces the current to avoid the CV stage to achieve the purpose of shortening the time. It usually consists of 4 to 5 levels of constant current charging [29-32].

A study [33] reported that lithium iron phosphate (LFP) batteries charged using a multi-stage (2 different CC stages) charging strategy had a capacity retention of 83% after 4200 cycles. Abdel-Monem and his team [34] conducted eight experiments, including several of the charging strategies mentioned previously: conventional CC-CV charging, multi-stage constant current charging and pulse charging strategies. They found that after 1700 cycles, the remaining discharge capacities using the multi-stage charging strategy and the pulse charging strategy were both higher than that of CC-CV, with the pulse charging strategy being the best. However, the multi-stage charging strategy does have some limitations. Zhang et al [35] concluded in their experiments that the battery capacity loss was faster when charged using the multi-stage charging strategy compared to 1C CC-CV with the same average C rate. Another limitation is mainly reflected in the experimental design of the multi-stage charging strategy. The current range is basically decreasing step by step, and the switch condition of each level of current is the cutoff voltage [36-38], which leads to the limited charging strategy.

1.3.3. Pulse Charging Strategy

The last common charging method is the pulse charging strategy, as shown in Figure 1.2(c). The principle of pulse charging is to break the constant charging current rate and direction to improve the battery performance by changing the current range, current direction, or temporarily stopping charging [39-42].

Most studies showed that pulse charging has a positive effect on improving the performance of lithium-ion batteries [43-45]. The pulse charging strategy optimizes the overall charging process, improves charging efficiency, and extends cycle life [46-49]. Pulse charging strategies improve battery performance in different ways:

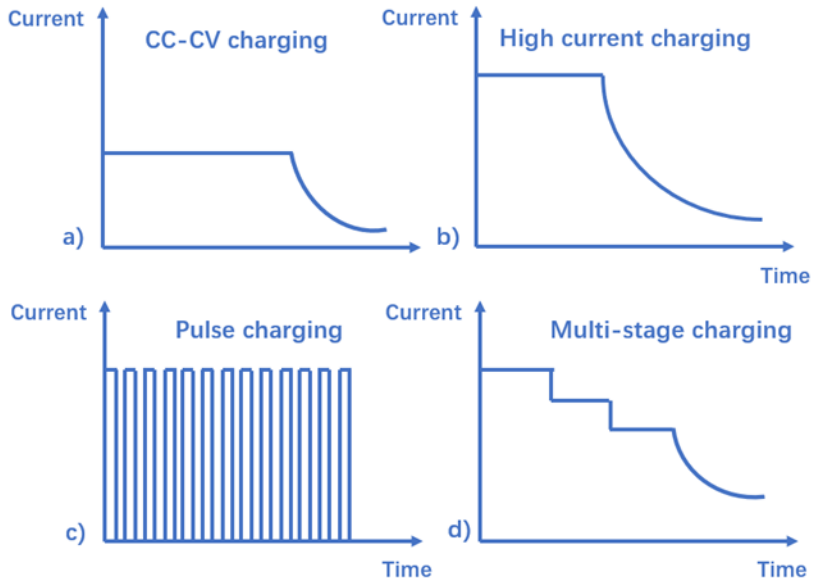

Figure 1.2: Schematic diagram of different charging strategies.

First, in low temperature environments, pulse charging can effectively preheat the battery [50]. Some specific pulse parameters, such as cutoff voltage and pulse frequency, have been studied, and their improvements on the preheating effect and temperature rise of lithium-ion batteries at low temperatures have been demonstrated [51]. The results show that a small pulse frequency of 0.5 Hz can effectively preheat the battery at low temperature without causing irreversible damage to the battery. In other words, reducing the pulse frequency means prolonging the pulse time, which plays a decisive role in the preheating of the battery at low temperatures. This serves as a theoretical basis for our research.

At room temperature, pulse charging strategies are expected to shorten charging time and extend battery cycle life [52-53]. Heng Yang et al [54] and Grecia García et al

[55] found that pulse charging can suppress the growth of lithium dendrites and promote the formation of a stable solid electrolyte (SEI) film. The pulse charging strategy can not only effectively extend the cycle life [56-57], but also improve charging efficiency compared to the constant current and constant voltage charging strategy [58-59]. Kohl et al [42] found that a pulse charging strategy can reduce concentration polarization and interfacial resistance of 18650 lithium cobalt oxide batteries produced by Samsung. However, Vermeer et al [60] showed that using pulse charging strategies can lead to battery degradation, which may be caused by a very high pulse frequency. Most of the previous literature highlights the advantages of pulse charging at room temperature, while a few studies also point out its disadvantages. This shows that the pulse charging strategy at room temperature has not been systematically studied or summarized. For example, some literature [55,58] only studies the performance improvement of a single pulse charging mode (pulse charging followed by rest) on a single aspect of the battery, such as cycle life, compared to the constant current and constant voltage charging mode. Additionally, different pulse patterns have been reported by different researchers, and their effects on the battery performance have not been thoroughly compared and studied.

Lithium-ion batteries have different charging strategies and charging targets at different temperatures. At low temperatures, charging strategies are needed to quickly increase cell temperature and shorten charging time. At room temperatures, charging strategies are needed to control temperature rise, shorten charging time, and extend battery life. The most common charging strategy at present is constant current and constant voltage charging. This charging strategy is safe but slow, and it does not take into account changes inside the battery. The multi-stage current charging strategy can

shorten charging time compared to the constant current and constant voltage charging strategy. However, previous studies have shown that under the same input current, the cycle life of a multi-stage current charging strategy is not as good as that of the constant current and constant voltage charging strategy. The pulse charging strategy, on the other hand, can be used for both low temperature and room temperature conditions. It also has the advantages such as high charging efficiency and long cycle life. However, there is currently a lack of systematic study on pulse charging at room temperature. Existing literature provides only a limited understanding of charging behavior at low temperatures. The effects of pulse parameters and various pulse patterns have not been thoroughly studied at different temperatures. Therefore, this dissertation aims to address these unanswered questions.

1.4 The State of Art of Lithium-ion Battery Modeling

Lithium-ion battery models are of great significance in research and application. Their uses include battery characterization analysis, state-of-charge and state-of-health estimation, system-level optimization, and real-time simulation for battery management system design. Currently, the most common battery models are equivalent circuit models and physics-based models. An equivalent circuit model is simple to calculate and can be used for real-time BMS applications. A physics-based model describes the ion transport and charge transfer process inside the battery in detail. It has high accuracy but complex calculations and is not suitable for real-time monitoring of batteries.

1.4.1 Equivalent Circuit Model

Equivalent Circuit Model (ECM) is a commonly used battery modeling method that simulates the dynamic behavior of the battery by using circuit elements such as

resistors, capacitors, and inductors [61-64]. This type of model is simple, has low computational complexity, and is suitable for real-time applications, especially in battery management systems (BMS). These simplified circuit components are used to represent various electrochemical and thermal characteristics of a battery. The equivalent circuit model does not consider the full electrochemical process within the battery. Instead, the main factors affecting battery performance are represented using various simplified circuit elements. In a simple ECM, the voltage source represents the open circuit voltage (OCV), and the resistor simulates the internal resistance. This ECM is simple and suitable for describing steady-state behavior, but cannot accurately simulate dynamic characteristics. In order to improve the accuracy of the model, more resistor–capacitor (RC) networks can be added to form a higher-order equivalent circuit model to simulate the dynamic behavior of the battery, including transient response and steady-state characteristics.

The equivalent circuit model is normally applied to the battery management system (BMS) to monitor and manage the battery status in real time, such as state estimation (SOC, State of Charge) and health status (SOH, State of Health) [65-68]. Since the equivalent model is extremely computationally efficient, real-time monitoring of SOC and SOH can be achieved by embedding a model-based algorithm in the microprocessor of the vehicle computer through the BMS.

Equivalent circuit models come in various forms [69-72]. The simplest is the internal resistance model (Thevenin model), which consists of an open circuit voltage source in series with an internal resistance. Both the open circuit voltage and the internal resistance are functions of state of charge (SOC), state of health (SOH) and temperature.

Hu et al [73] compared twelve equivalent circuit models for lithium-ion batteries and found that different models are suitable for different battery chemistries. The first-order RC model is the first choice for NMC lithium batteries, while the first-order RC model with single-state hysteresis seems to be the best choice for lithium iron phosphate batteries. Tang et al [74] used the ECM model to study pulse charging strategy and found that pulse charging not only shortens charging time compared to constant current and constant voltage charging, but also significantly reduces polarization voltage.

1.4.2 Physics-based Electrochemical Models

Electrochemical models are more complex than equivalent circuit models (ECM). Based on electrochemical kinetics and transport equations, they can simulate the characteristics and reactions of lithium-ion batteries [75]. Although more accurate than ECM, they require greater computational effort. The most common electrochemical-based models are the pseudo-two-dimensional (P2D) model and the single particle model (SPM).

The P2D model is based on porous electrode theory, concentrated solution theory, and kinetic equations [76-81]. The P2D model has been widely used in lithium-ion battery research [82-87]. It combines the one-dimensional electrode and electrolyte transport phenomena with the reaction kinetics in the electrode particles at the solid scale, hence the name pseudo-two-dimensional model. In this model, the intercalation of lithium in the electrode is modeled as a solid diffusion process. The concentration of lithium within the solid phase is solved using a pseudo-second-dimension along the radius of the particle. Intercalation processes are described with charge transfer kinetic expressions. Because P2D model simulation can be time consuming, a simplified P2D

model called single particle model (SPM) was developed to reduce calculation time. The SPM ignores the properties variation of the electrolyte and treats transport phenomena in a simple way [88]. This simplification, however, limits the model's application for currents higher than 1C.

In 1993, Doyle et al [81] used concentrated solution theory to establish a P2D model to simulate the behavior of polymer electrolyte batteries. The kinetic expression in this model adopts the Butler-Volmer equation. Fuller et al [89] extended Doyle's P2D model with lithium foil as the positive electrode by introducing a composite porous electrode for the positive electrode. This was the first P2D lithium battery model with two composite porous electrodes and a separator. These models were verified relatively accurately through experimental data [79, 84, 87]. Based on the work of Doyle and Newman, the P2D electrochemical models have been widely used in various battery studies, such as optimizing battery design [79], studying the impact of design parameters on battery performance [84], and predicting battery thermal behavior under various operating conditions [87].

In 2016, Jokar et al [90] used the inverse method to study the electrochemical parameter estimation for lithium-ion batteries with different materials, including LiCoO2, LiMn2O4 and LiFePO4. They used a least squares function as the objective function and applied a genetic algorithm for the optimization. The experimental results showed that the method remained accurate and stable under both low and high discharge rates. However, their study was limited to simple single charge and discharge process and did not validate the model's feasibility in complex charging modes, such as pulse charging.

The application of thermal modeling in P2D models is of great significance because the performance and life of lithium-ion batteries are greatly affected by temperature. Electrochemical-thermal models are a subset of electrochemical models that are specifically designed to understand the effects of electrochemical reactions on thermal behavior. The P2D electrochemical models [81,82,84] proposed by Doyle and Newman are isothermal models in which the temperature throughout the battery is assumed uniform and does not change with time. In order to incorporate thermal models into the porous electrode battery model, researchers [91-92] developed an electrochemical-thermal battery model. This model combines Doyle's electrochemical model [81,82,84] and the general energy conservation model proposed by Bernardi et al [92]. This electrochemical-thermal battery model allows the battery temperature to change with time.

In order to analyze the effect of temperature on battery performance, researchers have incorporated several temperature-related parameters, including the diffusion coefficient, ionic conductivity, and transference number of lithium ions. Botte et al [94] developed an electrochemical-thermal model that takes into account the temperature dependence of these parameters. Xu et al [95-96] developed an electrochemical–thermal coupled model for a single lithium iron phosphate battery. The model was applicable for currents up to 5C. The model was validated using the experimental voltage change and temperature rise. Despite these advancements, existing models have not been widely integrated with advanced charging technologies. Nonetheless, these studies provide a new direction toward future work, namely, integrating improved electrochemical–thermal

models with advanced charging technology to enhance the charging performance of lithium-ion batteries.

1.5 Optimization Algorithm

Optimizing charging parameters is the key to further improving the charging performance of lithium-ion batteries. The Non-dominated Sorting Genetic Algorithm II (NSGA-II) and Multi-Objective Particle Swarm Optimization (MOPSO) are two common multi-objective optimization algorithms used for lithium-ion batteries [98-105]. NSGA-II, proposed by Deb et al in 2002 [102], has fast non-dominated sorting, elite strategy and congestion comparison operator, making it a benchmark algorithm for multi-objective optimization [100-102]. MOPSO introduces dominance relationship judgment and elite solution maintenance (similar to NSGA-II), divides the target space into grids, and selects the global optimal solution based on density. However, its diversity remains weaker than that of NSGA-II [103-105]. In this study, the NSGA-II algorithm will be used to determine the optimal parameter combination of the pulse charging strategy through multi-objective optimization.

1.6 Objectives and Scope of Dissertation

As indicated in previous studies, the pulse charging strategy has many advantages and is worthy of further study. However, pulse charging has not been systematically studied in the existing literature, and most studies have focused only on the effects of a specific type of pulse charging protocol on battery performance.

The primary motivation of this work is to conduct a systematic study to better understand how different pulse parameters and pulse charging modes affect the performance of lithium-ion batteries under different temperatures. Since the goals of the

pulse charging are different at different temperatures, this study requires customized experimental design and extensive experimental testing to address different needs. No previous studies have systematically analyzed and defined pulse charging strategies, making this work innovative.

Compared to the ECM, the P2D model can more accurately capture the internal characteristics and electrochemical reactions of lithium-ion batteries. However, few studies have integrated the P2D model with pulse charging strategies. Therefore, another objective of this work is to combine these two approaches and explore the impact of different pulse charging strategies on battery performance from both experimental and modeling aspects.

Finally, this study aims to optimize pulse charging strategies. The motivation behind the optimization is to identify appropriate pulse charging parameters without changing the battery materials and to improve battery performance by adopting a more effective charging strategy.

CHAPTER TWO

DESIGN OF EXPERIMENTS

2.1 Experimental Objectives

Pulse charging is primarily characterized by pulse charging current, pulse discharging current, and pulse frequency. Previous studies have shown conflicting results regarding the effectiveness of these parameters on battery charging performance. For example, some researchers found that high pulse frequency can help improve battery performance [39], while others argue that high frequency pulses will accelerate battery degradation [51,60]. Many previous studies have focused on a single pulse charging parameter and a single pulse charging pattern, while the effects of pulse parameters across various ranges and in different pulse charging patterns on battery performance have not been systematically studied. This research aims to design experiments to study pulse charging parameters and their effects on the battery performance at both low and room temperatures.

The first major objective is to investigate the effectiveness of pulse charging strategies at low temperatures. Specifically, this research aims to evaluate the ability of these pulse charging strategies to preheat the battery even when the battery is at a very low state of charge (SOC) under low ambient temperature. While negative pulse currents can aid in preheating, they may also extend the total charging time [51]. Therefore, it is critical to design a pulse preheating strategy that minimizes overall battery charging time. This requires identifying and designing the key parameters of the pulse charging strategy and evaluating their impact on battery performance at low temperatures.

The second major objective is to explore the influence of pulse charging strategies on battery performance at room temperature. This includes studying the effects of pulse charging on charging time, internal resistance changes and cycle life. Amanor-Boadu and his team did not use the same average input current for a fair comparison between charging modes, making their results less convincing [40]. To ensure fairness in this study, all pulse charging strategies are designed to maintain the same average input charging current. Various pulse charging strategies, characterized by different current magnitudes and pulse frequencies, will be tested. The results will also be compared to the conventional constant current and constant voltage charging method. Additionally, these pulse charging strategies will also be applied at a moderately low temperature (around 0°C) to further evaluate their effectiveness under varying thermal conditions.

2.2. Experiment Equipment

At present, lithium iron phosphate (LFP) batteries and lithium nickel manganese cobalt oxide (NMC) batteries [32-39] are the most commonly used in electric vehicle battery packs. This research involves two types of lithium-ion batteries: one is INR21700-30T NMC battery from Samsung, and the other is 26650 m1b lithium iron phosphate battery from A123 Systems. Compared to NMC batteries, LFP batteries are safer and have a longer cycle life, making them more suitable for research on pulse charging. In this study, the A123 26650 m1b LFP batteries were used as the primary test subjects, while the Samsung NMC batteries were used as a control group to evaluate the performance of the same pulse charging strategy under specific conditions. The specifications of the two batteries are shown in Table 2.1.

Table 2.1. Technical data of two different lithium-ion batteries

ANR 26650 Lithium Iron Phosphate Cylindrical Cell	
Positive Electrode	LFP
Dimensions (D x H)	26mm x 65.15 mm
Weight	76 grams
Nominal Voltage	3.3V
Nominal Capacity	2500 mAh
Maximum Continuous Discharge	50A
Manufacturer	A123
INR21700-30T NMC Li-ion batteries	
Positive Electrode	NMC
Dimensions (D x H)	21.22mm x70.30mm
Weight	70 grams
Nominal Voltage	3.6V
Nominal Capacity	3000 mAh
Maximum Continuous Discharge	35A
Manufacturer	Samsung

A Maccor Model 4200 Cycler, shown in Figure 2.1, is used to charge and discharge the batteries. This machine has 10 channels for battery connection, and ten corresponding sockets for thermocouples. The maximum channel output current is 30 amps. The minimum full-scale current is available for 150 μA. The minimum step time for experimental programming is 10 ms.

Figure 2.1: Maccor system 4200 batter cycler.

A temperature chamber from Maccor is used to control the ambient temperature. This equipment can provide temperature control ranging from - 20°C to 100ºC, with an accuracy of ± 0.5°C. For low temperature testing, the chamber is set to -8.5°C, which is the lowest stable temperature the chamber can maintain. Three T-type thermocouples with an accuracy of ± 0.5°C are attached to the upper, middle, and lower surfaces of the battery to monitor the temperature rise of the lithium-ion battery in real time during the pulse charging process.

2.3. Pulse Charging Parameters

Figure 2.2 presents a classic pulse charging scheme, which serves as the basis for the pulse charging method used in this work. $I_{pospulse}$ and $T_{pospulse}$ are the pulse charging

current and pulse charging time, respectively. $I_{negpulse}$ is the discharge current and $T_{negpulse}$ is the discharge pulse duration. The combination of $T_{pospulse}$ and $T_{negpulse}$ defines the time required for a single pulse cycle, where the pulse frequency of the pulse charging strategy can be derived.

Prior research has not adequately addressed key questions such as when to initiate and terminate pulse charging, what pulse frequency should be used, and what the appropriate pulse current rate is. In other words, the control parameters related to pulse charging have not been sufficiently studied. Next, we will present a series of experiments to study these parameters under both low and ambient temperature conditions.

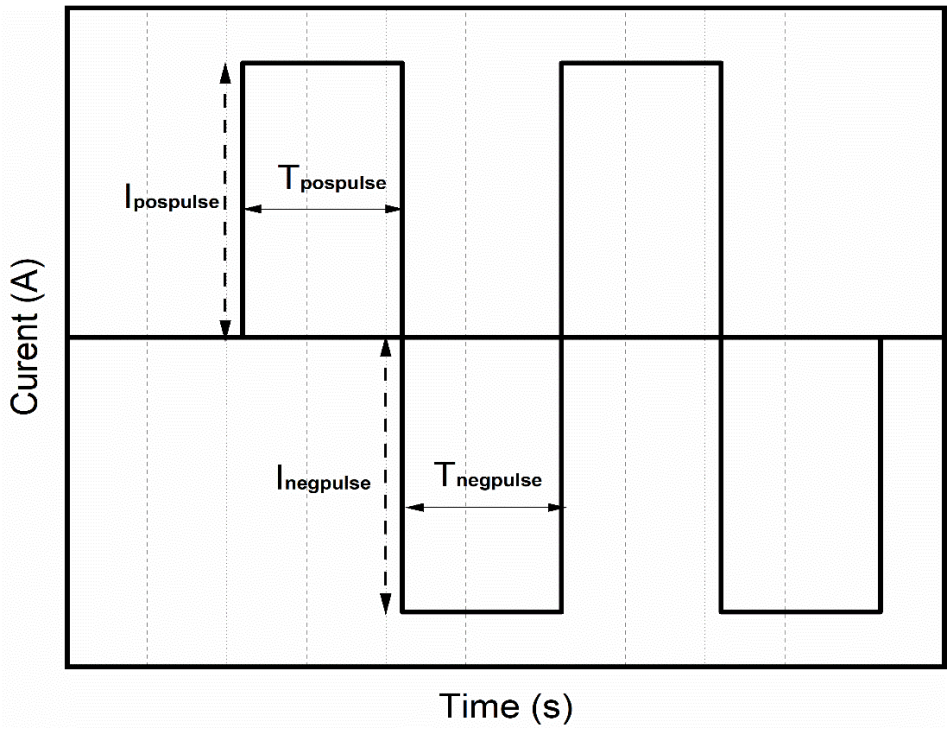

Figure 2.2: Parameters in a typical pulse charging strategy.

2.3.1 Pulse Charging Parameters at Low Ambient Temperatures

In this set of experiments, the ambient temperature is set to -8.5 °C. The objective is to develop a pulse charging strategy suitable for low temperatures, which can not only preheat the battery but also reduce the total charging time.

In order to implement the pulse current charging strategy under low ambient temperatures, we need to address two key questions: 1. At what battery temperature should pulse charging be stopped? 2. What are the appropriate pulse charge/discharge current rates and durations?

The first question is addressed through preliminary testing, as shown in Figure 2.3. After 11 pulse cycles, the battery temperature rises from -8.5 °C to approximately 0 °C, and after 16 pulse cycles, it increases to about 10 °C. However, reaching approximately 0 °C is sufficient to reduce the total charging time. This result will be explained in detail as shown in Figure 3.1 of Chapter 3. The experiments were conducted using two new lithium iron phosphate batteries with a result variation of no more than 2%. Based on these findings, a low-temperature charging strategy consisting of 11 pulse cycles is proposed.

The second question is addressed by introducing a new parameter, protection capacity ratio (PCR). The protection capacity ratio is used to quantify the relationship between the pulse discharge capacity and pulse charge capacity in the pulse charging stage, helping to prevent the battery from being over-discharged. This newly designed pulse parameter correlates all basic pulse parameters, and is defined as:

$$\text{Protection Capacity Ratio (PCR)} = 1 - \frac{pulse\ discharge\ capacity}{pulse\ charge\ capacity} \tag{2.1}$$

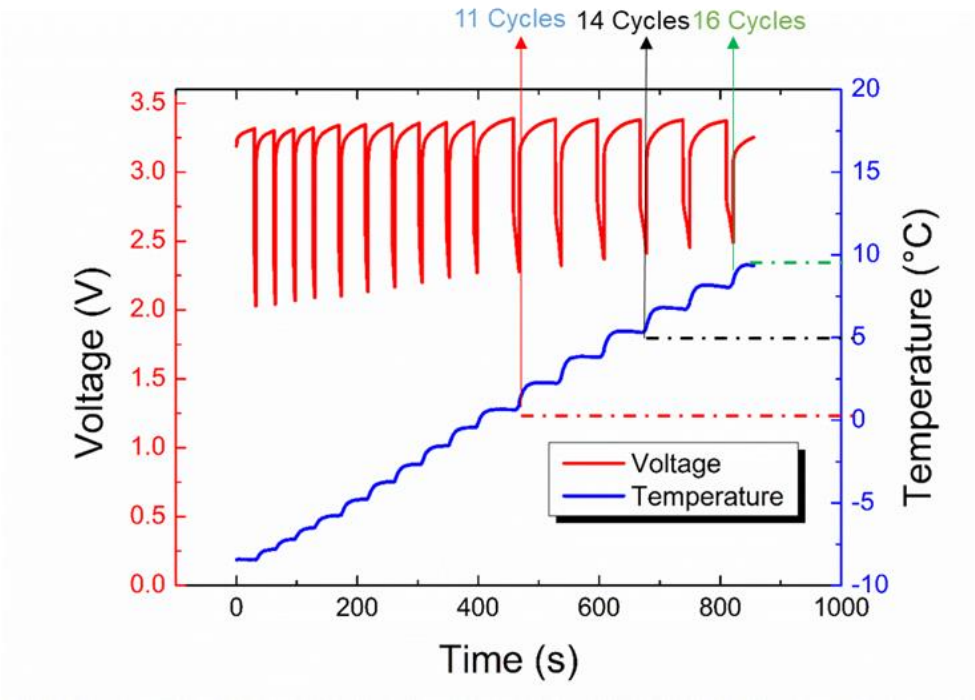

Figure 2.3: Schematic diagram of temperature rise due to increasing pulse heating cycles.

This protection capacity ratio ranges from 0 to 1. A value of 0 means the battery is not being charged at all while a value of 1 indicates charging with a constant current, meaning there is no pulse effect. In other words, higher PCR values correspond to less discharge within the pulse cycle.

2.3.2 Pulse Charging Parameters at Room Temperatures

The purpose of this group of experiments is to study how various pulse charging strategies can reduce charging time and prolong the cycle life of lithium-ion batteries at room temperature. Pulse charging strategies are generally classified into three types as shown in Figure 2.4:

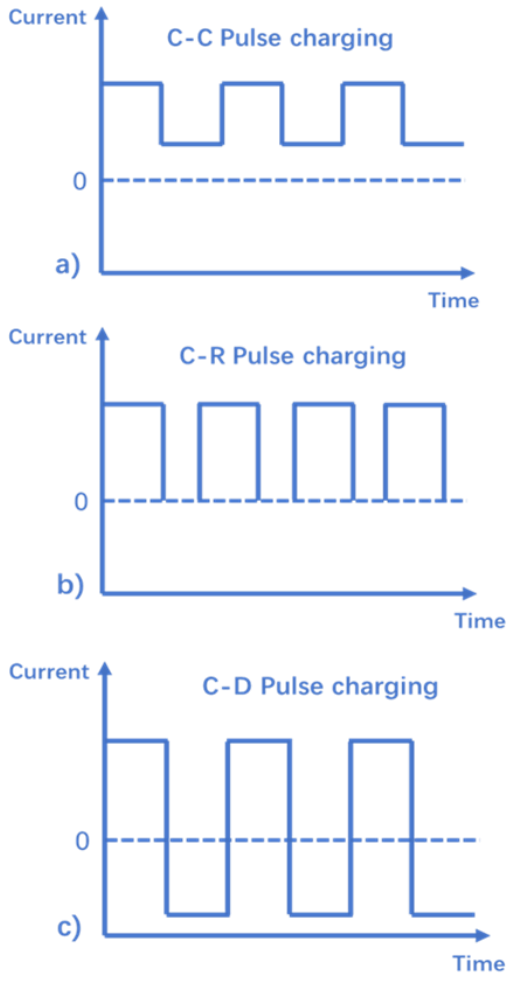

Figure 2.4: Schematic diagram of three pulse charging modes.

1-Charge-Charge (C-C): A charge current is followed by another charge current of a different magnitude (C–C), and the cycle repeats.

2- Charge-Rest (C-R): The battery is charged for a period of time, then allowed to rest and the cycle repeats.

3- Charge-Discharge (C-D): A charge current is followed by a discharge current (C-D) forming a charge/discharge cycle.

Consider a pulse cycle consisting of two-time intervals, T_1 and T_2. Figure 2.5(a) compares different pulse charging patterns with equal time intervals, i.e., $T_1=T_2$. For example, in a single pulse cycle of 20 seconds, the T_1 and T_2 of the 2C/0C C-R mode and the 3C/-1C C-D mode are both 10 seconds. This means that the average input current in all pulse charging modes is always kept at 1C. When the current in each time interval remains the same, it is a constant current charging strategy. If the two currents are different, it becomes a pulse charging strategy. Figure 2.5(b) shows the situation when T_1 is not equal to T_2. Similarly, when a single pulse cycle is 20 seconds, in order to ensure that the average current input is 1C, T_1 of the 4C/0C C-R mode is 5 seconds and T_2 is 15 seconds.

Various combinations of pulse parameters, including pulse current at T_1, pulse current at T_2, and pulse frequency, are applied for each of the three pulse charging strategies. A total of at least 120 different experiments were conducted with pulse currents ranging from 1.2C to 6C and frequencies ranging from 0.025Hz to 1Hz. Three lithium-ion batteries, A, B, and C, were used. By keeping the average input current fixed at 1C, and systematically varying one parameter at a time, such as frequency, we can obtain the relationship between the pulse charging current amplitude and the pulse discharging current amplitude at each frequency.

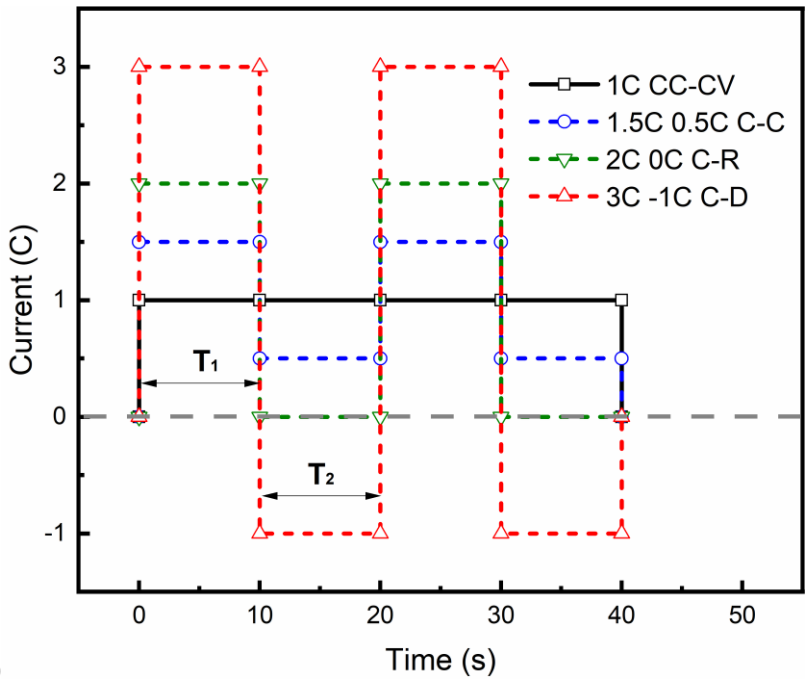

(a)

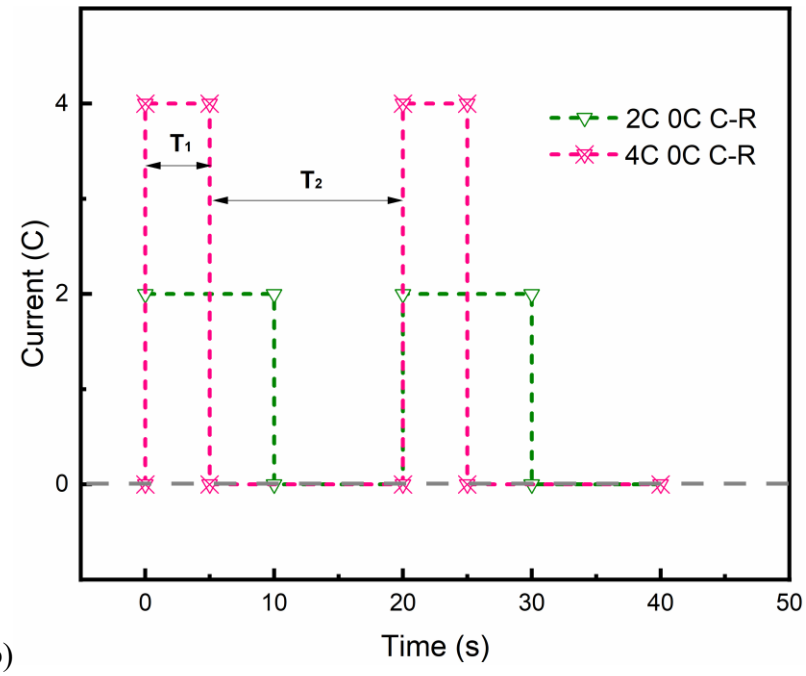

(b)

Figure 2.5: Schematic diagram of charging principle of partial charging patterns. (a) $T_1=T_2$. (b) $T_1 \neq T_2$.

2.4. Method-Taguchi Design

2.4.1 Taguchi Design - Introduction

The Taguchi design is an experimental design method used to select products or processes that perform more reliably under varying operating conditions [106]. Among the various design of experiments (DOE) methods, the Taguchi design method is very effective and convenient, because it reduces the number of experiments required while enabling the study of the influences of multiple parameters [36]. The Taguchi method emphasizes achieving quality goals through parametric design and is suitable for engineering design [107], Therefore, it is adopted as the experimental design method for this study.

Figure 2.6 describes the flow chart of a typical Taguchi design method. These steps include: 1 - determining input factors and factor levels of the experiment; 2 - calculating the orthogonal array (OA) size; 3 - conducting experiments and recording responses. 4 - analyzing the results. If the results do not meet the design requirements, the first and second steps should be reconsidered for redesign; and 5 - determining the correlation of each parameter and its impact factor.

2.4.2 Taguchi Design -Factors and Response

Control factors and noise factors are the two main factors in the Taguchi design method. Control factors are process or design parameters that people can control while noise factors are factors that cause system variability and are difficult to control. For example, in this research, the pulse discharge rate can be set as a control factor while manufacturing variability among batteries is considered a noise factor.

In the first major experiment, the objective is to fast charge a Li-ion battery at low ambient temperatures. Therefore, charging time is chosen as the response variable in the Taguchi design. In the second major experiment, the goal is to investigate the effects of pulse charging parameters on battery performance. Therefore, total charging time and temperature rise are selected as the response variables.

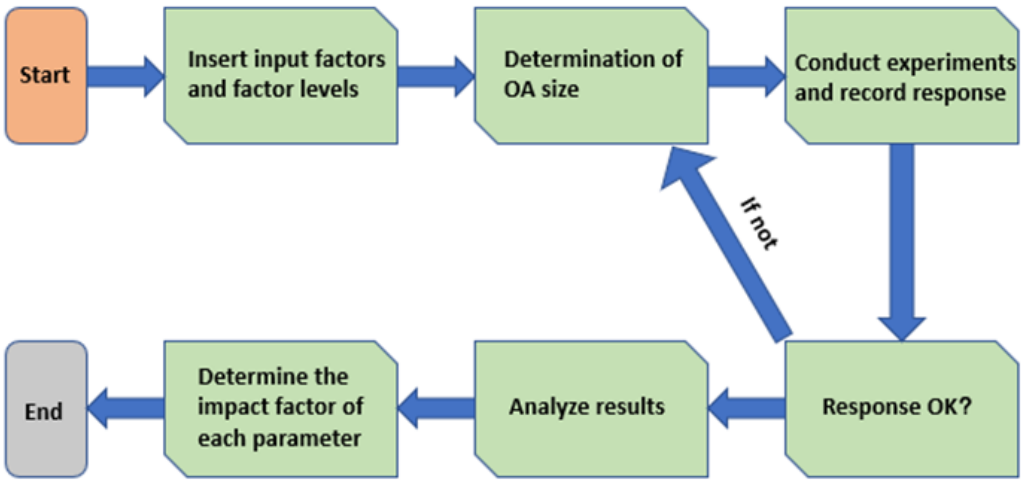

Figure 2.6: Flow chart of the Taguchi design.

2.4.3 Taguchi Design -S/N Ratio and Mean Values

In a typical response of a Taguchi design, both mean values and signal-to-noise (S/N) ratios are analyzed. The signal-to-noise ratio is a robustness measure used to determine control factors that can reduce the variability of products or processes by

minimizing the effects of noise factors. As shown in Table 2.2, the formula for calculating the signal-to-noise ratio varies depending on the specific design objectives.

Table 2.2. Signal to noise (SN) ratio formulas with respect to different conditions [106]

Signal-to-noise ratio	Goal of the experiment	Data characteristics	Signal-to-noise ratio formulas
Larger is better	Maximize the response	Positive	$S/N = -10 * \log[\Sigma(1/Y^2)/n]$
Nominal is best	Target the response and you want to base the signal-to-noise ratio on standard deviations only	Positive, zero or negative	$S/N = -10 * \log(\sigma^2)$
Nominal is best (default)	Target the response and you want to base the signal-to-noise ratio on means and standard deviations	Non-negative with an "absolute zero" in which the standard deviation is zero when the mean is zero	$S/N = 10 * \log[(\overline{Y}^2) \div \sigma^2]$
Smaller is better	Minimize the response	Non-negative with a target value of zero	$S/N = -10 * \log[\Sigma(Y^2)/n]$

In the first experiment, the objective is to fast charge a battery at either a low ambient temperature or room temperature. The response variable is charging time, which is consistent with the "smaller is better" criterion in the Taguchi design. The corresponding S/N ratio formula is:

$$S/N = -10 * log\left[\sum(Y_i^2)/n\right] \quad (2.2)$$

If the objective is to investigate the effect of pulse charging parameters on battery cycle life, the response variable is the remaining discharge capacity, which is consistent with the "larger is better" criterion in the Taguchi design. Then the corresponding S/N ratio formula is:

$$S/N = -10 * log\left[\sum(1/Y_i^2)/n\right] \quad (2.3)$$

where Y is the response of a given combination of factor levels, and n is the number of responses of a combination of factor levels. In other words, Y_i represents the total charging time of each experimental test, and n represents numbers of tests conducted.

2.4.4 Taguchi Design at Low Ambient Temperatures

Preliminary tests show that at an ambient temperature of -8.5 °C, using a pulse charging strategy to heat the battery to ~0°C reduces the total charging time by nearly 11 minutes compared to the traditional 1C CC–CV method. This charging method will be used as a baseline for the Taguchi design. The parameters of this preliminary design are summarized in Table 2.3, and the first eleven cycles are selected for further design.

As with all Taguchi designs, the first step is to determine the input control factors and their levels. For the input control factors, there are two parameters: the protection capacity ratio and the pulse discharge current rate. Each factor is designed with three

levels. After selecting the control factor and factor levels, the orthogonal array (OA) size is determined.

To achieve fast charge at low ambient temperatures, the setting range of protection capacity ratio needs to be large in order to observe the effect on the results. Hence three levels of protection capacity ratio are 5%, 25%, 50%. The range of protection capacity ratio is between 0 and 1. If the value is equal to 0, it means that the battery cannot be effectively charged at low temperatures. If the value is equal to 1, the battery charging mode becomes constant current charging, and effective pulse charging preheating cannot be performed.

Previous literature [108] has shown that a high discharge current rate can be used to preheat batteries at low temperatures, with the highest setting being 21C. However, due to the cycler's output current limit of 30A, the current rate for pulse discharge stage must be high enough to generate heat to preheat the battery at low temperature, but still within a reasonable range. Therefore, three levels of pulse discharge current rates, 4C, 8C and 12C, are selected based on this current limit.

The control factors and levels for low ambient temperature experiments are summarized in Table 2.4, and the orthogonal array, which includes 9 cases, is shown in Table 2.5.

2.4.5 Taguchi Design for C-R Mode at Room Temperatures

Based on previous Taguchi design experience, we began our room temperature pulse charging study by focusing on the C-R mode.

For the C-R mode, there is no current input in the second half of each pulse. Therefore, we investigated the effects of pulse charging current amplitude and frequency on battery charging time and temperature rise. To evaluate the effect of current amplitude,

the setting range of pulse current rate needs to be large in order to effectively observe the effect. Hence five levels of pulse current rate are chosen as 2C, 3C, 4C, 5C, 6C. Similarly, the frequency is set at five levels: 0.05Hz, 0.1Hz, 0.25Hz, 0.5Hz, and 1Hz. By maintaining a consistent average current input in the C-R pulse mode, the influence of these two parameters on the battery performance can be systematically analyzed. The control factors and their corresponding levels for the pulse charging experiment in C-R mode at room temperature are summarized in Table 2.6.

Table 2.3. Parameter settings of 16 pulse charging cycles at low temperature

Cycle No	Charging current(C)	Charging time(s)	Discharging current(C)	Protection capacity ratio (%)
1	0.75	30	10	5
2	0.75	30	10	5
3	0.85	30	10	5
4	0.95	30	10	5
5	1	40	10	5
6	1.1	40	10	5
7	1.2	40	10	5
8	1.3	40	10	5
9	1.4	40	10	5
10	1.5	40	10	5
11	1.6	60	10	5
12	1.7	60	10	5
13	1.8	60	10	5
14	1.9	60	10	5
15	2.0	60	10	5
16	2.0	60	10	5

Table 2.4. Control factors and their levels at low temperature

Control factors	Factor levels		
	1	2	3
Protection capacity ratio	5%	25%	50%
Pulse discharge current rate	4C	8C	12C

Table 2.5. Orthogonal array for low temperature experiments using the Taguchi design

Case No.	Protection capacity ratio (%)	Pulse discharge current rate (C)
1	5	4
2	5	8
3	5	12
4	25	4
5	25	8
6	25	12
7	50	4
8	50	8
9	50	12

Table 2.6. Control factors and their levels at room temperature

Control factors	Factor levels				
	1	2	3	4	5
Pulse current rate	2C	3C	4C	5C	6C
Frequency	0.05Hz	0.1Hz	0.25Hz	0.5Hz	1Hz

2.5. Internal Resistance Testing and Cycle Life Testing

The cycle life test and internal resistance test of lithium-ion batteries are the two core methods to evaluate the performance, cycle life and safety of lithium-ion batteries. While they are independent tests, they are also closely related and together provide key data support for evaluating pulse charging strategies.

2.5.1 Internal Resistance Testing

The internal resistance test of lithium-ion batteries is an important method for evaluating battery performance, state of health (SOH) and safety. Common test methods include the alternating-current (AC) impedance test, direct-current (DC) pulse test and the high-power pulse characterization (HPPC) test, as described by USABC standards [6]. According to the USABC manual, the internal resistance of a battery can be quickly measured using a pulse current as shown in Figure 2.7. The internal resistance of the battery can be determined by the following formula:

$$R_d = \frac{\Delta V_{discharge}}{\Delta I_{discharge}} = \left|\frac{V_{t1} - V_{t0}}{I_{t1} - I_{t0}}\right| \quad (2.4)$$

2.5.2 Cycle Life Testing

The cycle life test of lithium-ion batteries is a key experiment to evaluate capacity degradation and performance stability of batteries over repeated charge and discharge cycles. It directly affects the lifespan of the battery in practical applications.

The purpose of cycle life testing is to determine the maximum number of charge and discharge cycles that a battery can undergo under specific conditions (such as different temperatures and various charging strategies) before reaching failure. The failure condition of lithium-ion batteries is generally defined as the capacity dropping to 80% or less of the initial value.

As shown in Figure 2.8, each cycle life test begins by charging the lithium-ion battery with either constant current and constant voltage (CC-CV) or pulse current and constant voltage (PC-CV) until the cutoff current is reached, which is considered fully charged. The battery is then allowed to rest for half an hour to one hour to eliminate polarization effects. Afterwards, the battery is discharged at a constant current (D-CC) to the lowest cutoff voltage (considered to be fully discharged), where the discharge capacity of the battery is recorded. Finally, the battery rests again for half an hour to one hour to be ready for another cycle. All the experiments for comparison are conducted under the same cutoff conditions and rest times to ensure consistency and reliability of the experimental results.

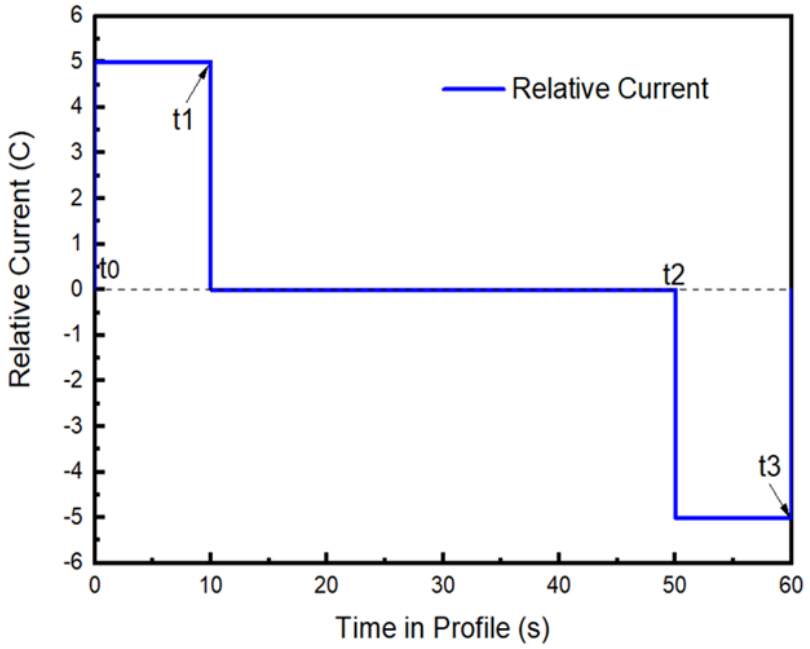

Figure 2.7: Schematic of current for pulse internal resistance measurement.

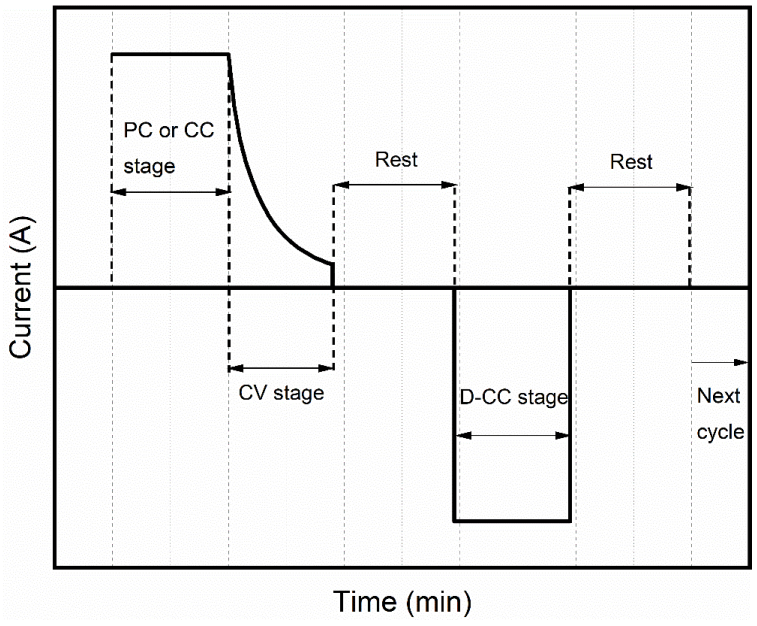

Figure 2.8: Schematic of lithium-ion battery cycle life test.

CHAPTER THREE

EXPERIMENTAL RESULTS AND DISCUSSION

3.1 Introduction

The previous chapter established the experimental objectives and described the experimental design. This chapter presents the experimental results based on the previously proposed assumptions and procedures, and then organizes and analyzes the findings.

For the low temperature tests, the preheating pulse duration was first determined through preliminary experiments. Next, Taguchi analysis was used to determine and analyze the effects of various pulse parameters on the performance of lithium-ion batteries at low temperatures. Through a combination of two pulse parameters, an improved pulse charging strategy at low temperatures was developed.

For the room temperature tests, the feasibility of the pulse charging strategy was first determined through preliminary experiments. Next, the influence of each pulse parameter on the performance of lithium-ion batteries at room temperature was determined and analyzed through Taguchi analysis. Three pulse charging modes were then proposed and defined: C-C, C-R and C-D. Finally, changes in the internal resistance and the cycle life test results of the pulse charging strategy were compared with those of the conventional CC-CV charging strategy at different temperatures.

Each test was conducted on at least two batteries with the same capacity. The performance difference between the batteries in the same experimental test did not exceed 2%.

3.2. Low Temperature Experimental Results and Discussion

For the low temperature experiments, a preliminary experiment was conducted to establish the basic experimental benchmark, such as conducting an initial set of 11 pulse cycles first to bring the temperature to around 0 °C. Based on this, a Taguchi experimental design was implemented to study the effects of different pulse parameters on the performance of the Li-ion battery at low temperatures. The low temperature tests used 26650 lithium iron phosphate batteries from A123 Systems as the test subjects.

3.2.1 Preliminary Test Results

For this experiment, a series of pulse cycles was applied at the beginning of charging, followed by the traditional CC-CV step at an ambient temperature of -8.5 °C (note: this is the lowest stable temperature that our environmental chamber can maintain). The CV charging stage ended when the charging current dropped to 0.04C. After each charge-discharge cycle, the battery was removed from the environmental chamber and rested at room temperature (23 °C) for 3.5 hours to ensure that it reached thermal equilibrium. The soak time in the cold environmental chamber was also set to 3.5 hours to ensure that the battery reached and remained at -8.5 °C. The cell voltage and temperature were recorded during the charging process. Table 2.3 presents the pulse charging pattern, in which the pulse charging current gradually increases from 0.75C to

2C. Figure 2.3 presents that the cell temperature rose to around 10 °C after 16 cycles, 5 °C after 13 cycles, and 0 °C after 11 cycles.

Next, three different pulse ending conditions were compared. They are: -8.5 °C to 0 °C, -8.5 °C to 5 °C, and -8.5 °C to 10 °C. After the cell temperature was raised from -8.5 °C to the specified target temperature (i.e. 0 °C, 5 °C or 10 °C) by pulse charging, a standard 1C CC-CV charging step was applied until the battery was fully charged. Figure 3.1(a) and Figure 3.1(b) show how the cell voltage and cell surface temperature change with time under three different pulse-ending temperatures. The cell reaches the cutoff voltage earlier using the CC-CV charging method than using the pulse charging method. At an ambient temperature of -8.5 °C, the cell is charged nearly 11 minutes (9%) faster using the pulse preheating charging method than using the traditional 1C CC-CV charging method. There is a preheating with 1C CC-CV, but it is very minor due to low current. Note that in pulse preheating charging method, pulse preheating stops once the cell reaches around 0 °C, and is then followed by 1C CC-CV charging. This charging method will serve as the benchmark for the subsequent Taguchi design analysis due to its excellent performance. The results from the other two tests indicate that even if the temperature rise at the end of pulse charging is higher, the total charging time is longer due to the extended duration of the initial pulse heating phase.

3.2.2 Low Ambient Temperature Taguchi Results

Charging a battery at low temperatures presents several challenges due to slow diffusion rates and high internal resistances. To reduce battery degradation under these conditions, a very low charging current (typically less than 1/2C) is usually applied. The

purpose of this series of experiments is to find a pulse charging strategy at low temperatures, which can not only preheat the battery but also reduce total charging time. Two parameters related to pulse charging are defined: the protection capacity ratio and the pulse discharge current rate. The pulse discharge current rate can be set to a high value to preheat the battery through ohmic heating at low temperatures, while the protection capacity ratio is used to prevent the battery from being over-discharged.

The Taguchi design method is used for experimental design to reduce the number of experiments and study the effects of multiple parameters simultaneously. In this experimental design, the protection capacity ratio and pulse discharge current rate are selected as input control factors. Each factor is designed with three levels. The control factor combination has been introduced in the previous chapter and will not be repeated here.

The experiment sets up a control group, namely two batteries, A and B, which undergo the same test. Battery C is used as a blank control group where no pulse charging testing is performed. Therefore, battery C can serve as a benchmark to detect whether the designed low temperature charging experiment degrades the performance of battery. A total of 18 tests were conducted. Table 3.1 shows the average pulse preheating time and the total charging time of batteries A and B with a difference of no more than 2% for nine charging patterns in the Taguchi experiment design. Different pulse charging preheating times can be obtained from different protection capacity ratios and different pulse discharge current rates. The shortest among them is 7.45 minutes, the longest is 8.95 minutes, and the maximum difference is only 1.50 minutes. For the total charging

time, the experimental results seem to indicate that it is the result of the joint action of two input factors. Next, we will conduct Taguchi analysis on the results.

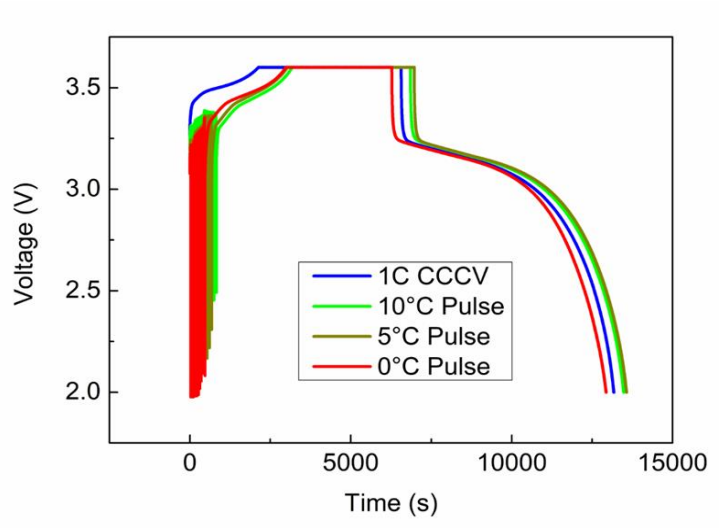

(a)

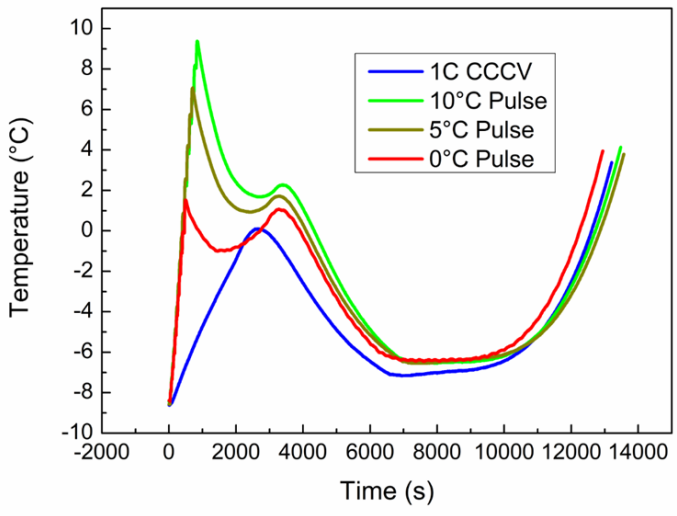

(b)

Figure 3.1: Comparison between CC-CV, CC-CV with different pulse ending conditions patterns at -8.5°C (a) Voltage. (b) Temperature.

Table 3.1. Preheating time and total charging time of different cases

Case No.	Pulse discharge current rate (C)	Protection capacity ratio (%)	Preheating time (min)	Total charging time (min)
1	4	5	8.95	123.08
4		25	8.65	112.50
7		50	8.36	116.61
2	8	5	7.97	120.05
5		25	7.83	103.50
8		50	7.69	105.98
3	12	5	7.65	115.65
6		25	7.5	98.30
9		50	7.45	105.72

In this experiment, the objective is to fast charge a battery at low ambient temperatures. The response variable is the total charging time. Therefore, this work is consistent with the “smaller is better” criterion. For the analysis of Taguchi design results, higher values of the signal to noise (SN) ratio are more desirable to achieve the goal - the smaller the time, the better. Figure 3.2 shows that the protection capacity ratio has a greater impact on total charging time while the pulse discharge current rate has a smaller effect. Figure 3.2 also indicates that the optimal combination for minimizing charging time is a 25% protection capacity ratio and a 12C pulse discharge current rate.

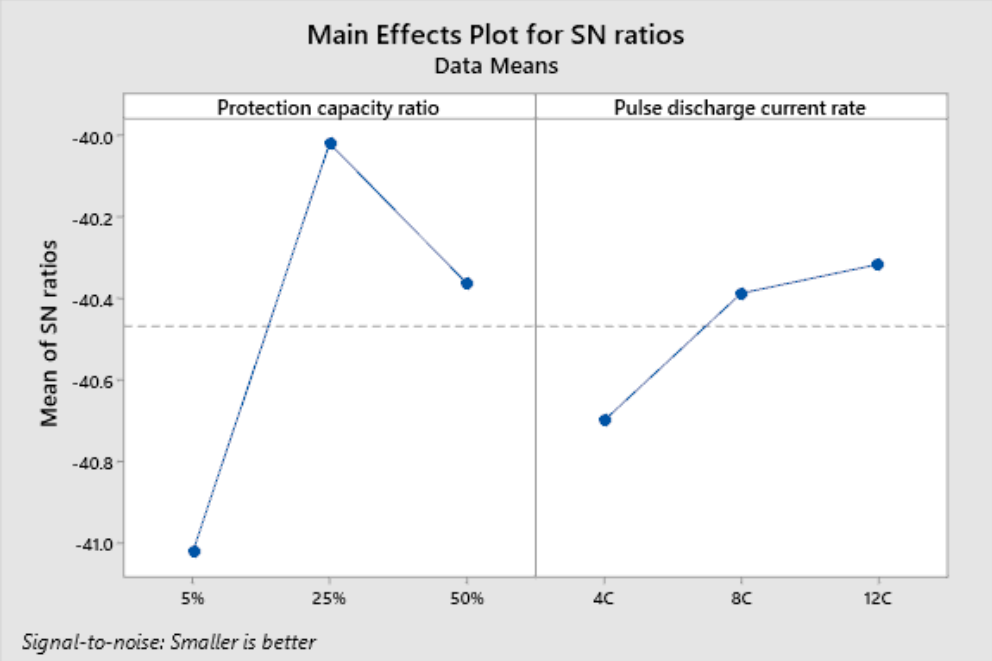

Figure 3.2: Taguchi design results analysis-main effects plot for SN ratios -Total charging time.

We can now compare the battery charging time of the optimal pattern with that of the baseline pattern at low temperatures. The baseline charging pattern shown in Figure 3.3(a) contains two stages: a CC (1C) stage to 3.6V and a CV stage. The CC stage takes about 36 minutes, and the CV stage takes about 76 minutes. The optimal charging pattern shown in Figure 3.3(b) uses a specific pulse charging method (25% protection capacity ratio and 12C pulse discharge current rate) and contains 3 stages: a pulse current stage, a CC stage to 3.6V, and a CV stage. The pulse current stage takes about 7.5 minutes, the CC stage about 43 minutes and the CV stage about 49 minutes. Figure 3.4(a) compares the total charging time of the traditional CC-CV charge shown in Figure 3.3(a) and the optimal pulse charge pattern shown in Figure 3.3(b). Based on the results of the two

batteries, the optimal pulse charging pattern saves about 11% charging time when compared to the traditional CC-CV charging pattern. Although the optimal charging pattern consumes 7.5 minutes in the pulse current stage, the cell reaches the upper cutoff voltage later, which saves 43% of the time in the final CV stage when compared to the baseline charging pattern.

The fully charged batteries from both charging methods were discharged at a constant current of 0.5C to a low cutoff voltage of 2.0 V. Figure 3.4(b) shows that when the optimal charging pattern is used, the discharge capacities of the two batteries are about 1.3% greater than those obtained using the baseline charging pattern. Therefore, the pulse charging method developed here saves the total charging time without sacrificing the cell capacity.

After low-temperature charging, the two batteries A and B were taken out from the environmental chamber and placed at room temperature for 3.5 hours for actual discharge capacity testing. Figure 3.5 shows the discharge capacity of both batteries, and their comparison with the benchmark cell C. The two batteries charged using the pulse charging method at low temperature show no degradation compared to their initial states. Further testing will be conducted to evaluate the cycle life of pulse charging at low temperature.

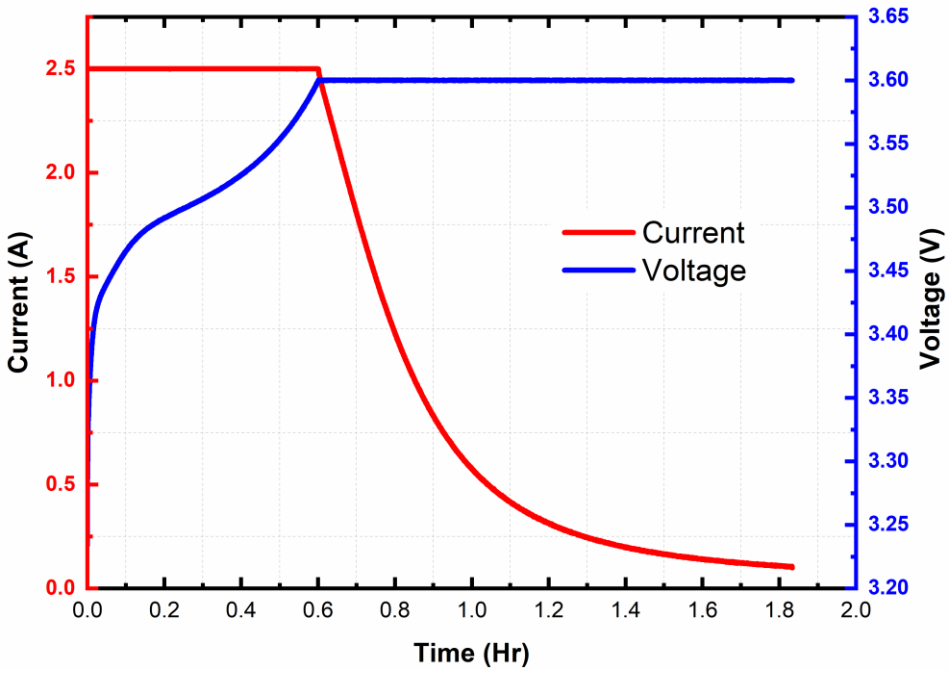

(a)

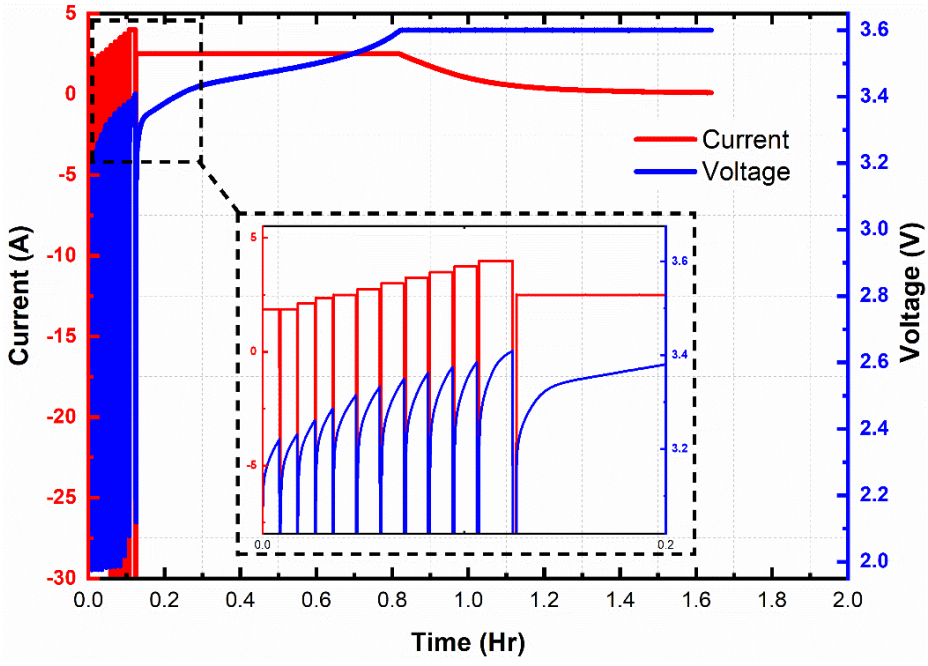

(b)

Figure 3.3: Comparison of the optimal pulse charging pattern with the baseline charging pattern: (a) Baseline CC-CV charging pattern. (b) Optimal pulse charging pattern.

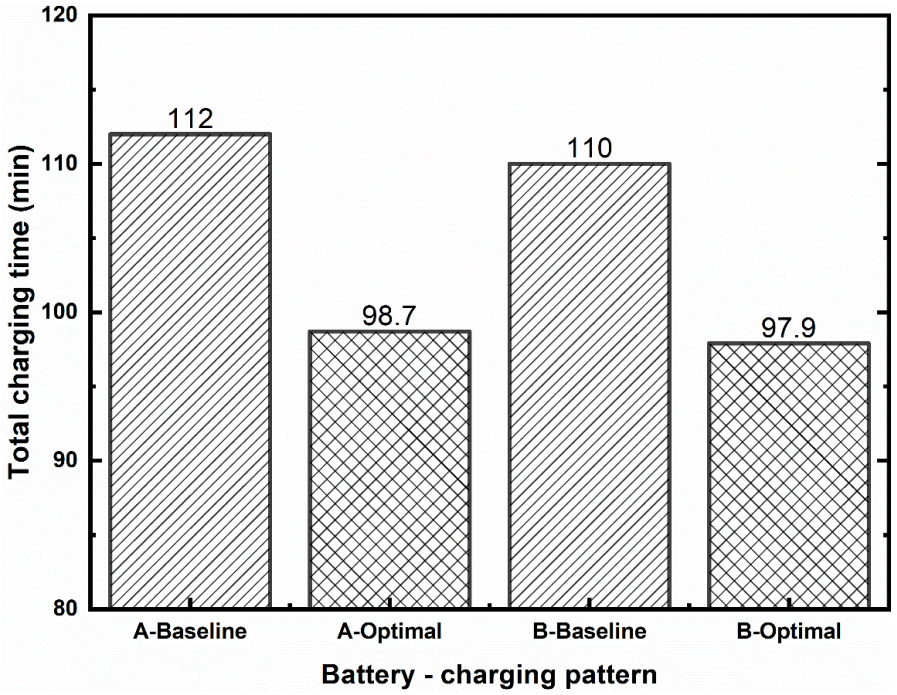

(a)

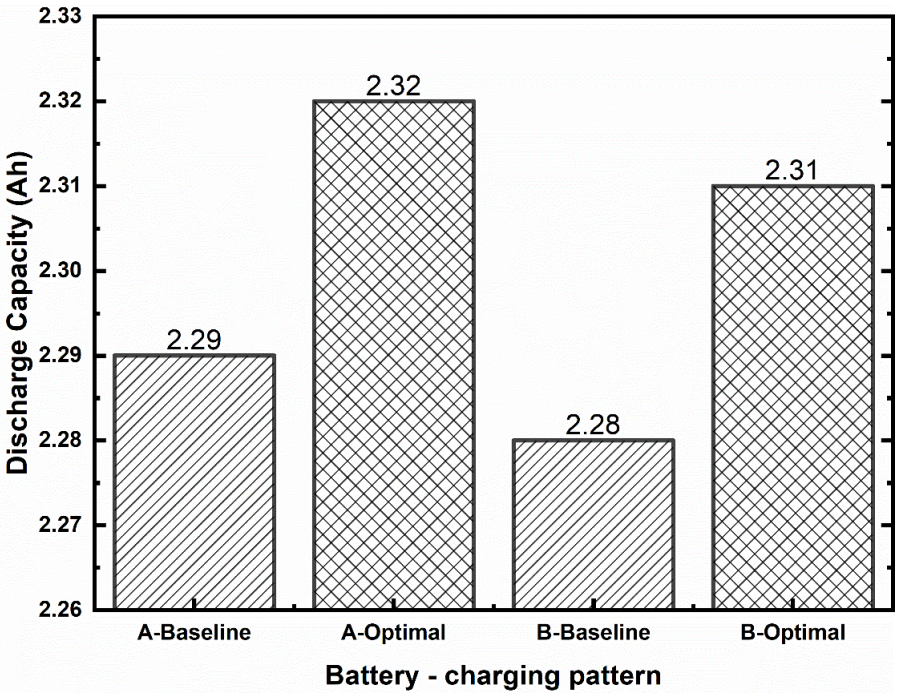

(b)

Figure 3.4: Comparison of the optimal pulse charging pattern with the baseline charging pattern: (a) Total charging time. (b) Total discharge capacity.

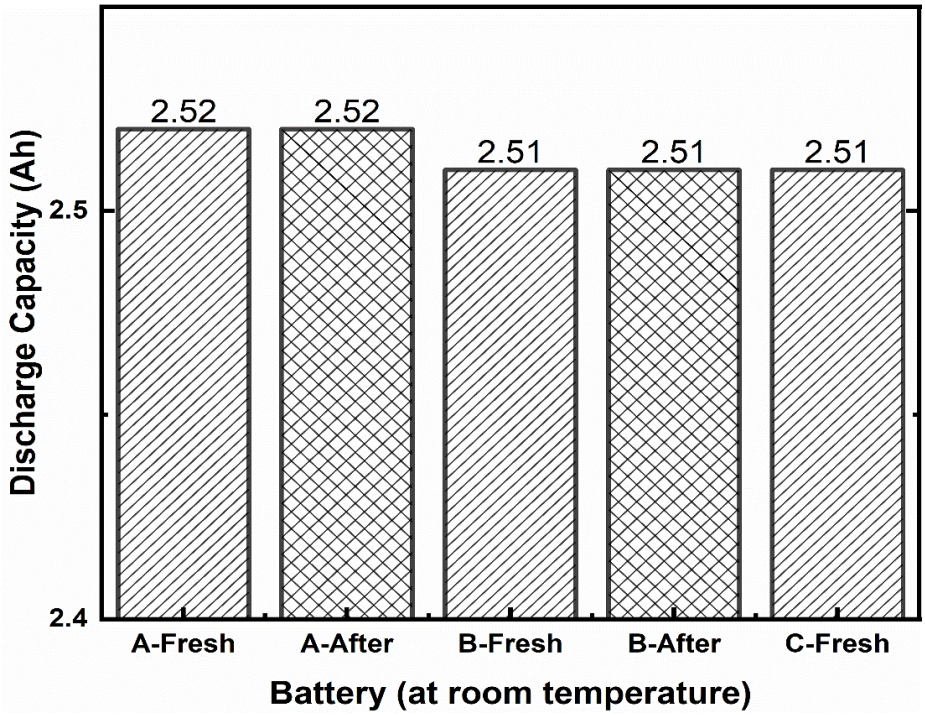

Figure 3.5: Battery remaining discharge capacity after low temperature test.

3.3. Room Temperature Experimental Results and Discussion

We now focus on studying pulse charging of lithium-ion batteries at room temperature. Previous results have shown that pulse charging can reduce charging time when its frequency is increased to 50 Hz or higher [39]. A preliminary experiment using a 2C-Rest pulse charging mode at 50 Hz was conducted to verify this finding. However, it was found that the excessively high pulse frequency made it difficult to reach the cutoff voltage of 3.6V during the entire charging process. In other words, it took longer to fully charge the battery using such a high frequency pulse charging strategy.

We then redesigned the frequency parameters and conducted experiments, finding that the new method improved the performance of both LFP and NMC lithium-ion batteries. The ranges of pulse parameters, such as pulse current amplitude and pulse frequency, were adjusted, and a Taguchi design was used to analyze their influence on the experimental results of the C-R mode. Finally, we analyzed and discussed the results of the two additional defined modes: C-C and C-D.

In these experiments, different pulse methods involve charging the lithium-ion battery to its maximum cutoff voltage using a specific pulse pattern, followed by constant-voltage charging until the current is reduced to 0.1C. The average current of each pulse charging pattern is maintained at 1C, ensuring a fair comparison between the proposed pulse charging methods and the traditional charging method (constant current and constant voltage charging) in terms of battery performance. The total charging time of the 1C CC-CV charging method is used as the experimental baseline.

3.3.1 Selection of Charging Frequency

In a preliminary experiment, we used the A123 LFP battery as an example and applied the 2C 50Hz C-R charging protocol. The total charging time was 135 minutes, significantly longer than the 67 minutes required by the 1C CC-CV charging method. This finding contradicts with conclusions drawn in a previous paper [39], indicating that high pulse frequency values can greatly prolong the time needed for the battery to reach the cutoff voltage, thereby increasing the overall charging time. We also tested different pulse frequencies ranging from 5 to 50 Hz, but the results did not reduce the total charging time as expected. Based on this, we formulated the hypothesis that lower

frequencies, which involve longer time duration for each proposed pulse current, may better reveal the effect of pulse charging on battery performance. Therefore, the charging frequencies selected for this study range from 0.025Hz to 1Hz.

3.3.2 Taguchi Results for the C-R Mode

First, we selected 2C C-R pulse charging protocol to charge the A123 LFP battery and Samsung NMC battery. Each experiment included three batteries as a reference group. Four different frequencies (0.05Hz,0.1Hz,0.25Hz,0.5Hz) were applied, and the average total charging time was compared with the 1C CC-CV method. It can be seen from Figure 3.6(a) and 3.6(b) that this pulse charging method consistently reduced the total charging time for both batteries, compared to the traditional 1C CC-CV charging method, regardless of frequency. This demonstrates that when the average charging current remains the same (i.e,1C in this study), the efficiency of pulse charging is slightly higher than that of the traditional 1C CC-CV charging method.

Subsequently, we conducted a more in-depth analysis of the C-R mode. The two most critical parameters in the pulse charging protocol, namely the pulse current rate and frequency, were selected as control factors for Taguchi experimental design and analysis. Each control factor has 5 factor levels, the input pulse current rate ranges from 2C to 6C, and the frequency is from 0.05Hz to 1Hz. These details are summarized in Table 2.6 as discussed in previous chapter. A total of 25 sets of experiments were conducted, with each set comprising three batteries as a control group. The testing results are summarized in Figure 3.7.

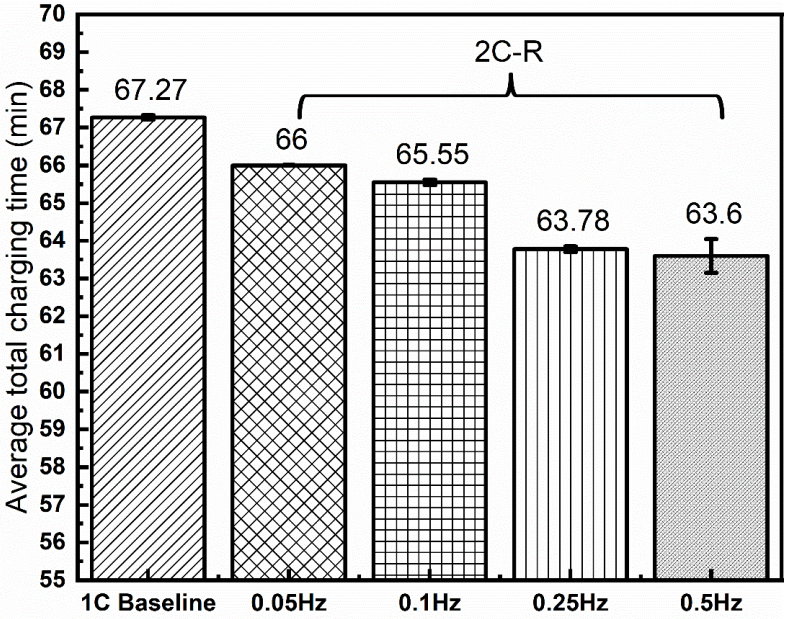

(a)

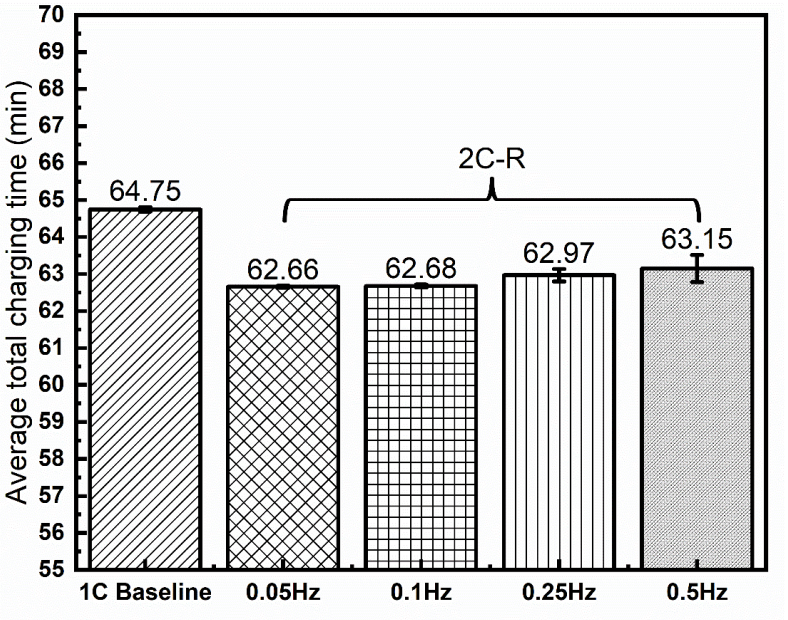

(b)

Figure 3.6: Comparison of average total charging time after two different lithium batteries were charged in the same way. (a) A123 LFP batteries. (b) Samsung NMC batteries.

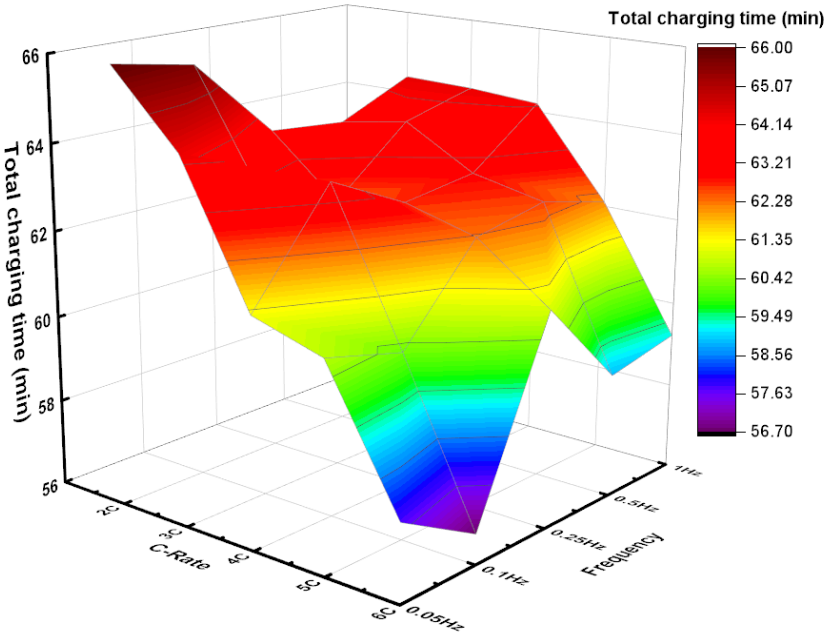

(a)

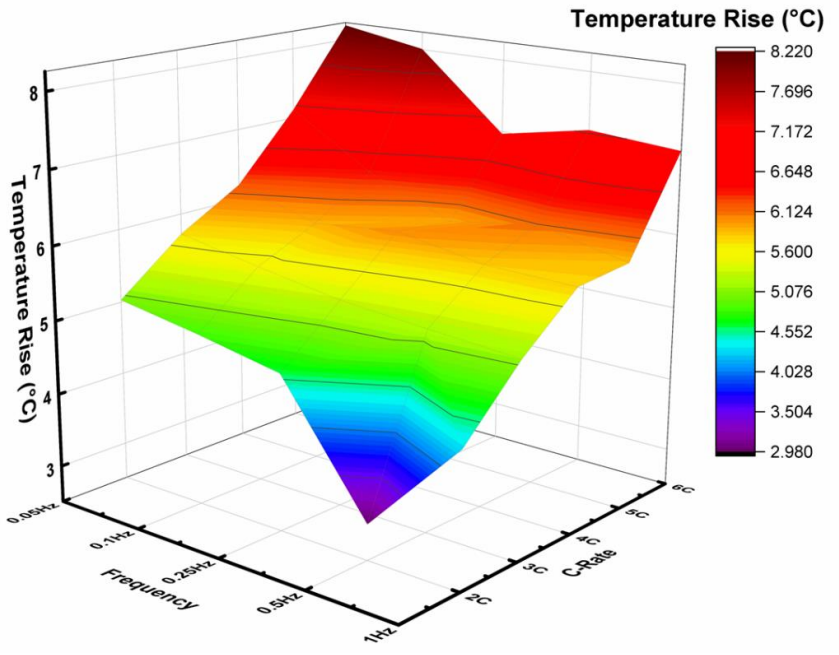

(b)

Figure 3.7: Overview of output results in C-R mode. (a) Total charging time. (b) Temperature rise.

As shown in Figure 3.7(a), the total battery charging time tends to decrease as the current increases and the frequency decreases, up to 3C. Beyond 3C, the current amplitude becomes the dominant factor in reducing the total charging time. Figure 3.7(b) shows that the temperature rise of the battery in C-R mode increases as the input pulse current increases. As the C-rate increases, the overall battery temperature rise ranges from about 3.2°C (baseline 1C CC-CV) to a maximum of 8.2°C (6C C-R mode).

According to the Taguchi analysis presented in Figure 3.8(a) and 3.8(b), the input pulse current amplitude shows a large gradient change. Further analysis using Minitab software shows that the influence factors of the pulse current amplitude are 0.84 and 0.78, respectively, while the influence factors of the pulse frequency are 0.15 and 0.23. This confirms that within the tested range, the input pulse current amplitude has a greater influence on charging time than the pulse frequency. While high input pulse current can reduce the total charging time, it comes at the cost of a higher temperature rise. Additionally, a large input pulse current diminishes the effect of pulse frequency. Therefore, in designing the next mode, we will limit the pulse input current to no more than 3C, which allows us to continue to effectively evaluate the effects of both parameters.

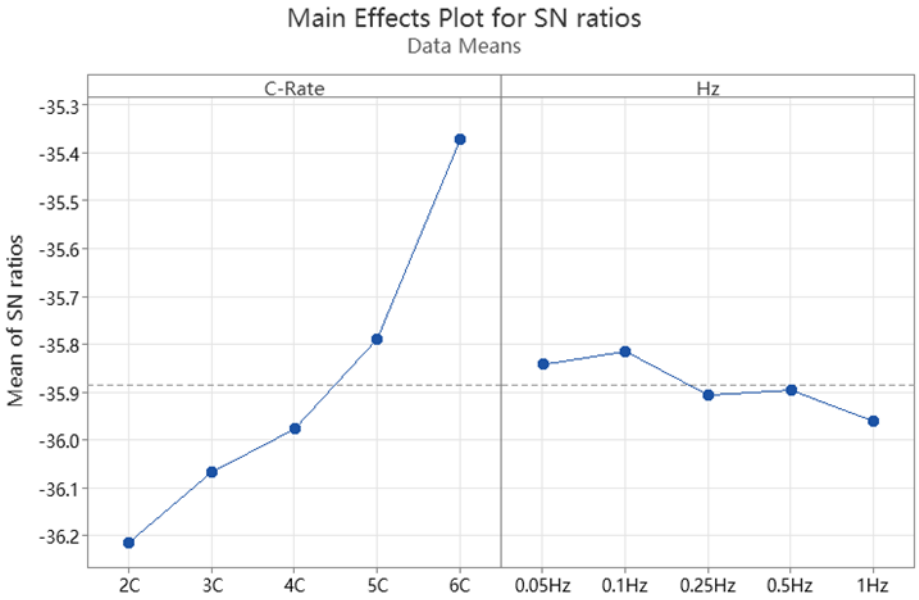

(a)

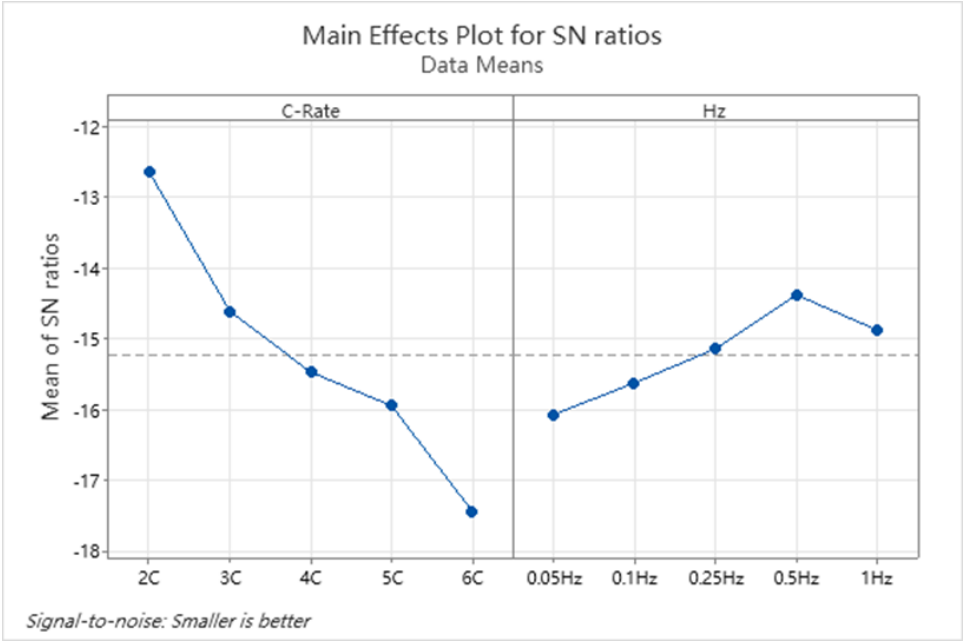

(b)

Figure 3.8: Taguchi results for C-R mode. (a) Total charging time. (b) Temperature rise.

3.3.3 C-C and C-D Modes Experimental Design and Results

Compared with the C-R mode, the C-C and C-D pulse modes change the amplitude and/or direction of the pulse current. Figure 3.9 shows a schematic diagram of different charging methods. Each single pulse period is divided into two time periods: T_1 and T_2. Figure 3.9(a) presents the case where $T_1 = T_2$ while Figure 3.9(b) shows the example where $T_1 \neq T_2$. In Figure 3.9(a), the pulse charging current in the T_1 stage gradually increases, and the pulse charging current in the T_2 stage gradually decreases, and eventually transits to a pulse discharge current. The average charge rate in each pulse duration is equivalent to 1C. For example, the 1C CC-CV charging method charges with the same current (1C) during both the T_1 and T_2 time periods. The 2C/0C charging method charges at 2C during the T_1 period and rests during the T_2 period, which has the same charging capacity as 1C charging in both the T_1 and T_2 time periods. Figure 3.9(b) shows an example of a pulse charging pattern where $T_1 \neq T_2$. At a frequency of 0.05Hz, i.e., in a 20-second cycle, the durations of the two stages T_1 and T_2 in the C-D pulse mode of 2C/-1C are not equal, and the selection of T_1 and T_2 should ensure that the input average current is 1C.

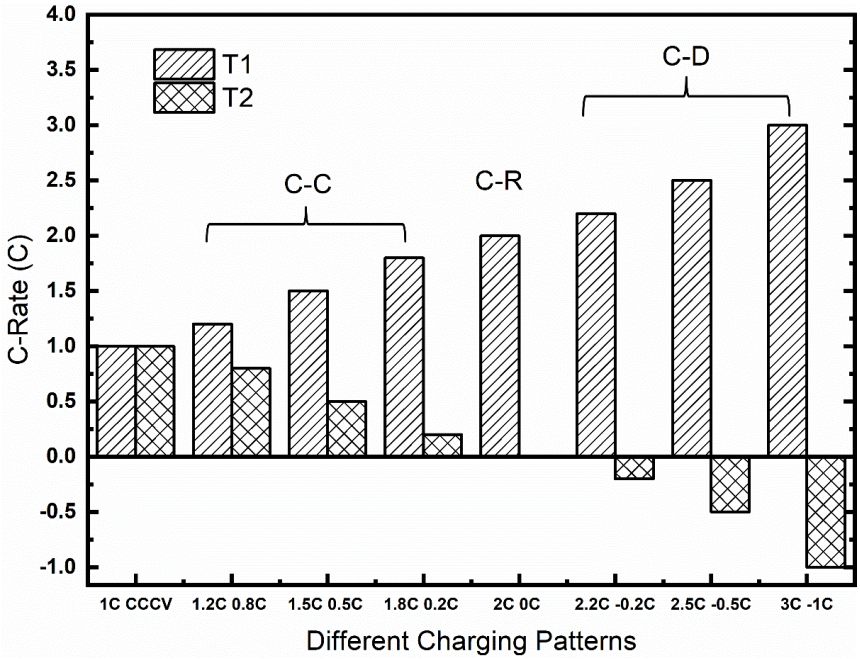

(a)

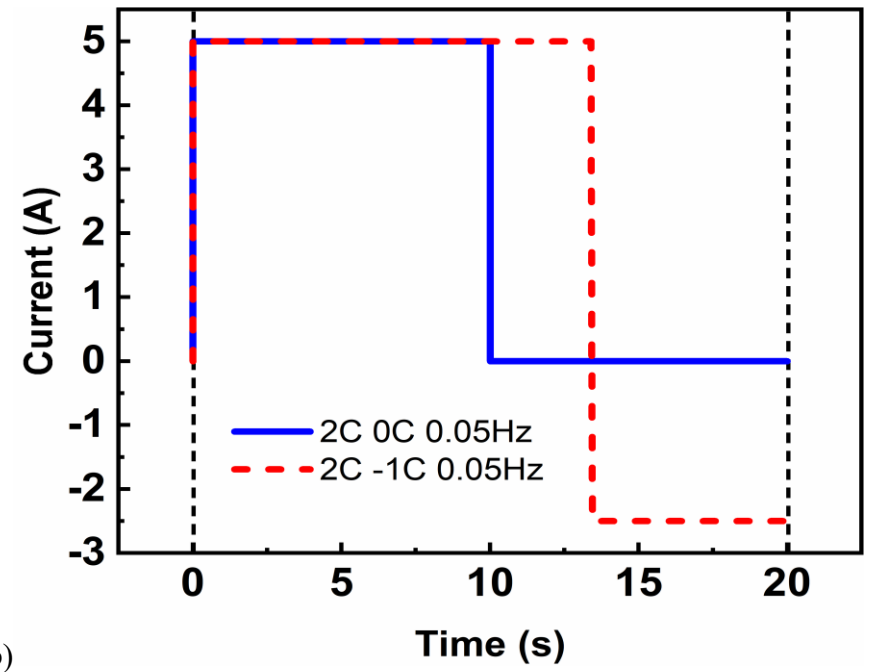

(b)

Figure 3.9. Schematic diagram of charging principle of different charging patterns. (a) $T_1=T_2$. (b) $T_1 \neq T_2$.

Table 3.2 summarizes the total charging time, the discharge capacity, and the ending cell temperature rise for each of the seven pulse charging methods, shown in Figure 3.9(a) at frequencies of 0.05Hz, 0.1Hz, 0.25Hz, and 0.5Hz. The results were compared with those using the 1C CC-CV charging method. Interestingly, only one set of total charging time exceeded the baseline of 1C CC-CV, which was the 3C/-1C at 0.5Hz. This may be because the charging current was discharged shortly after being applied, leading to a delayed attainment of the cutoff voltage. These data results offer valuable insights for selecting the appropriate pulse charging and discharging ranges. A high frequency and high C-D pulse amplitude difference tend to prolong the charging time, as the large negative pulse current will delay the voltage's approach to the cutoff voltage. The battery shows the shortest total charging time with the lowest frequency (0.05Hz) in the 3C/-1C charging mode. The average discharge capacities and the average temperature rises are similar for the seven cases of three pulse modes since the batteries were all fully charged by including a constant CV stage.

Table 3.2. Summary of key results for different pulse modes (T_1=T_2)

Mode (with CV)	Case	Frequency (Hz)	Total Charging Time (min)	Discharge capacity (Ah)	Ending Temperature Rise (°C) (averaged value)
1C CC-CV			67.26	2.511	3.21
C-C	Case 1 (1.2C/0.8C)	0.05	64.8	2.516	4.56
		0.1	64.38	2.520	4.37
		0.25	64.85	2.517	3.97
		0.5	64.3	2.521	4.04
	Case 1 Average		64.58	2.518	4.23
	Case 2 (1.5C/0.5C)	0.05	65.75	2.505	4.26
		0.1	63.8	2.517	3.93
		0.25	63.6	2.522	3.85
		0.5	64.2	2.519	3.78
	Case 2 Average		64.33	2.516	3.955
	Case 3 (1.8C/0.2C)	0.05	63.5	2.517	4.78
		0.1	65.18	2.508	4.31
		0.25	64.38	2.517	3.95
		0.5	65	2.514	4.02
	Case 3 Average		64.52	2.514	4.26
C-R	Case 4 (2C/0C)	0.05	66	2.511	5.03
		0.1	65.55	2.508	4.55
		0.25	63.78	2.521	4.32
		0.5	63.6	2.521	2.95
	Case 4 Average		64.73	2.515	4.21
C-D	Case 5 (2.2C/-0.2C)	0.05	64.23	2.513	4.87
		0.1	64	2.517	4.58
		0.25	64.5	2.521	3.96
		0.5	67	2.510	3.91
	Case 5 Average		64.93	2.515	4.33
	Case 6 (2.5C/-0.5C)	0.05	63.36	2.517	4.95
		0.1	63.86	2.517	4.77
		0.25	64.6	2.518	3.69
		0.5	65.88	2.521	2.97
	Case 6 Average		64.42	2.518	4.10
	Case 7 (3C/-1C)	0.05	**62.73**	2.519	5.41
		0.1	64.68	2.513	5.23

Table 3.2.-Continued

Mode (with CV)	Case	Frequency (Hz)	Total Charging Time (min)	Discharge capacity (Ah)	Ending Temperature Rise (°C) (averaged value)
C-D	Case 7 (3C/-1C)	0.25	66.22	2.516	4.55
		0.5	68.3	2.521	3.98
	Case 7 Average		65.48	2.517	4.79

The C-D mode with a larger pulse input current and at a lower pulse frequency (3C/-1C 0.05Hz) demonstrated good charging performance when $T_1=T_2$. Consequently, we mainly use the C-D mode for our next round of experimental study where $T_1 \neq T_2$. Another 15 sets of experiments were designed, and the results are summarized in Table 3.3. The first 10 sets in Table 3.3 all use the same pulse charging amplitude of 2.5C (no more than 3C to limit temperature rise). The amplitude of pulse discharge was gradually increased from 0C to 5C, with the pulse time within each pulse duration adjusted to ensure a 1 C equivalent charging capacity per pulse. These sets differ only in frequency: one at 0.05Hz and the other at 0.025Hz. The results indicate that the frequency has a minimal impact on battery charging performance. Subsequently, we selected 2C as the pulse charging amplitude and 0.05Hz as the frequency. Compared to the 2.5C range, the pulse discharge amplitude was proportionally reduced, i.e., 2C/-1C corresponds to 2.5C/-1.25C in a ratio of 2:1, 2C/-2C corresponds to 2.5C/-2.5C in a ratio of 1:1, 2C/-4C corresponds to 2.5C/-5C in a ratio of 1:2. The results show that decreasing the charge and discharge range can effectively reduce the final cell temperature rise but tend to have

relative longer total charging time (i.e., 2.5C/-5C has the largest applied charge and discharge current range, the highest temperature rise and the shortest total charging time).

Other currents, such as 4C or even 6C, can speed up the charging rate, but also results in a higher temperature rise. Hence, we need to opt for a compromise solution, choosing a pulse charging strategy that not only reduces the charging time but also keeps the temperature increase within a certain range. Notably, the 2C/-1C at 0.05Hz mode charges faster and results in a reasonable final temperature rise, suggesting the necessity of further research using this mode. Because 2C is selected as the pulse charging current rate for the C-D mode (2C/-1C 0.05Hz), therefore 2C/0.5C at 0.05Hz and 2C/0C at 0.05Hz will be used to represent the C-C and C-R modes, respectively, for further comparative analysis.

Table 3.3. Summary of key results for different pulse modes ($T_1 \neq T_2$)

Mode (with CV)	Frequency (Hz)	Case	Total Charging Time (min)	Discharge capacity (Ah)	Ending Temperature Rise (℃)
2.5C C-R	0.05	2.5C/0C	63.56	2.513	5.23
2.5C C-D		2.5C/-0.5C	63.36	2.517	4.95
		2.5C/-1.25C	62.83	2.519	5.68
		2.5C/-2.5C	62.5	2.519	6.64
		2.5C/-5C	61.65	2.522	7.12
2.5C C-R	0.025	2.5C/0C	63.58	2.506	5.34
2.5C C-D		2.5C/-0.5C	62.95	2.513	5.69
		2.5C/-1.25C	62.38	2.515	5.98
		2.5C/-2.5C	61.83	2.519	7.58
		2.5C/-5C	61.5	2.520	8.21
2C C-R	0.05	2C/0C	66	2.511	5.03
2C C-D		2C/-0.5C	63.87	2.511	4.23
		2C/-1C	**62.63**	**2.515**	**4.31**
		2C/-2C	63.5	2.512	4.87
		2C/-4C	61.76	2.517	6.09

3.4. Internal Resistance and Cycle Life Testing Results

After analyzing the experimental results of the three modes at room temperature, we conducted internal resistance tests and cycle life tests for different charging strategies to further confirm that the pulse charging mode has a positive impact on battery performance. This includes not only comparative tests of different charging modes at room temperature, but also comparative tests at 25 °C and 0 °C.

3.4.1 Internal Resistance Testing Results

Using the internal resistance measurement method described in Chapter 2, we measured the internal resistance of the pulse charged cell at 10% increment of the state of charge for four different charging modes: 1C CC-CV mode, C-D mode (2C/-1C), C-R mode (2C/0C), and C-C mode (2C/0.5C). All pulse charging modes were set at 0.05 Hz. The average current of all pulse charging modes was designed to be 1C, which is equivalent to the 1C CC-CV mode.

Figure 3.10 shows the variation in measured cell internal resistance at different states of charge (SOC) for three pulse charging modes along with the CC-CV charging as a baseline for comparison. Among the four modes, the C-D mode exhibits the smallest internal resistance, followed by the C-R mode, and then the C-C mode. Their internal resistances are smaller than that of the baseline 1C CC-CV mode across all SOC levels. Specifically, the average internal resistance in the C-D mode is nearly 14.5% lower than that of the CC-CV mode, indicating that the pulse charging may be able to enhance battery cycle life and efficiency.

Since the C-D mode shows excellent performance results, we set up two different temperature conditions to observe the performance of batteries charged using the C-D mode and the CC-CV mode. At a low temperature of 0 °C, to prevent over-discharge, the battery was pre-charged to 10% SOC before internal resistance testing under different charging modes. As shown in Figure 3.11, at 0 °C, the internal resistance of both modes at 10% SOC is basically the same. As charging continues, the internal resistance trends diverge. Compared with the CC-CV mode, the C-D pulse charging mode can effectively

reduce the internal resistance for the entire charging process. However, the internal resistance at 0 °C is still greater than that at 25 °C due to the reduced electrolyte ion conductivity and lithium diffusivity at low temperature. Despite this, the 2C/-1C pulse charging mode can still effectively reduce the increase in internal resistance, thereby improving the charging performance.

In order to more intuitively observe the difference in internal resistance between different charging modes, Figure 3.12 shows the percentage reduction in internal resistance of the 2C/-1C pulse charging mode relative to the CC-CV charging mode. It can be seen that the pulse charging mode significantly reduces internal resistance through the entire charging process, whether at 0 °C or 25 °C. At 0 °C, near the end of charging (80% SOC-90%SOC), the pulse charging mode reduces internal resistance by more than 30% compared to the CC-CV method.

3.4.2 Cycle Life Testing Results

To further evaluate the influence of pulse charging on battery performance, we conducted cycle life tests. We selected the pulse mode (2C/-1C at 0.05Hz), which resulted in the smallest internal resistance, and compared it with the 1C CC-CV charging mode. To ensure a fair comparison, both charging methods had an average input current of 1C, and included a CV stage.

In the pulse charge mode, the battery was charged using a 2C/-1C pulse current at 0.05Hz to reach the cutoff voltage of 3.6V, followed by CV charging until the current dropped to 0.1C. After charging, the battery rested for one hour to eliminate internal polarization, then was discharged to 2V at 0.5C, followed by another one-hour rest. In the

CC-CV charging mode, the battery was charged with a 1C constant current to the cutoff voltage of 3.6V, then continued with CV charging until the current decreased to 0.1C. This was followed by one-hour rest, a discharge to 2V at 0.5C, and another one-hour rest. Each charge and discharge cycle was repeated 800 times for both charging modes.

Figure 3.13 shows that, as the number of cycles increases, the remaining discharge capacity of the 2C/-1C at 0.05Hz pulse mode is higher than that of the baseline 1C CC-CV mode. This indicates that compared to the traditional CC-CV charging mode, the C-D pulse charging mode not only reduces the total charging time, but also effectively extends the battery's cycle life. This result also aligns with the lower resistance demonstrated in Figure 3.11 for the C-D pulse charging mode.

Figure 3.14(a) shows that after 800 cycles, the internal resistance of the battery increased under both charging modes. The resistance in the pulse charging mode remains lower than that of the CC-CV mode across the 10%-90% SOC range. The increase in resistance after 800 cycles is significantly smaller in the pulse charging mode, which explains why the pulse charging mode shows better battery cycle life.

Figure 3.14(b) indicates that initially, there is little difference in the open-circuit voltage (OCV) between the two charging modes. However, after 800 cycles, both charging modes exhibit a rightward shift on the x-axis (i.e., SOC position) to maintain the same open-circuit voltage. This is caused by battery degradation. Compared to the pulse charging (C-D) mode, the CC-CV mode shows a larger shift, confirming the conclusion drawn from Figures 3.14 (a) and (b) that CC-CV charging leads to greater battery degradation.

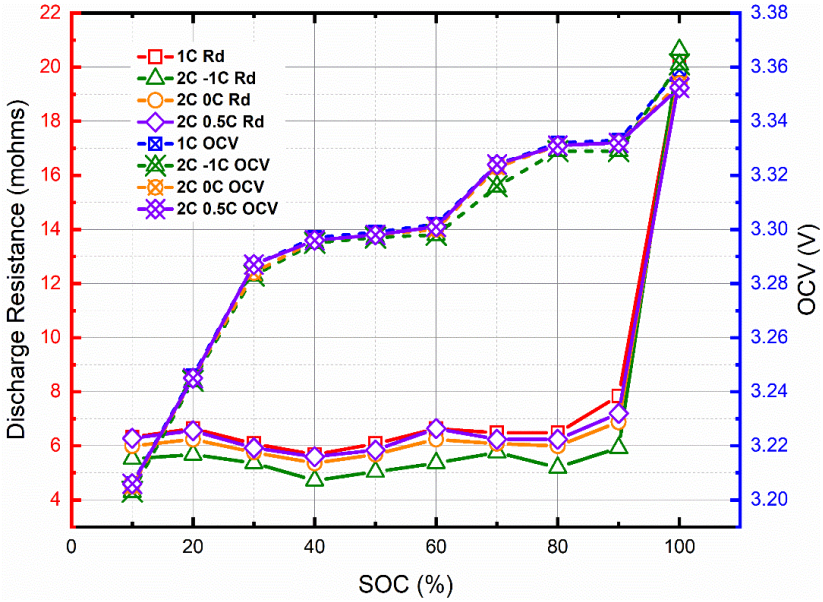

Figure 3.10: Comparison of cell pulse internal resistance for 1C CC-CV mode, C-D mode (2C/-1C), C-R mode (2C/0C) and C-C mode (2C/0.5C).

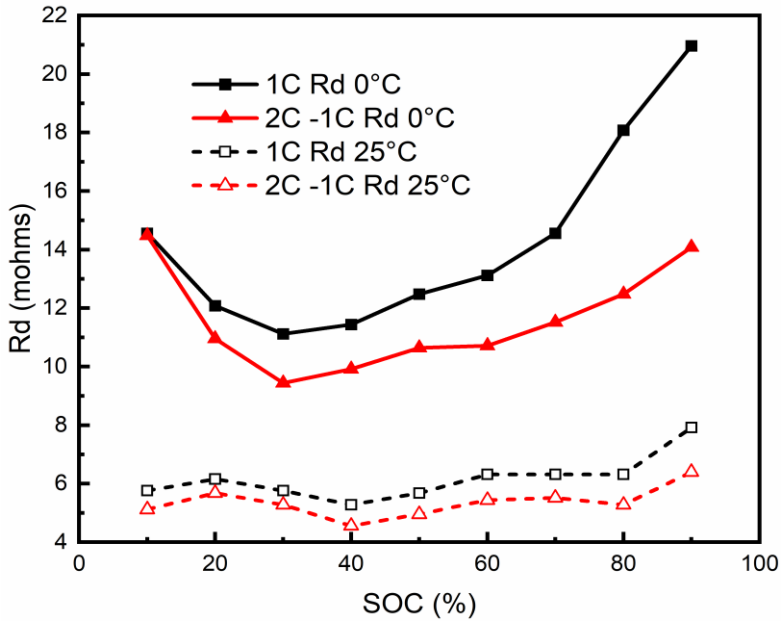

Figure 3.11: Comparison of internal resistance between 2C/-1C C-D mode and 1C CC-CV charging mode at different temperatures.

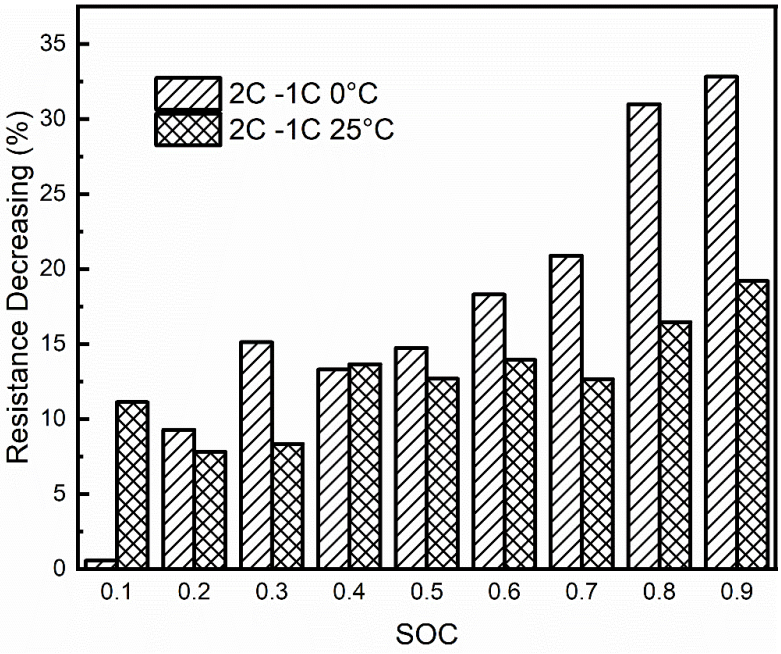

Figure 3.12: The percentage reduction of internal resistance in 2C/-1C C-D mode compared with 1C CC-CV charging mode at different temperatures.

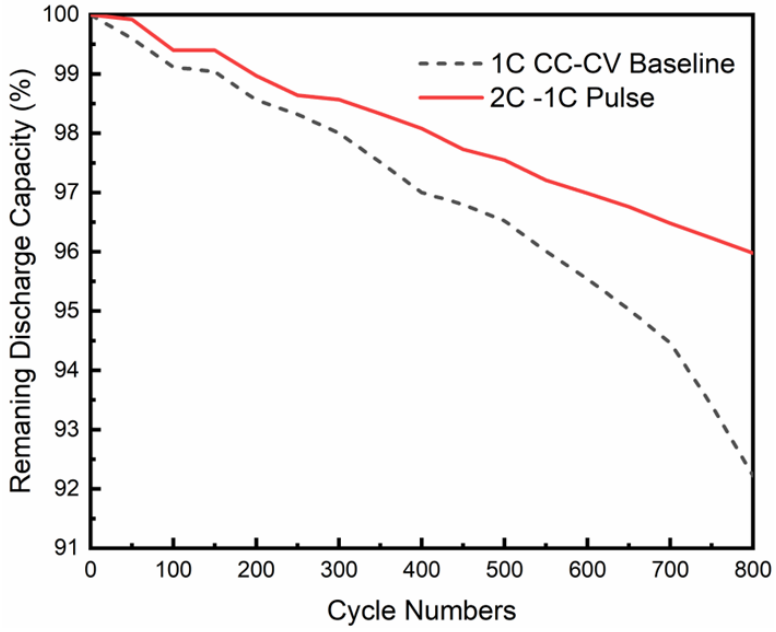

Figure 3.13: 1C CC-CV vs C-D mode (2C/-1C) 800 cycles -Remaining discharge capacity.

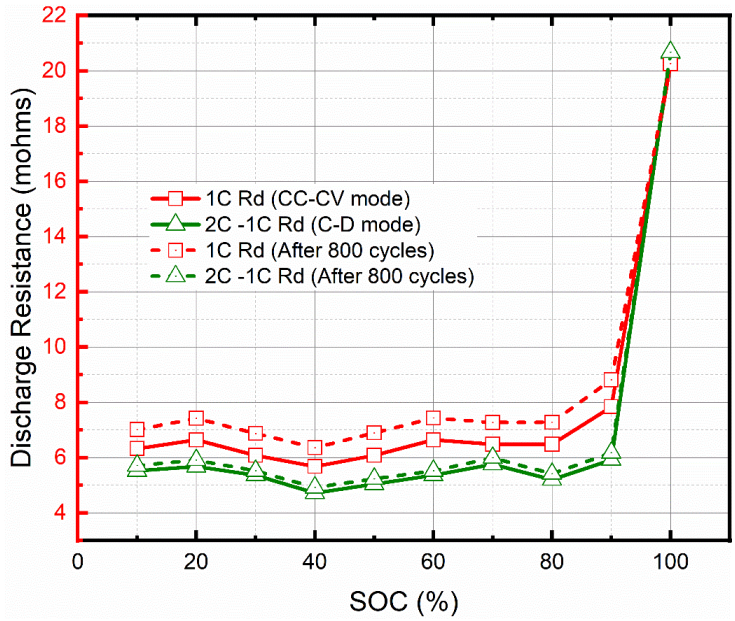

(a)

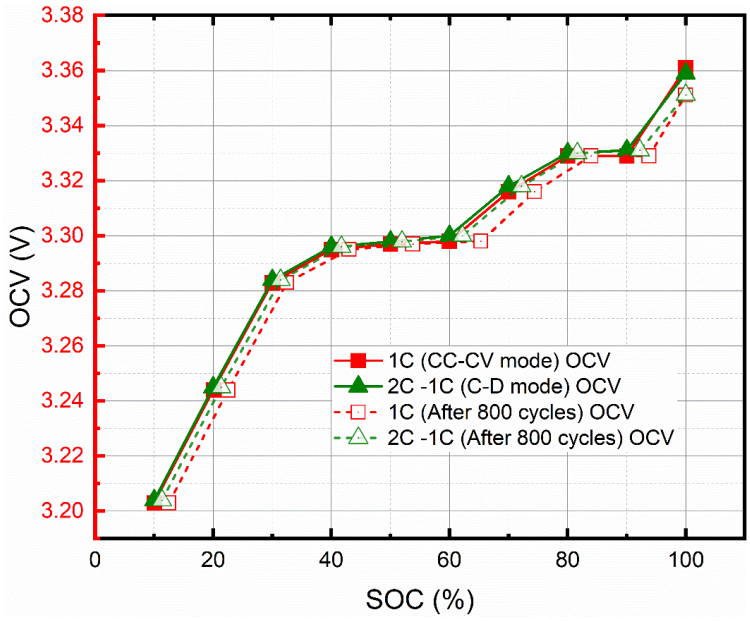

(b)

Figure 3.14: Cycle test results. (a) 1C CC-CV vs C-D mode (2C/-1C) before and after 800 cycles - Comparison of cell pulse internal resistance for 1C CC-CV mode, C-D mode (2C/ -1C). (b) 1C CC-CV vs C-D mode (2C/-1C) before and after 800 cycles - Comparison of cell OCV for 1C CC-CV mode, C-D mode (2C/-1C).

CHAPTER FOUR

NUMERICAL SIMULATION AND MODEL RESULTS

4.1 Introduction

This study mainly uses an electrochemical-thermal model that combines a pseudo two-dimensional electrochemical model and a two-dimensional thermal model to study the performance of LiFePO4 lithium-ion batteries under different pulse charging strategies. This combined electrochemical-thermal model was established and further developed based on previous studies [95-96]. This model is used to analyze the electrochemical behavior and performance of batteries. It describes the intercalation and deintercalation processes of lithium ions within the electrode materials, as well as the diffusion and migration of Li-ions in the electrolyte, both of which directly affect the charge and discharge performance of the battery. In addition, the model helps explain experimental phenomena by examining the distribution of lithium ions in the electrolyte and the lithium concentration distribution within each electrode particle. The model is used for simulation analysis under different operating conditions, including CC-CV charging strategies and pulse charging strategies, as discussed in Chapter 3. In addition, this model is also used for multi-objective optimization of batteries.

4.2 Model Setup

Figure 4.1 shows an overview of the electrochemical-thermal model. The model domain includes the negative electrode, separator, and positive electrode. The electrolyte exists everywhere inside the battery. In the model, the current flow direction is defined as

the x axis, and the solid particle dimension is defined as the r axis. During the charging process, lithium ions are transported from the positive electrode to the negative electrode through the electrolyte, while electrons flow from the positive electrode to the negative electrode through the external circuit. Figure 4.1 illustrates the discharging process, which is exactly the opposite of the charging process. The thermal model is a two-dimensional axisymmetric cylindrical model, where R represents the radial direction and Z represents the longitudinal direction of the battery.

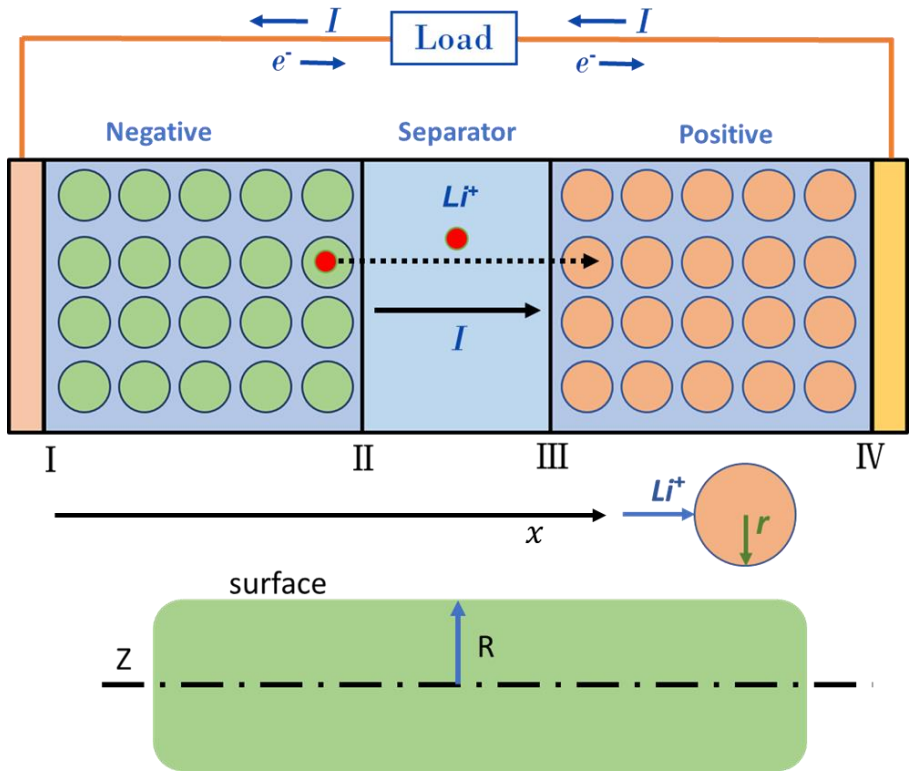

Figure 4.1: Schematic of electrochemical-thermal LiFePO4 battery model.

The model predicts battery performance primarily by coupling charge conservation, mass conservation, and electrochemical reactions. In this model, the active material is considered as a uniformly spherical particle, and lithium diffusion is described by Fick's law in the radial direction (r) of the spherical active material particle. Lithium-ion transport in the electrolyte phase is described along the through-plane direction (x) of the cell.

The charge conservation in the cell is expressed as:

$$\frac{\partial i_s}{\partial x} + \frac{\partial i_l}{\partial x} = 0 \tag{4.1}$$

where the electrical current density $i_s(x,t)$ describes the transport of electrons in the solid phase, and the ionic current density $i_l(x,t)$ describes the transport of lithium ions in the electrolyte. This charge conservation equation indicates that the total current is always equal to the sum of the solid phase and liquid phase currents.

Mass conservation includes both solid and liquid phases. In the solid phase, Fick's second law is used to describe the conservation of mass for lithium ions in a single spherical active material particle:

$$\frac{\partial c_s}{\partial t} = \frac{D_{s,eff}}{r^2}\frac{\partial}{\partial r}\left(r^2 \frac{\partial c_s}{\partial r}\right) \tag{4.2}$$

where t is time, $c_s(x,r,t)$ is the concentration of lithium in the active material of the electrode, r is the radial coordinate inside a spherical particle, and $D_{s,eff}$ represents the effective diffusion coefficient of lithium in the solid phase. In the x direction, the diffusion rate in the liquid phase is at least one order of magnitude faster than that in the solid phase, and therefore it is not considered [109-110].

The mass conservation of lithium ions in the liquid phase can be presented as:

$$\varepsilon_l \frac{\partial c_l}{\partial t} = \frac{\partial}{\partial x}\left(D_{l,eff} \frac{\partial c_l}{\partial x}\right) + S_a \frac{(1-t_+)}{F} j_n \tag{4.3}$$

where ε_l denotes the porosity, $c_l(x,t)$ is the concentration of lithium ions in the electrolyte phase, $D_{l,eff}$ represents the effective diffusion coefficient of lithium ions in the electrolyte phase, t_+ is the transference number of lithium ions, j_n represents the local transfer current density per unit area of the solid-electrolyte interface, S_a is the volume-specific surface area, and F is Faraday's constant.

The electrochemical reaction process on the interface of electrode and electrolyte is explained by Butler–Volmer equation:

$$j_n = j_0\{\, exp\left(\frac{\alpha_a F \eta}{\bar{R}T}\right) - exp\left(\frac{-\alpha_c F \eta}{\bar{R}T}\right)\} \tag{4.4}$$

where j_n is the local charge transfer current density and j_0 is the exchange current density. α_a and α_c are the anodic and cathodic charge transfer coefficients, η is the local surface overpotential, F is Faraday's constant, $\bar{R}$ is the universal gas constant, and T is the temperature.

To predict the temperature rise, an energy conservation equation (along the R direction of the battery radius and the Z direction of the battery length respectively) is used in the thermal model, which is defined as:

$$\rho C_p \frac{\partial T}{\partial t} = \frac{1}{R}\frac{\partial}{\partial R}\left(R \cdot \lambda_R \frac{\partial T}{\partial R}\right) + \frac{\partial}{\partial Z}\left(\lambda_Z \frac{\partial T}{\partial Z}\right) + q_{\,tot} \tag{4.5}$$

where ρ is the cell density, C_p is the heat capacity and λ is the thermal conductivity. $q_{\,tot}$ is the total heat generation rate consisting of reversible heat due to entropy change, irreversible heat due to reaction, and irreversible ohmic heat.

The model describes the transport related phenomena and electrochemical reactions occurring inside the battery. The transport phenomena include transport and diffusion of lithium and lithium ions in each solid or electrolyte phase, the transfer of electrons in the solid phase, and the transfer of thermal energy through heat conduction. The boundary conditions corresponding to each of the governing equations are listed in Table 4.1. A finite element-based software, COMSOL Multiphysics 6.3, was used to solve these coupled governing equations. A time-dependent solver with a relative tolerance of 0.001 is used for simulation calculations. The specific parameters of the battery used in the model are shown in Table A.1. This model can be used to study both the electrochemical performance and thermal performance of the battery, such as battery voltage changes, temperature rise, and lithium-ion concentration distribution.

Table 4.1 Boundary conditions of the electrochemical-thermal model

Governing Equations	**Boundary Conditions**
Charge Conservation	$i_s\|_{\mathrm{I}} = i_l\|_{\mathrm{II}} = i_l\|_{\mathrm{III}} = i_s\|_{\mathrm{IV}} = I_{app}/A;\ \ \emptyset_s\|_{\mathrm{I}} = 0$
Mass Conservation	$\frac{\partial c_l}{\partial x}\|_{\mathrm{I}} = \frac{\partial c_l}{\partial x}\|_{\mathrm{IV}} = 0$; $D_{l,eff}\frac{\partial c_l}{\partial x}\|_{\mathrm{II}} = D_{l,eff}\frac{\partial c_l}{\partial x}\|_{\mathrm{III}} = I_{app}/AF;$ $\frac{\partial c_s}{\partial r}\|_{r=0} = 0\ ;\ \ -D_{s,eff}\frac{\partial c_s}{\partial r}\|_{r=R_s} = \frac{j_n}{F}$
Energy Conservation	$\frac{\partial T}{\partial x}\|_{\mathrm{I}} = \frac{\partial T}{\partial x}\|_{\mathrm{IV}} = 0\ ; T\|_{\mathrm{I}} = T\|_{\mathrm{IV}} = T_{amb}$

4.3 Model Validation

To validate the model, experimental testing results are used. The experiments are divided into two categories: low temperature experiments and room temperature experiments. The testing conditions for the low temperature experiments are described in Table 2.3, where the battery is charged with a pulse current at an ambient temperature of -8.5°C, and the pulse cycle is repeated 11 times with a protection capacity ratio of 5% and a pulse discharge rate of 10C. Figures 4.2(a) and 4.2(b) compare the experimental and simulation results for voltage and temperature rise under this pulse charging condition. Additionally, Figure 4.3(a) and 4.3(b) show the model validation results using experimental data obtained at room temperature, where the battery is charged using a pulse charging strategy of 2C/0C at 0.05Hz in C-R mode. Figures 4.3(a) presents the cell voltage comparison between the experimental and model results while Figure 4.3(b) shows the temperature rise comparison under the specified pulse charging condition.

From the results obtained under both temperature conditions, it can be seen that the trends in voltage and temperature change predicted by the model are basically consistent with those observed in the experimental test. Therefore, the model will be used to further explore the impact of pulse charging on battery performance.

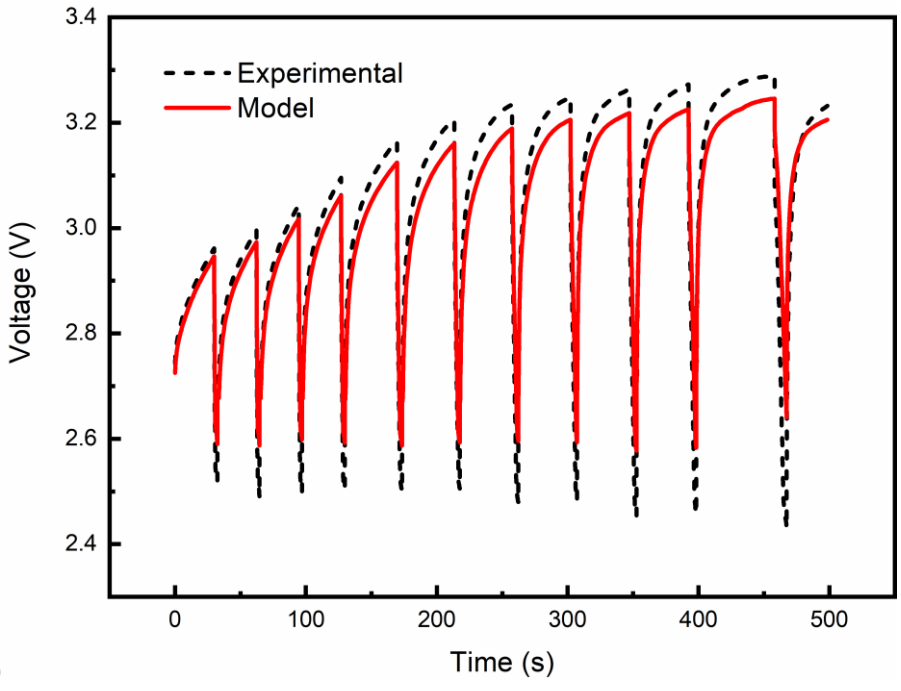

(a)

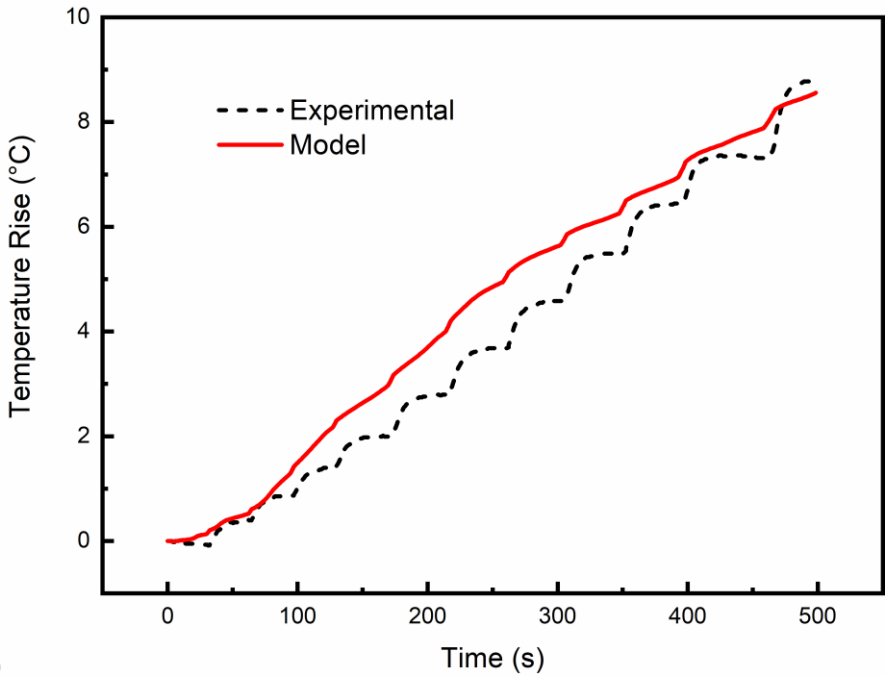

(b)

Figure 4.2: Experimental results vs modeling results at low temperature pulse charging. (a) Voltage. (b) Temperature rise.

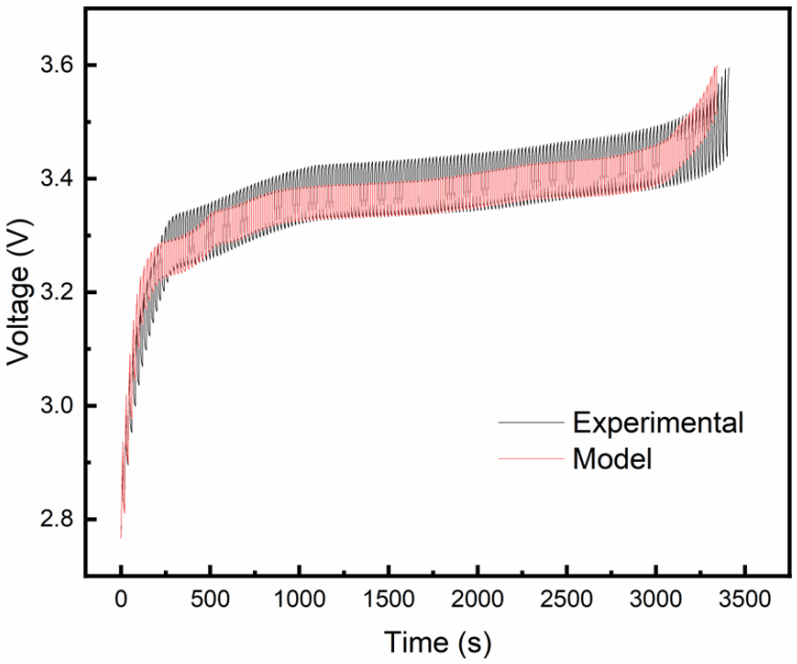

(a)

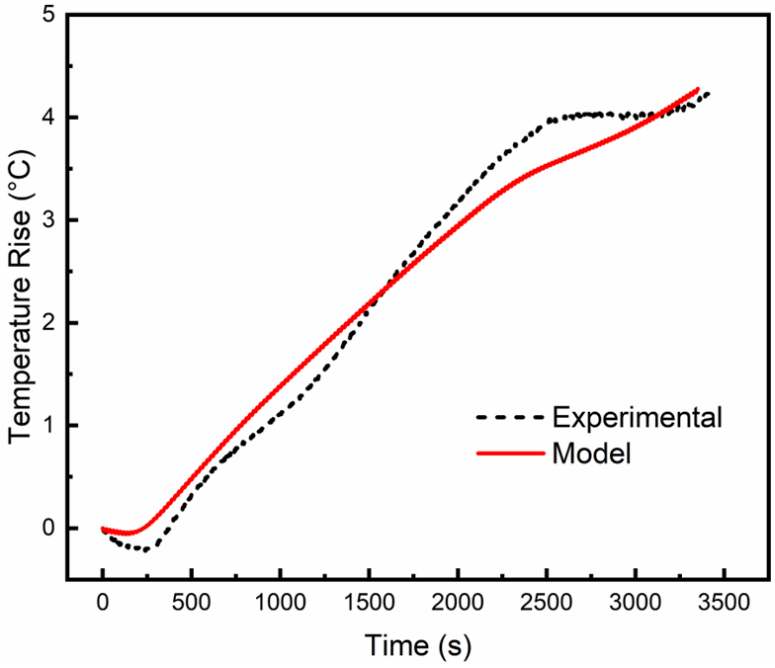

(b)

Figure 4.3: Experimental results vs modeling results at room temperature pulse charging. (a) Voltage. (b) Temperature rise.

4.4 Results and Discussion

4.4.1 Low Temperature Model Results

This section compares the model results for two charging methods at low temperatures: the traditional 1C CC-CV charging method, as shown in Figure 3.3(a), and the optimal pulse charging method (pulse CC-CV), as shown in Figure 3.3(b). The optimal pulse CC-CV method includes a pulse charging stage where the protection capacity ratio is 25% and the pulse discharge current rate is 12C, followed by a 1C CC stage to 3.6V and a CV stage.

Figures 4.4 through 4.6 present the internal characteristics of the Li-ion battery at 5% SOC and 80% SOC when the battery is charged using the pulse CC-CV method versus the traditional CC-CV charging method. Figures 4.4 and 4.5 show the distributions of electrolyte salt concentration and electrolyte potential across the cell, and Figure 4.6 presents the lithium concentration distribution within the solid electrode at each SOC level.

Figure 4.4 shows that Li-ions are deintercalated from the active material on the positive electrode and transported to the negative electrode during the charging process. As a result, the electrolyte salt concentration on the positive electrode is higher than that on the negative electrode. Under the pulse CC-CV charging method, lithium ions are deintercalated from the graphite particles during the pulse charging stage, resulting in an increase in the electrolyte salt concentration on the negative electrode. This is particularly true at 5% SOC, but it is not evident at 80% SOC. It should also be noted that the pulse charging stage ends at about 5% SOC, which results in a relatively uniform electrolyte

salt concentration profile due to the pulse effect. In contrast, the difference in electrolyte salt concentrations between the two charging protocols gradually narrows at 80% SOC. This is due to the subsequent CC-CV charging stage, which begins after the battery temperature reaches 0 °C after pulse charging. Therefore, the pulse charging method promotes a more uniform electrolyte salt concentration distribution across the electrodes, thereby enhancing the performance of the battery.

Figure 4.5 shows the electrolyte potential distribution across the cell at 5% SOC (a) and 80% SOC (b) for the two charging methods, respectively. Under pulse CC-CV charging, the electrolyte potential at the positive electrode is lower and its distribution across the battery is more uniform than that under conventional CC-CV charging. The lower electrolyte potential corresponds to a higher battery potential, indicating that the battery is more effectively charged with pulse CC-CV charging. This is particularly true immediately after the pulse charging stage (around 5% SOC), where the electrolyte potential at the positive electrode becomes lower than that of the baseline pattern, and the potential distribution across the cell becomes more uniform. At 80% SOC, the difference in electrolyte potential between the two charging patterns becomes smaller. The electrolyte potential also decreases as SOC increases from 5% to 80%.

Figure 4.6 shows the lithium concentration within the electrode particles of the battery at 5% SOC (a) and 80% SOC (b) for the two charging methods. In each plot, the solid line represents the lithium concentration at the particle surface, while the dashed line represents the lithium concentration at the particle center. At 5% SOC, the distribution of lithium concentration within electrode particles on both the positive and

negative electrodes is relatively flat in both charging methods, since it is at the beginning of charging. However, a lithium concentration gradient is present between the particle surface and center under the conventional 1C CC-CV charging method even at 5% SOC. This is due to the very slow diffusion of lithium within the solid particle at low temperatures. In contrast, with pulse charging, the cell temperature increases due to the high pulse discharge rate, which enhances lithium diffusion in the solid phase. Therefore, the lithium concentration difference between the particle surface and center is reduced under pulse charging. When charged to 80% SOC, the lithium concentration increases in the negative electrode, and decreases in the positive electrode. A lithium concentration gradient is formed on both electrodes. This gradient is more pronounced under conventional 1C CC-CV charging compared to pulse CC-CV charging, reflecting the improved mass transport and reduced concentration polarization enabled by the pulse charging method.

To further study the impact of pulse charging parameters on battery performance, a total of six charging protocols are compared, as shown in Figure 4.7. The protection capacity ratio varies among 5%, 25%, and 50%, and the pulse discharge current rate is set to 4C, 8C, and 12 C.

Figure 4.7(a) shows that under a specified protection capacity ratio (25%), a higher pulse discharge current rate (12C) makes the electrolyte salt concentration distribution inside the cell more uniform, thereby improving the performance of the battery. This is because a higher pulse current rate results in an increase in cell

temperature, leading to faster diffusion, which in turn improves the charging efficiency of the battery at low temperatures.

Figure 4.7(b) shows that the charging patterns with the 5% and 25% protection capacity ratios result in more uniform electrolyte salt concentration distribution compared to the 50% protection capacity ratio for a specified pulse discharge current rate of 12C. Generally, a higher protection capacity ratio corresponds to a longer constant current charging time. However, this may not be the case under low temperature charging conditions. A lower protection capacity ratio means more pulse discharging, which in turn increases the battery temperature, and improves the charging effect.

Figure 4.7(c) presents the corresponding experimental temperature rise of the three pulse charging protocols shown in Figure 4.7(b). All three pulse charging protocols reach their peak temperature rise within about 500 seconds. The pulse charging protocol with a 5% protection capacity ratio and a 12C pulse discharge rate results in the highest ending temperature but with longer pulse discharge time, which in turn leads to longer total charging time. In contrast, the pulse charging protocol with a 50% protection capacity ratio and a 12C pulse discharge rate has the highest pulse charging capacity and the shortest pulse discharge time, which results in the lowest peak temperature rise but a longer charging time due to slow diffusion at low temperatures. The pulse charging protocol with a 25% protection capacity ratio and a 12C pulse discharge rate is a balance between the aforementioned two protocols. It retains more charging capacity than the protocol with a 5% protection capacity ratio, and achieves a higher temperature rise than

the protocol with a 50% protection capacity ratio. Therefore, it results in the shortest charging time.

Both the experimental and modeling results demonstrate that the battery's charging performance at low temperatures is governed by the combined effect of the pulse discharge current rate and protection capacity ratio. These results are consistent with our findings from the Taguchi design experiments.

In order to further study the impact of the pulse charging induced preheating on the overall charging process, the effects of various ambient temperatures are analyzed. In this analysis, ambient temperatures of 10°C and -10°C are used. Figures 4.8 through 4.10 present the internal characteristics of the Li-ion battery at the same SOC (80%), but under different ambient temperature conditions (10°C and -10°C) when the battery is charged using the pulse CC-CV method and by the conventional CC-CV charging method. Figures 4.8 and 4.9 show the electrolyte salt concentration and electrolyte potential distributions across the cell, and Figure 4.10 shows the lithium concentration distribution within the solid electrode at each SOC.

Figure 4.8 shows that at the same SOC (80%) but under different ambient temperatures, the pulse CC-CV charging method continues to produce a more uniform electrolyte salt concentration distribution, thereby improving the charging performance of the battery. The influence of pulse preheating charging is more pronounced at low temperatures (i.e., -10°C). On the other hand, the lithium and lithium-ion diffusion rates are faster at 10 °C than at -10 °C, resulting in a more uniform electrolyte salt concentration distribution at higher temperatures.

Figure 4.9 shows the electrolyte potential distribution across the cell at -10°C (a) and 10°C (b) for the two charging methods, respectively. Under pulse CC-CV charging, the electrolyte potential distribution across the battery is more uniform than that under conventional CC-CV charging. The lower electrolyte potential corresponds to a higher battery potential, indicating that the battery is charged more efficiently under pulse CC-CV charging. These results are consistent with those observed in Figure 4.5, regardless of temperature. This further illustrates the positive impact of the pulse charging phase on improving battery charging.

Figure 4.10 shows the lithium concentration within the electrode particles of the battery at -10°C (a) and 10°C (b) for the two charging methods. In each plot, the solid line represents the lithium concentration at the particle surface, and the dashed line represents the lithium concentration at the particle center. When charged to 80% SOC, the lithium concentration increases in the negative electrode, and decreases in the positive electrode. A lithium concentration gradient forms in both electrodes. This gradient is more pronounced under conventional 1C CC-CV charging compared to the pulse CC-CV charging, particularly at -10 °C. As the temperature increases, the difference in the gradient between the two charging methods is significantly reduced due to the faster diffusion rate at 10 °C.

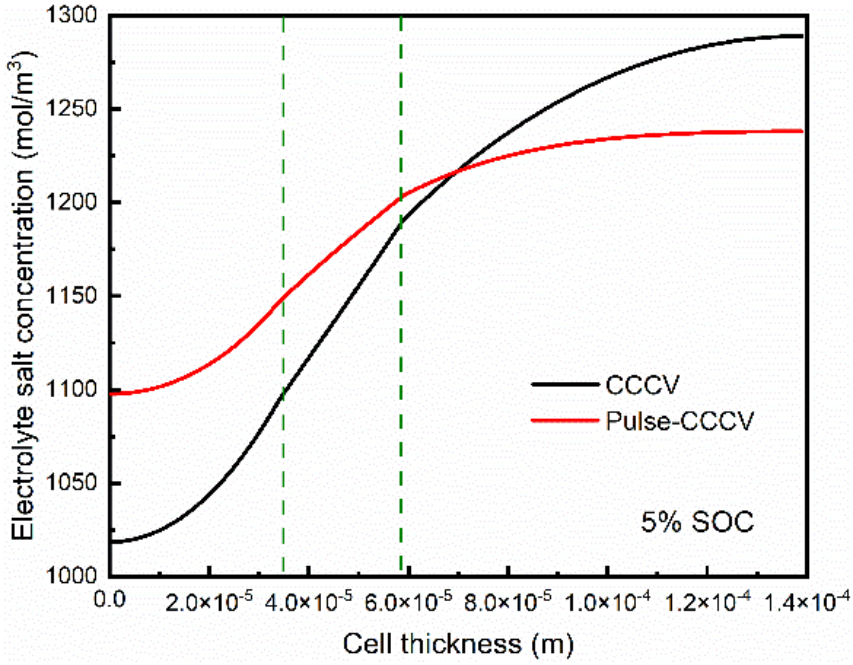

(a)

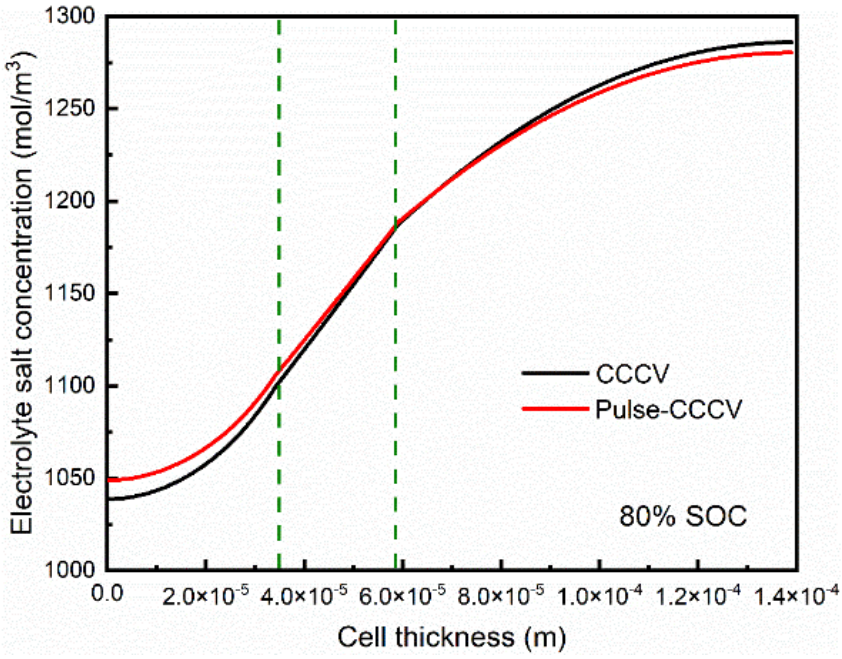

(b)

Figure 4.4: Electrolyte salt concentration across the cell for the optimal pulse pattern (pulse CC-CV) compared with the conventional 1C CC-CV charging pattern at (a) 5% SOC. (b) 80% SOC.

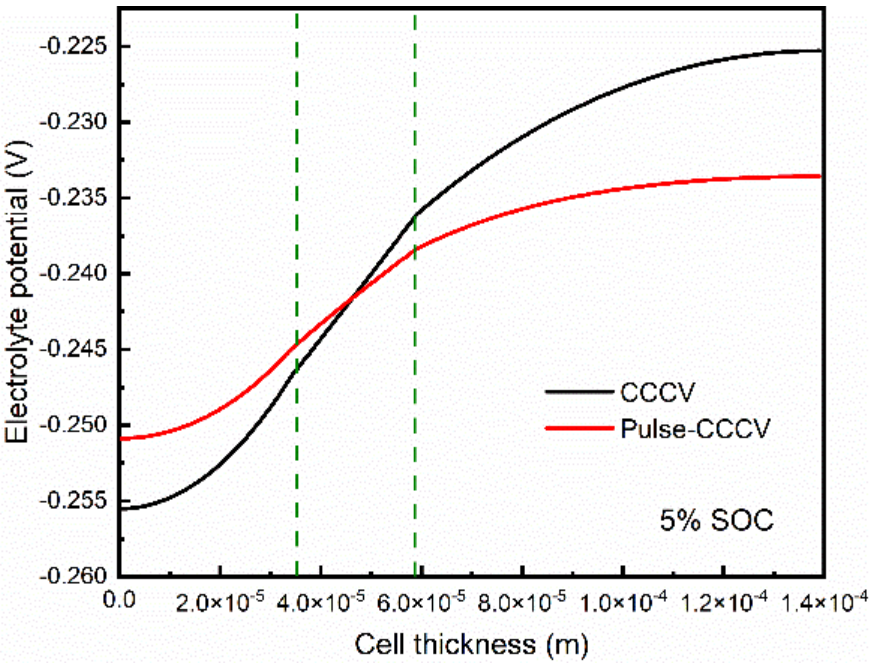

(a)

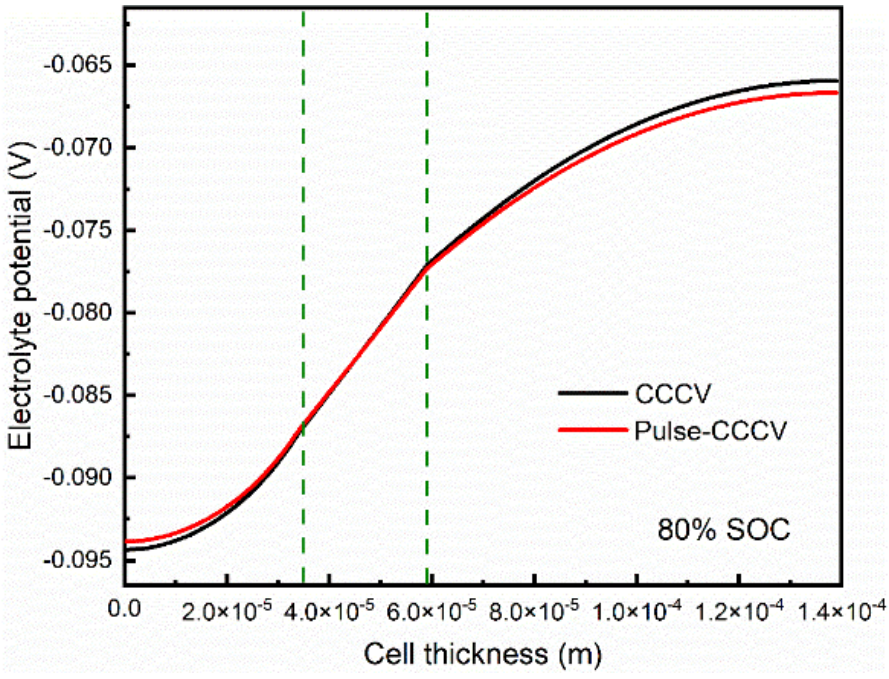

(b)

Figure 4.5: Electrolyte potential across the cell for the optimal pulse pattern (pulse CC-CV) compared with the conventional 1C CC-CV charging pattern at (a) 5% SOC. (b)80% SOC.

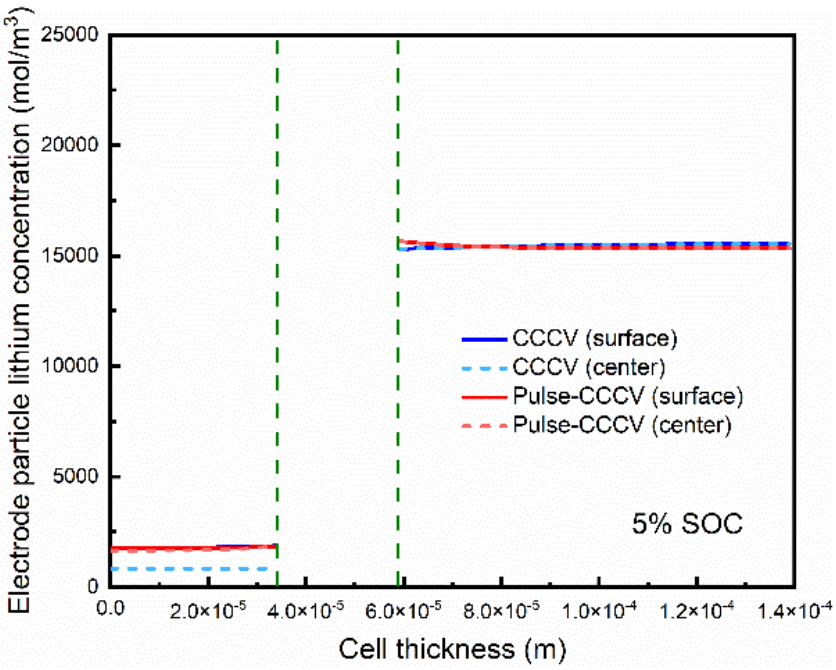

(a)

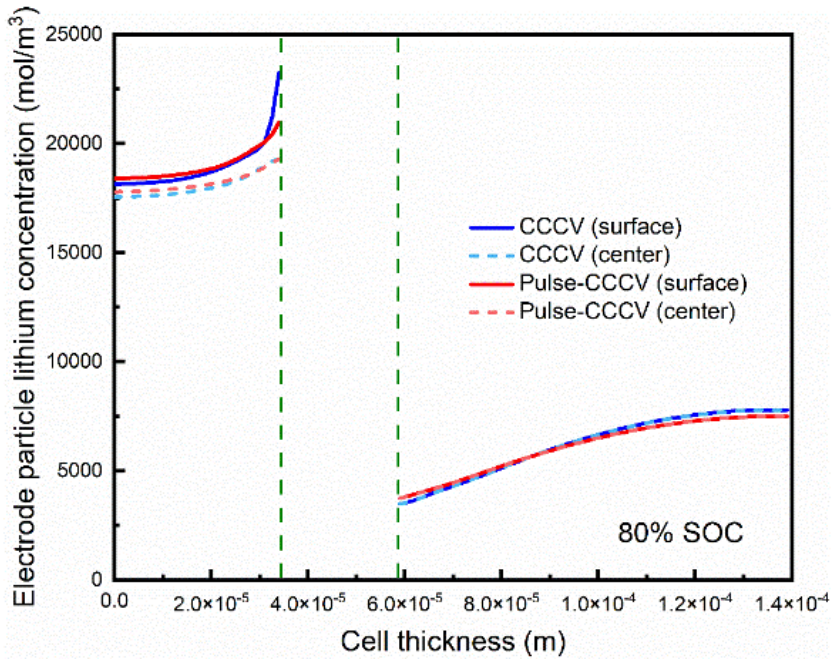

(b)

Figure 4.6: Electrode particle lithium concentration across the cell for the optimal pulse pattern (pulse CC-CV) compared with the conventional 1C CC-CV charging pattern at (a) 5% SOC. (b) 80% SOC.

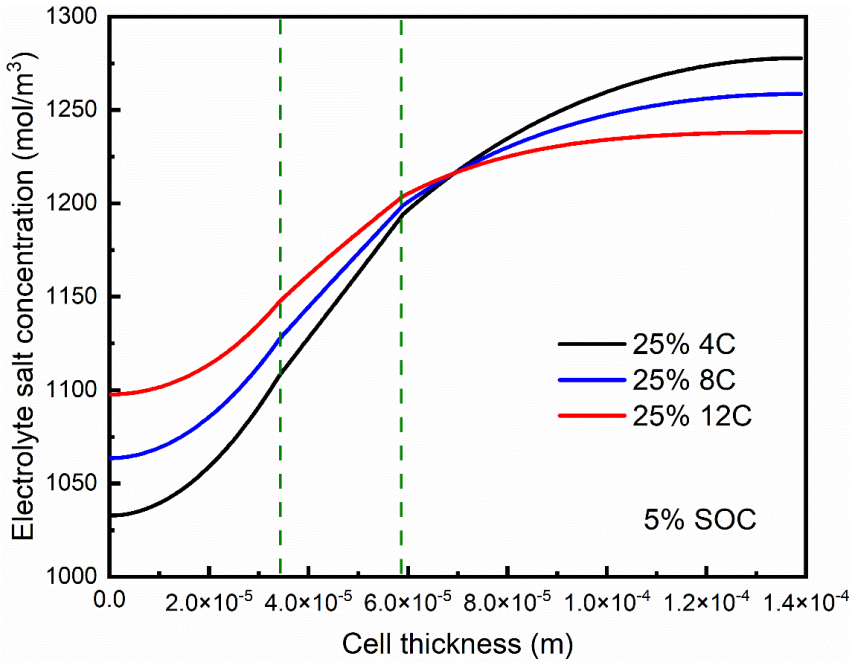

(a)

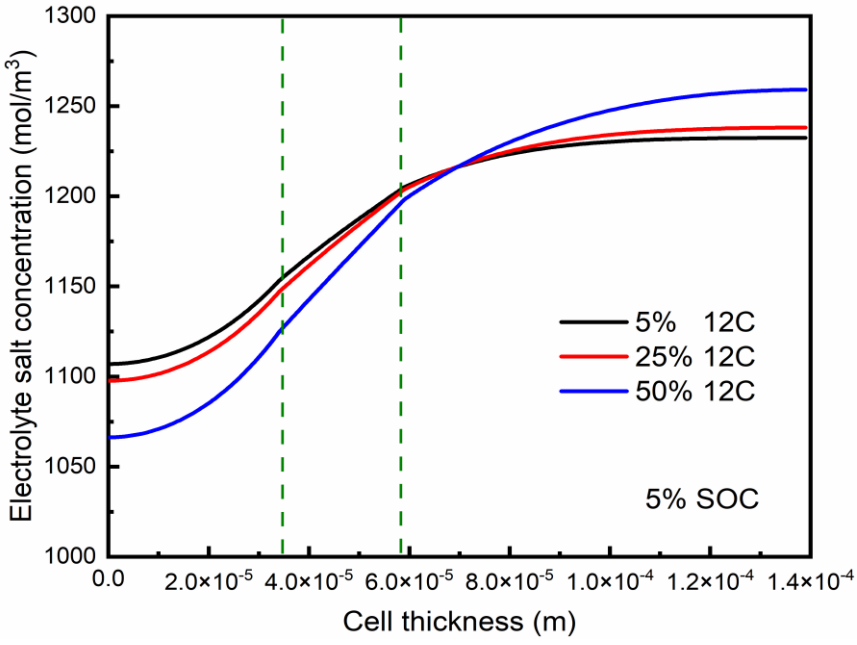

(b)

Figure 4.7: Electrode particle lithium concentration across the cell for different pulse patterns. (a) Same protection capacity ratio but different pulse discharge current rates. (b) Same pulse discharge current rate but different protection capacity ratios. (c) Peak temperature rise in the case b.

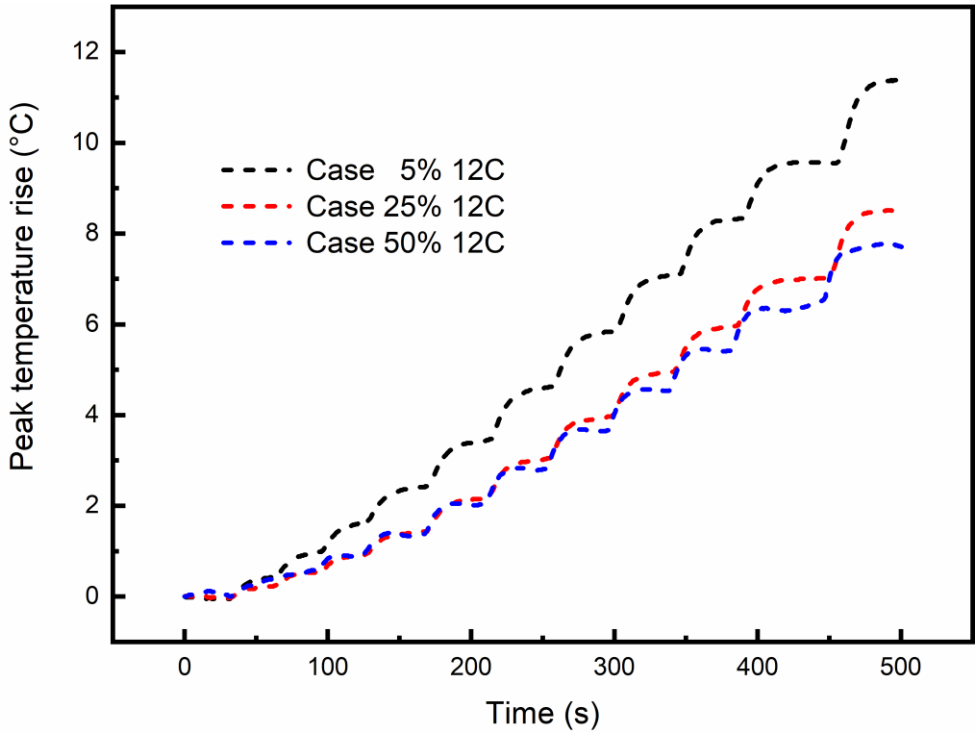

(c)

Figure 4.7: -Continued.

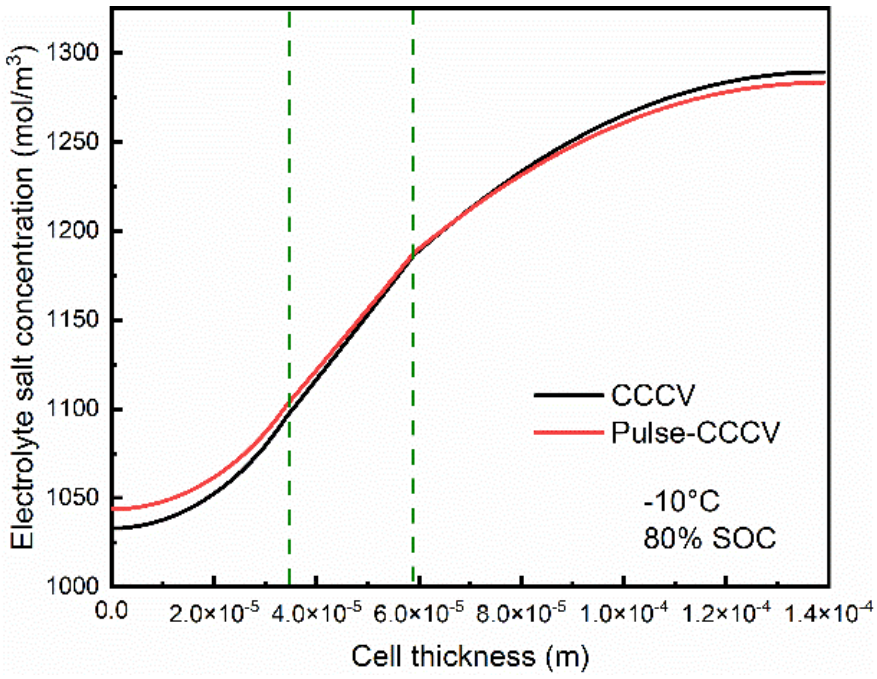

(a)

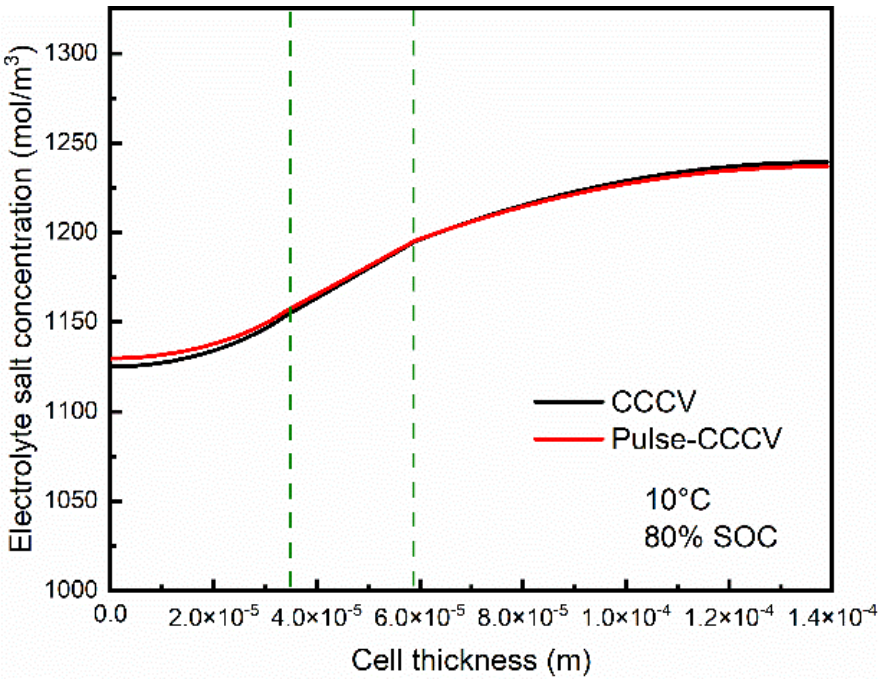

(b)

Figure 4.8: Electrolyte salt concentration across the cell for the optimal pulse pattern (pulse CC-CV) compared with the conventional 1C CC-CV charging pattern at (a) 5% SOC. (b)80% SOC.

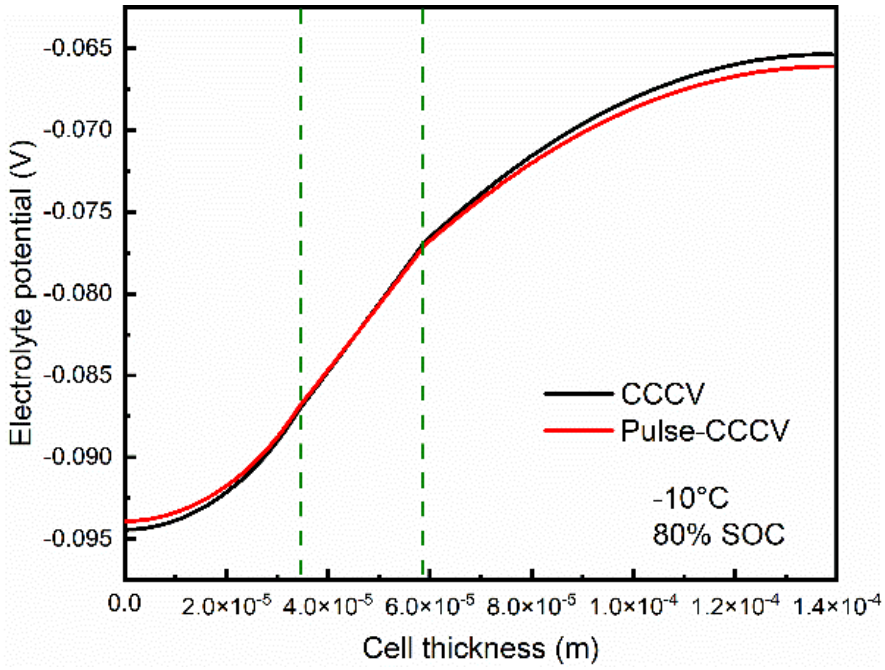

(a)

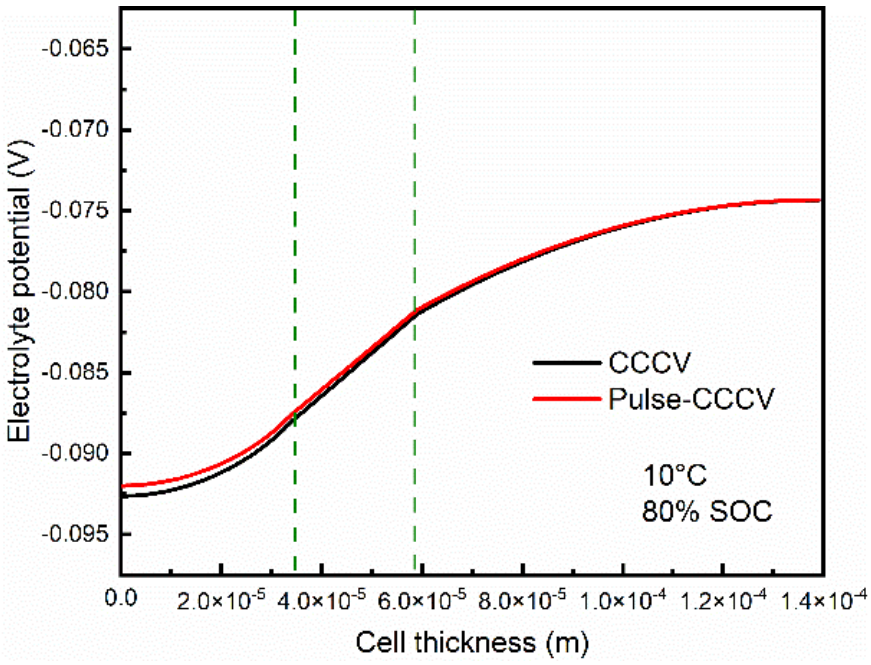

(b)

Figure 4.9: Electrolyte potential across the cell for the optimal pulse pattern (pulse CC-CV) compared with the conventional 1C CC-CV charging pattern (80% SOC) under (a) -10 °C. (b) 10°C.

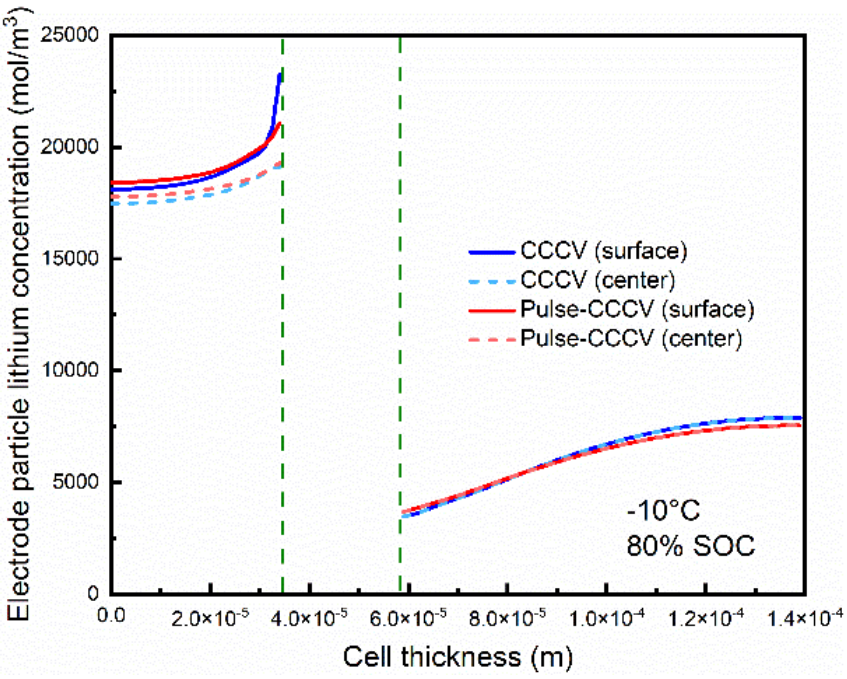

(a)

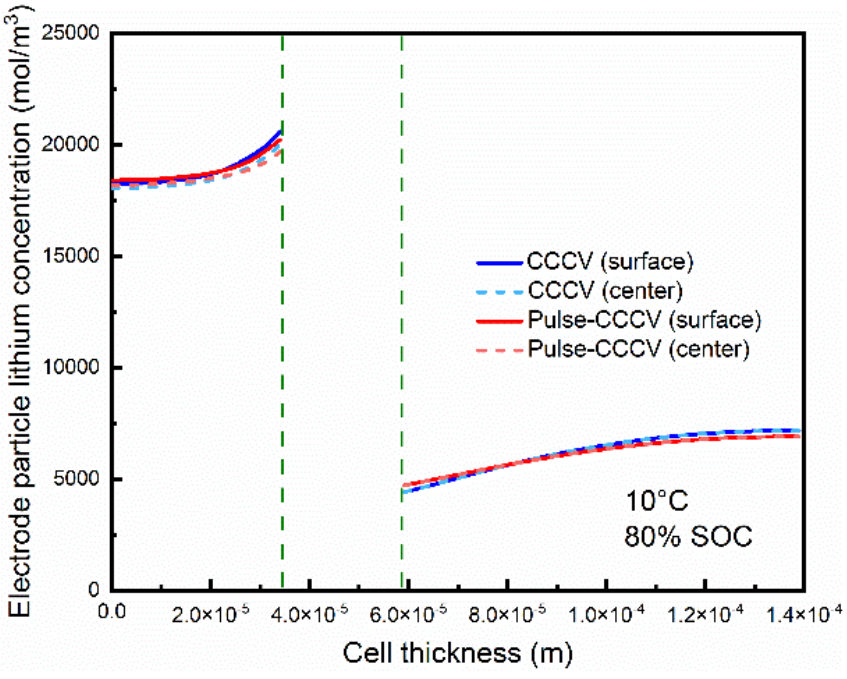

(b)

Figure 4.10: Electrode particle lithium concentration across the cell of the optimal pulse pattern (pulse CC-CV) compared with the conventional 1C CC-CV constant current charging pattern (80% SOC) under (a) -10 °C. (b) 10°C.

4.4.2 Room Temperature Model Results

For the room temperature tests, the three previously studied pulse charging modes (2C/0.5C at 0.05Hz, 2C/0C at 0.05Hz, 2C/-1C at 0.05Hz), are simulated and compared with the baseline 1C CC-CV charging mode.

Figure 4.11(a) presents the electrolyte salt concentration at 10% SOC for the four charging methods: 1C CC-CV, 2C/0.5C at 0.05Hz (C-C pulse mode), 2C/0C at 0.05Hz (C-R pulse mode), and 2C/-1C at 0.05Hz (C-D pulse mode). It is evident that during the charging process, Li-ions are deintercalated from the active material in the positive electrode and migrate toward the negative electrode. Consequently, the electrolyte salt concentration in the positive electrode is higher than that in the negative electrode.

In the pulse charging modes, the process involves the deintercalation of lithium ions from the graphite particles specifically during the pulse discharging stage. This process leads to an increase in the electrolyte salt concentration in the negative electrode. Therefore, compared to the conventional 1C CC-CV mode, the pulse charging modes promote a more uniform electrolyte salt concentration distribution across the two electrodes, thus improving battery performance. According to the model results, the 2C/-1C at 0.05Hz pulse charging pattern (C-D mode) has the most uniform electrolyte salt concentration distribution. This is consistent with the experimental results showing that it has the lowest internal battery resistance, as shown in Figure 3.9.

As SOC increases, at 80% SOC, as shown in Figure 4.11(b), the differences in the electrolyte salt concentration distribution among the four charging modes become more pronounced, but the relative ranking remains unchanged. This is the result of continuous

constant current or pulse charging. These findings further demonstrate that the C-D pulse mode promotes a more uniform distribution of the electrolyte salt concentration within the battery, thereby improving battery performance.

Figure 4.12 shows the lithium concentration within electrode particles at 80% SOC for the four charging methods. The dashed line illustrates the lithium concentration at the particle center. At the beginning of charging, the lithium concentration in the negative electrode is significantly lower than that in the positive electrode. Moreover, the differences in lithium concentration distribution among the four charging modes are minimal during the early stages of charging (such as at 10% SOC). Therefore, we primarily focus on the lithium concentration distribution after the battery is substantially charged under each of the four charging modes.

At 80% SOC, lithium concentration increases at the negative electrode and decreases at the positive electrode. A lithium concentration gradient develops in the negative electrode. This gradient is more pronounced under the conventional baseline 1C CC-CV charging method compared to the pulse-based charging modes (C-C, C-R, C-D). The C-D pulse charging mode using 2C/-1C 0.05Hz shows the smoothest lithium concentration gradient. This indicates that pulse charging methods can effectively reduce the lithium concentration gradient within the negative electrode during the charging process, thereby enhancing the performance of lithium-ion batteries. However, further improving the battery charging performance remains a challenge. Therefore, an optimization section can be introduced for further research.

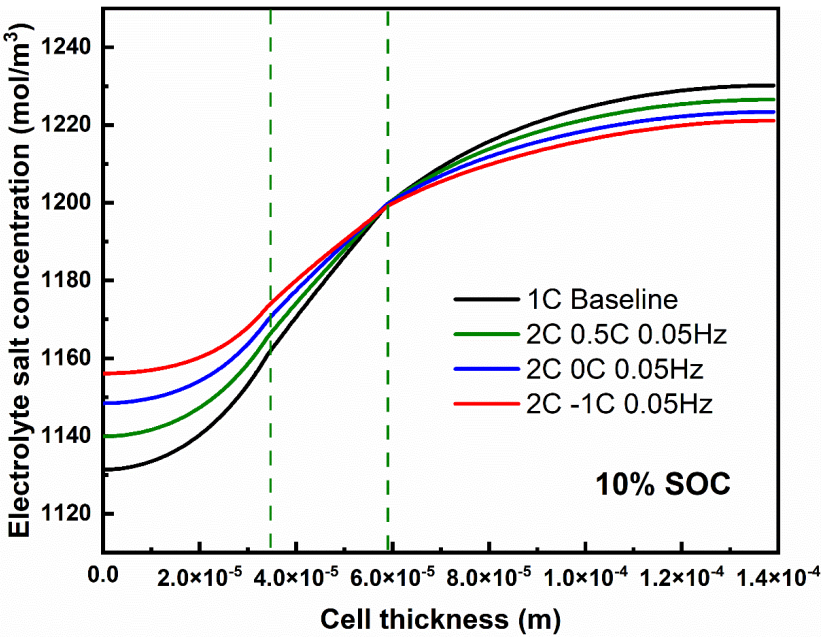

(a)

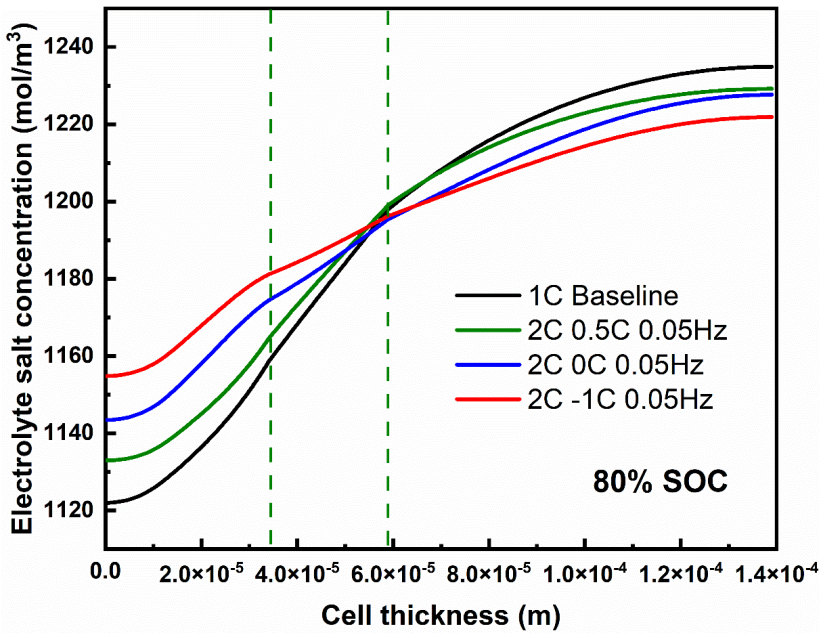

(b)

Figure 4.11: Electrolyte salt concentration across the cell for three different pulse charging patterns (2C/0.5C of C-C Mode, 2C/0C of C-R Mode, 2C/-1C of C-D Mode at 0.05Hz) compared with the conventional 1C CC-CV charging pattern at (a) 10% SOC. (b) 80% SOC.

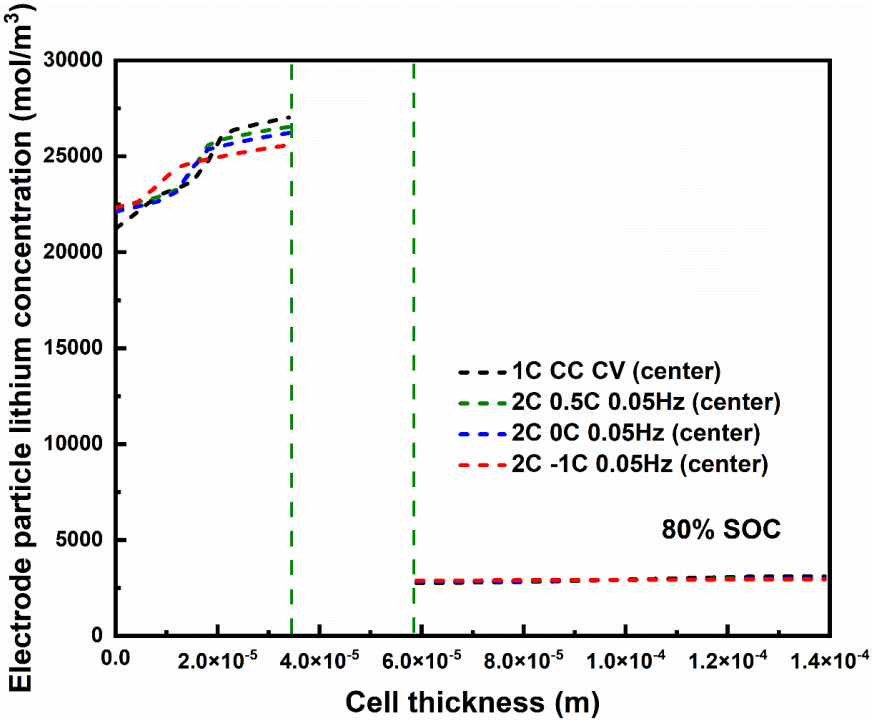

Figure 4.12: Electrode particle lithium concentration across the cell for the three different pulse charging patterns compared with the conventional 1C CC-CV charging pattern at 80% SOC.

4.5 Pulse Charging Optimization

NSGA II [101-103] is an elitist non-dominated sorting genetic algorithm that is widely used in multi-objective optimization applications. It not only employs elite preservation strategies but also explicitly uses diversity preservation techniques. To apply the NSGA II algorithm to optimize the pulse charging strategy, an objective function must be established first, such as maximizing the capacity after charging while minimizing the total charging time. Meanwhile, the optimization method should include constraints, such as limiting the amplitude and duration of the input positive/negative pulse current. After setting the population size to 100 and functional tolerance as 1E-6, an

initial charging mode can be generated. Based on the battery characteristics used in this research, the maximum charging current should be set to be less than 4C, i.e., 10A. The next step is to integrate the electrochemical-thermal model with the optimization process to evaluate each possible charging strategy. Although the model-based simulations provide high accuracy, they require significant computing time. The optimization process is illustrated in the flow chart as shown in Figure 4.13.

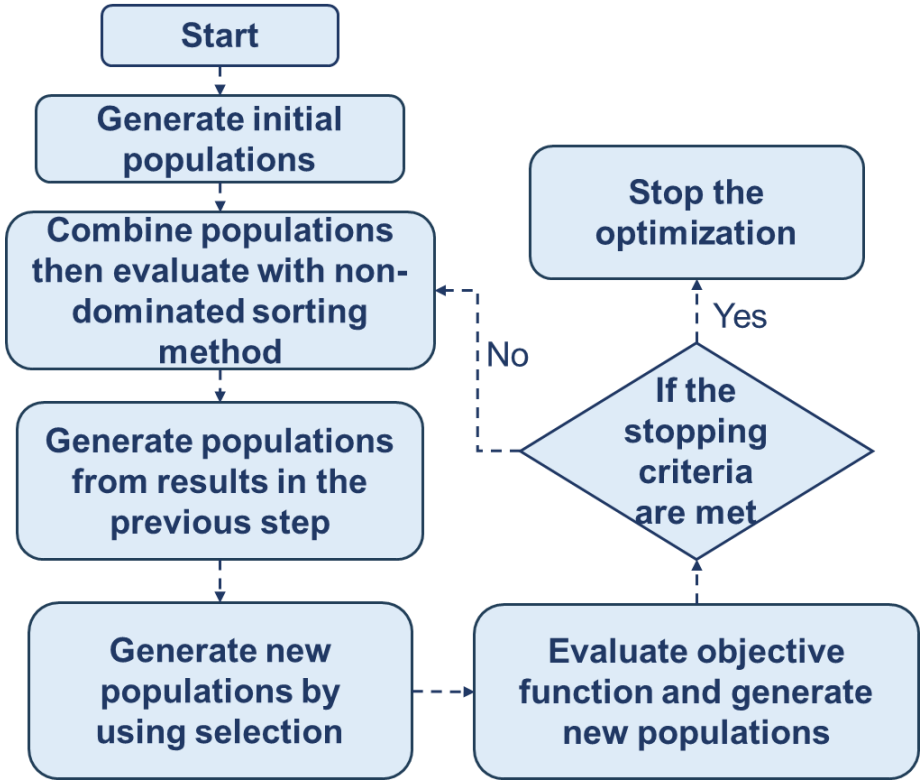

Figure 4.13: Flow chart of the NSGA-II method to find the optimal pulse charging pattern.

4.5.1 Objective Function and Parameters

Based on the results of our previous experiments and model studies, the pulse charging strategy at room temperature is designed to achieve the following goals: shorter charging time (t_{total}), lower temperature rise (ΔT_{max}) and improved charging efficiency (η). To meet these objectives, the pulse strategy is optimized by studying four key pulse parameters: pulse charging current (I_c), pulse discharging current (I_d), pulse charging time (t_c), and pulse discharging time (t_d). Each design factor is denoted by i, which represents the four design parameters in the pulse strategy. Therefore, this optimization problem involves three objectives and four design parameters. Each objective may be constrained and influenced by others, so the following objective equation is proposed to guide the optimization process:

$$Objective\ function = W_1 * t_{total} + W_2 * \Delta T_{max} + W_3 * \eta \quad (4.6)$$

where W_1 through W_3 are weight factors corresponding to respective objectives.

4.5.2 Optimization Constraints

Table 4.2 presents the constraints for the design parameters used in the multi-objective optimization. These constraints are determined based on experience from previous experiments to ensure sufficient pulse charging/discharging time within each single pulse cycle, compatibility with our testing capability, and compliance with battery safety guidelines. The lower limit of the pulse charging current is set to 1.5C, and the upper limit is 4C. The lower limit of the pulse discharging current is set to -4C, and the upper limit is -0.5C, with the negative sign indicating the direction of current flow. The upper and lower limits of the pulse charging time are 18 seconds and 5 seconds,

respectively, while the upper and lower limits of the pulse discharging time are 15 seconds and 5 seconds, respectively. The total charging time is limited to between 30 minutes and 69 minutes. The maximum temperature is set to 38°C, ensuring that the net temperature rise does not exceed 15°C so that the cell remains in a controlled temperature environment. The lower limit for charging capacity is set to 2.0Ah, which means that the battery must be charged to 80% of its capacity. The lower limit of charging efficiency is 90% and the upper limit is 100%, ensuring effective energy use during charging. Finally, the low voltage boundary of the lithium iron phosphate battery is 2V and the high voltage boundary is 3.6V. These limits are imposed to prevent the battery from being over-discharged or over-charged, which can accelerate battery degradation or lead to safety issues.

Table 4.2. Summary of constraints for different parameters.

Parameter	Symbol	Constraint
Pulse charging current (C)	I_c	$1.5 \leq I_c \leq 4$
Pulse discharging current (C)	I_d	$-4 \leq I_d \leq -0.5$
Pulse charging time (s)	t_c	$5 \leq t_c \leq 18$
Pulse discharging time (s)	t_d	$5 \leq t_d \leq 15$
Total charging time (min)	t_{total}	$30 \leq t_{total} \leq 69$
Maximum temperature rise (°C)	ΔT_{max}	$0 \leq \Delta T_{max} \leq 15$
Charging capacity (Ah)	C_{charge}	$2.0 \leq C_{charge} \leq 2.55$
Charge efficiency (%)	η	$90\% \leq \eta \leq 100\%$
Cell Voltage (V)	V	$2 \leq V \leq 3.6$

In addition, it is worth mentioning that, based on previous experimental and simulation results, the optimization model is built on the pulsed C-D mode at room temperature with a frequency of 0.05 Hz. Therefore, two major constraint formulas are applied:

$$I_c * T_c - I_d * T_d - 1C * 20s = 0 \tag{4.7}$$

$$T_c + T_d - 20s = 0 \tag{4.8}$$

Equation 4.7 ensures that the average current input across different pulse design parameter combinations is 1C, which provides a fair basis for comparing various pulse charging modes with the conventional 1C CC-CV charging mode. Equation 4.8 constrains each individual pulse cycle duration to 20 seconds, corresponding to a fixed frequency of 0.05Hz.

4.5.3 Optimization Results

Table 4.3 lists the simulation and experimental results from the multi-objective optimization. Due to the applied constraints, once the pulse charge and discharge current amplitudes are determined, the corresponding pulse charge and discharge times are also fixed. Setting W_1 through W_3 to 1, that is, assigning highest weight factor to each objective, produces three pulse parameter combinations, corresponding to the shortest charging time, the smallest temperature rise and the highest charging efficiency. Their respective pulse modes are 4C/-4C at 0.05Hz, 1.5C/-0.5C at 0.05Hz and 2.4C/-3.2C at 0.05Hz. If the weight factors are evenly distributed and a balanced multi-objective optimization is sought, the resulting pulse charging mode is 2.2C/-1.2C at 0.05Hz.

Table 4.3. Summary of simulation & experimental results for different weight factors

Case	Weight factors			Parameter combination	Total charging time (min)		Maximum temperature rise (°C)		Charging efficiency (%)	
					Sim	Exp	Sim	Exp	Sim	Exp
1	1	0	0	4C/-4C	60.7	61.1	5.8	6.46	99.4%	99.51%
2	0	1	0	1.5C/-0.5C	63.8	64.7	2.2	2.55	99.4%	99.59%
3	0	0	1	2.4C/-3.2C	63.6	64.3	3.3	3.59	99.9%	99.84%
4	1/3	1/3	1/3	2.2C/-1.2C	62.5	63	2.5	2.77	99.7%	99.75%
5				1C	66.9	67.6	2.7	3.01	99.3%	99.38%

Figure 4.14(a), (b), (c) show the comparison between the model and experimental results for charging time, maximum temperature rise, and charging efficiency, respectively, across different pulse modes and CC-CV modes. Experiments were conducted to verify the simulation data, and the two trends are consistent with the experimental results closely matching the simulation results.

From the numerical simulation results shown in Figure 4.14 and Table 4.3, the shortest charging time is reduced by nearly 9.2% compared to the CC-CV charging mode, but at the cost of a higher temperature rise. The lowest observed temperature rise is 18.5% lower than that of the CC-CV charging mode, and the highest single charging efficiency improves by about 0.6%. When the weight factor is evenly distributed, the resulting pulse charging combination is 2.2C/-1.2C at 0.05Hz. Compared to the CC-CV charging mode, this balanced pulse strategy reduces charging time by 6.5%, lowers

temperature rise by 7.4% and increases charging efficiency by 0.4% in a single charging process.

Figure 4.15 summarizes the experimental results of different pulse charging modes compared with the CC-CV charging mode. The 4C/-4C at 0.05Hz pulse charging mode reduces the total charging time by nearly 9.8%, but results in a higher temperature rise compared to the CC-CV mode. The 1.5C/-0.5C at 0.05Hz pulse charging mode lowers the total temperature rise by 15%, but the charging efficiency is not significantly improved. The 2.4C/-3.2C at 0.05Hz shows higher charging efficiency but cannot effectively control the slightly higher temperature rise. In contrast, the 2.2C/-1.2C at 0.05Hz pulse charging mode achieves balanced performance: it reduces charging time by 6.8%, lowers temperature rise by 8.0%, and improves charging efficiency 0.37% in a single charging process compared to the CC-CV charging mode. These results are consistent with those obtained by numerical simulation presented in Table 4.3 and Figure 4.14.

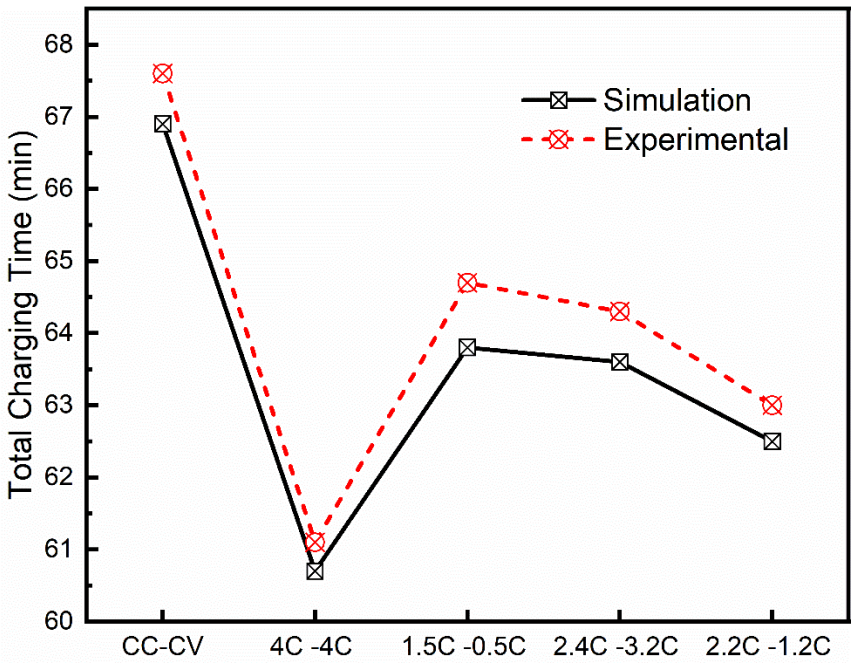

(a)

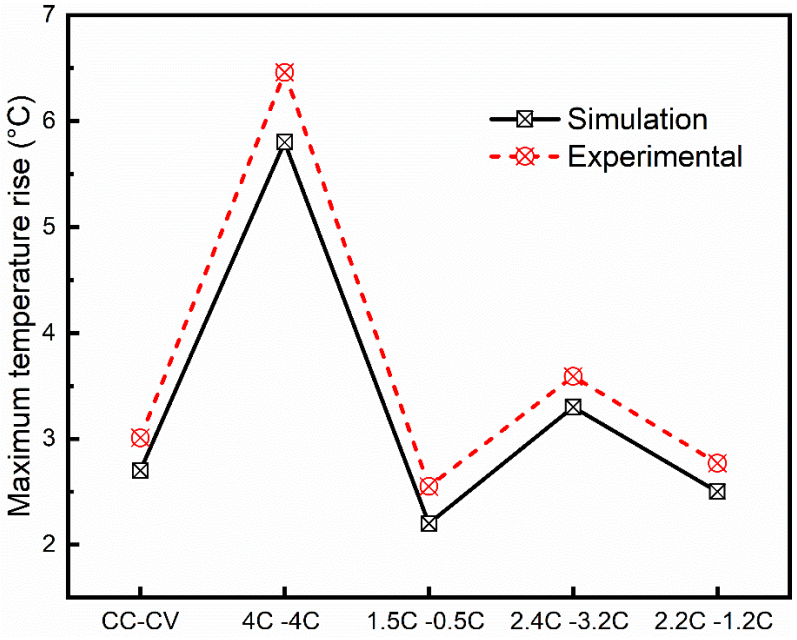

(b)

Figure 4.14: Simulation and experimental results for pulse charging patterns (4C/-4C, 1.5C/-0.5C, 2.4C/-3.2C, and 2.2C/-1.2C of C-D Mode at 0.05Hz) compared with the conventional 1C CC-CV charging pattern. (a) Total charging time. (b) Maximum temperature rise. (c) Charging efficiency.

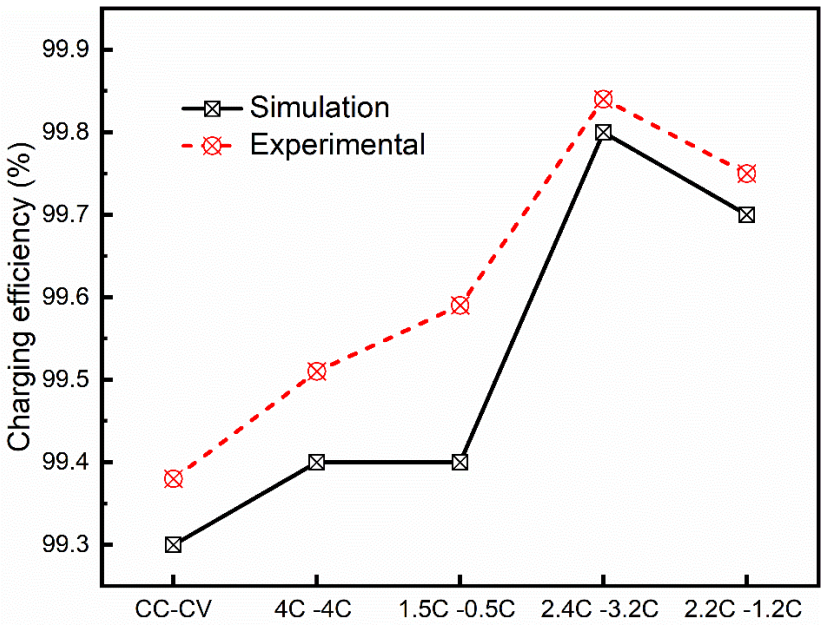

(c)

Figure 4.14: -Continued.

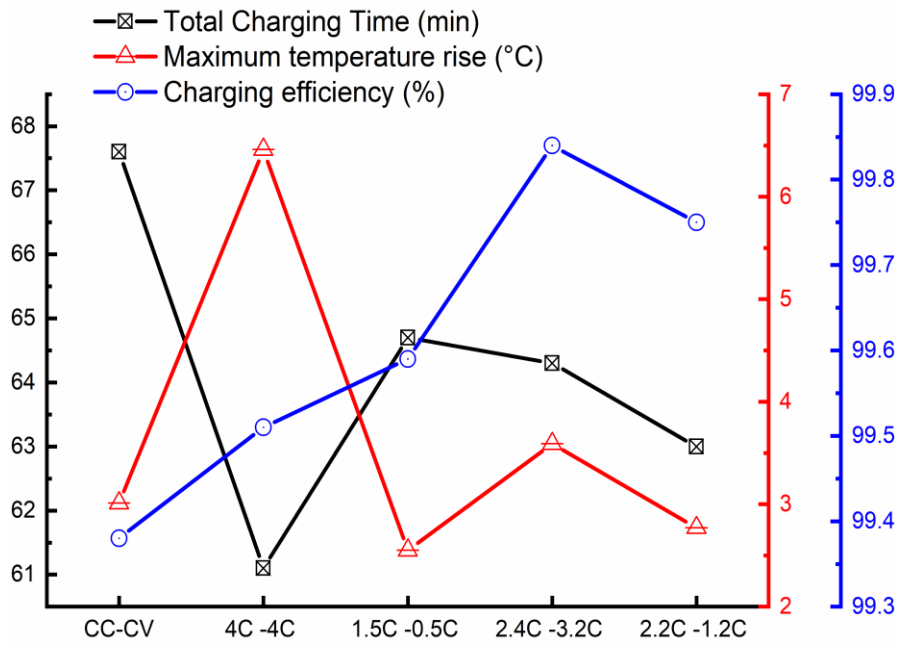

Figure 4.15: Experimental results for pulse charging patterns (4C/-4C, 1.5C/-0.5C, 2.4C/-3.2C, and 2.2C/-1.2C of C-D Mode at 0.05Hz) compared with the conventional 1C CC-CV charging pattern with three different objectives.

CHAPTER FIVE

CONCLUSIONS AND FUTURE WORK

5.1 Conclusions

This dissertation combines experimental research with physics-based numerical simulations to study the impact of pulse charging strategies on the performance of lithium-ion batteries. It also investigates how these pulse charging strategies affect charging time, resistance change and cycle life of lithium-ion batteries at different temperatures. It is crucial to understand the parameters and modes of pulse charging strategies, as they significantly affect the performance, safety and various applications of lithium-ion batteries.

This research first studies the pulse charging strategy at low ambient temperatures, with the objective of quickly increasing temperature rise and shortening charging time. Preliminary experiments determine that the preheating period consists of 11 pulse cycles. To explore the influence of pulse parameters on the low-temperature charging performance, a Taguchi design is used for experimental design and data analysis. The optimal combination of pulse charging parameters is identified as a 25% protection capacity ratio and a 12C pulse discharge current rate. The protection capacity ratio is an innovative design parameter that ensures that the battery is not over-discharged during the test. Based on the results from two battery samples, the pulse charging mode using these optimal parameters reduces charging time by about 11% compared to the conventional CC-CV charging mode.

Second, this study further investigates the effects of pulse charging strategies on the performance of lithium-ion batteries at room temperature. Three basic pulse modes are introduced and defined as C-C, C-R and C-D pulse charging modes. Based on preliminary experiments with different battery types, the pulse frequency range for room temperature experiments is determined to between 0.025Hz and 1Hz. Under the condition of equal average current (1C), both LFP and NMC batteries show shorter charging times in the 2C C-R mode compared to the conventional CC-CV charging mode. A Taguchi design and analysis are conducted for the C-R mode. It is observed that the input current should not exceed the 3-4 C range, as higher input pulse currents reduce the influence of pulse frequency. For the C-C and C-D modes, regardless of whether the pulse durations T_1 and T_2 are equal, most pulse charging modes reduce charging time compared to CC-CV charging while maintaining the same average input current.

Third, in the subsequent internal resistance test, the C-D (2C/-1C) pulse charging mode reduces the internal resistance by an average of 14.5% compared to the CC-CV mode. Even under low temperature conditions (0°C), at the end of charging (80% SOC - 90% SOC), the C-D pulse charging mode reduces the battery's internal resistance by more than 30% compared to CC-CV charging. These results demonstrate that pulse charging improves the charging performance of lithium-ion batteries. In addition, in the cycle life test, the pulse charging mode greatly alleviates battery degradation after 800 cycles when compared to the CC-CV charging mode.

Fourth, a P2D electrochemical-thermal model was developed to explore the mechanism of pulse charging. Simulation results at both low and room temperatures

show that the pulse charging method leads to a more uniform electrolyte salt concentration and a flatter lithium concentration distribution at both low SOC and high SOC. At low temperature, the pulse charging mode improves concentration uniformity through the combined effects of ionic shuttling and heat generation. At room temperature, the improvement is mainly attributed to the shuttling effect. These uniform distribution at different temperatures further illustrates the positive impact of pulse charging on battery charging performance.

Finally, pulse parameters are optimized by the NSGA-II method. Under consistent average current, the optimized pulse charging process reduces the charging time by 6.8%, lowers the temperature rise by 8.0%, and improves the charging efficiency by 0.37% in a single charging cycle compared to the conventional constant current and constant voltage charging mode at room temperature.

In conclusion, this dissertation helps to deepen understanding of design and mechanism of pulse charging strategies for lithium-ion batteries and provides a solid foundation for future research in this area.

5.2 Future Work

The experimental and theoretical methods proposed in this study for pulse charging need to be further extended and improved in the future. On the experimental side, additional studies can be conducted to explore pulse modes, pulse stage positions, and pulse strategies based on fast charging. For numerical models, the aging mechanism and degradation behavior of lithium-ion batteries should be further considered in pulse charging simulations. In addition, for the multi-objective optimization strategy of pulse

charging, a real-time dynamic combination of pulse parameter changes should be considered.

1. Study pulse modes and pulse stage positions. This study proposed and defined three basic pulse modes, namely C-C, C-R, and C-D. New pulse modes are also worth in-depth investigation. For example, the pulse mode "C-R-D-R", that is, the stages of pulse charge-rest-pulse discharge-rest are carried out in sequence. This new mode is a derivative of the C-D mode. Will adding a rest stage better eliminate battery polarization? With such questions, more pulse modes can be explored and studied. According to the findings in this study, battery's internal resistance generally increases at the later charging stage (High SOC). Applying pulse charging under only during high SOC conditions is worth studying. In other words, it is critical to study when and where to apply pulse charging in the battery charging process.
2. Pulse strategies based on fast charging. Fast charging generally charges the battery with an extremely high current, usually in a constant current mode. This study uses 1C as the average input current. It is worth investigating whether increasing the average input current to 1.5C, 2C or even 4C would allow the pulse charging strategy to produce the same improvement effects. Under the average input currents of 1.5C and 2C, it has been measured that the C-R and C-D modes can increase the battery charging speed by about 4.6% and 5%, respectively. However, due to the current limitation of the experimental instrument, further testing with higher average input currents is

not currently possible. Therefore, whether fast charging with pulse charging can improve battery performance, shorten charging time and slow down aging remains a question worthy of further studying.

3. Aging mechanism and degradation model of lithium-ion batteries. In the long-cycle charge and discharge experiment, this research completed 800 cycles. However, additional cycles are needed to more thoroughly verify the lithium-ion battery aging model. The aging model is crucial for studying the degradation mechanism and principle of lithium-ion batteries, so this work can be further improved in future research.
4. AI-driven intelligent pulse charging system. This study achieved multi-objective optimization by optimizing the combination of pulse parameters, but there are still some limitations. For further research, real-time optimization could be applied to determine the appropriate pulse parameter combination based on the changes of the battery's SOC and SOH. A reinforced machine learning framework can be used to achieve self-evolution of pulse charging strategies.

The completion of these proposed topics will greatly help advance understanding of the impact of pulse charging on the performance of lithium-ion batteries, observe their complex internal transfer processes and charging changes through models, and potentially incorporate more accurate pulse parameters and experimental phenomena into physics-based lithium-ion battery models, which will have a positive impact on pulse charging optimization.

APPENDICES

Table A.1. Model parameters for lithium-ion battery electrochemical-thermal model

Parameter	Symbol	Unit	Negative Electrode	Separator	Positive Electrode
Electrode thickness	δ	μm	34 [111]	25 [111]	80 [111]
Particle radius	R_s	μm	8.8 [e]	-	1.15 [e]
Volume fraction of solid phase	ε_s	-	0.593 [e]	0.55 [e]	0.354 [e]
Volume fraction of electrolyte (Porosity)	ε_l	-	0.387 [e]	0.45 [e]	0.593 [e]
Initial Li concentration in solid	$c_{s,0}$	$mol \cdot m^{-3}$	16000 [e]	-	471 [e]
Initial Li concentration in electrolyte	$c_{l,0}$	$mol \cdot m^{-3}$	1193[e]		
Li diffusion coefficient in solid	D_s	$m^2 \cdot s^{-1}$	$1.6 \times 10^{-14}(1.5 - x)^{3.5}$[111] where x=SOC		1.25×10^{-15}[111]
Li diffusion coefficient in electrolyte	D_l	$m^2 \cdot s^{-1}$	1.5×10^{-6} [112]		
Bruggeman tortuosity exponent	β	-	1.5 [111]	1.5 [111]	1.5 [111]
Electronic conductivity in solid	σ_s	$S \cdot m^{-1}$	100 [e]	-	3.8 [e]
Ionic conductivity	κ_l	$S \cdot m^{-1}$	$\kappa_l(c_l) = 8e^{-11}{c_l}^3 - 4e^{-7}{c_l}^2 + 0.0006c_l + 0.0151$		
Transference number	t_+	-	0.363		
Charge-transfer coefficient	α_a, α_c	-	0.5[113]	-	0.5[113]

Table A.1.-Continued

Parameter	Symbol	Unit	Negative Electrode	Separator	Positive Electrode
Gas constant	R	$J \cdot mol^{-1}K^{-1}$	8.314		
Faraday constant	F	$C \cdot mol^{-1}$	96485		
Applied current density at 1C	$i_{app,1C}$	$A \cdot m^{-2}$	11.4[e]		
Cell density	ρ	$Kg \cdot m^{-3}$	2047 [m]		
Reference temperature	T_{ref}	K	298.15		
Thermal conductivity	λ	$W \cdot m^{-1}K^{-1}$	0.35		
Heat transfer coefficient	h	$W \cdot m^{-2}K^{-1}$	21 [f]		
Heat capacity	c_p	$J \cdot Kg^{-1}K^{-1}$	1110		

e-estimated; m-measured; f-fitted to experimental data.

REFERENCES

[1] https://investmentpolicy.unctad.org/investment-policy-monitor/measures/4004/-369-billion-in-investment-incentives-to-address-energy-security-and-climate-change-/

[2] https://news.gm.com/home.detail.html/Pages/news/us/en/2025/jul/0714-Ultium-Cells-upgrade-Tennessee-plant-low-cost-EV-battery-cell-production.html

[3] https://www.fromtheroad.ford.com/us/en/articles/2025/ford-owned-american-battery-plant-future-electric-vehicles

[4] Masiero, Gilmar, et al. "Electric vehicles in China: BYD strategies and government subsidies." RAI Revista de Administração e Inovação 13.1 (2016): 3-11.

[5] https://electrek.co/2024/06/06/catl-dominates-ev-battery-market-but-byd-gains-ground/

[6] https://uscar.org/battery/usabc-awards-2-6-million-lithium-electrode-based-cell-development-and-manufacturing-contract-to-farasis-energy-usa/

[7] Reddy, Thomas B., and David Linden. "Linden's handbook of batteries." (2011).

[8] Fergus, Jeffrey W. "Recent developments in cathode materials for lithium ion batteries." Journal of power sources 195.4 (2010): 939-954.

[9] Liu, Chaofeng, Zachary G. Neale, and Guozhong Cao. "Understanding electrochemical potentials of cathode materials in rechargeable batteries." Materials Today 19.2 (2016): 109-123.

[10] Nitta, Naoki, et al. "Li-ion battery materials: present and future." Materials today 18.5 (2015): 252-264.

[11] Kam, Kinson C., and Marca M. Doeff. "Electrode materials for lithium ion batteries." Material Matters 7.4 (2012): 56-60.

[12] Endo, M., et al. "Recent development of carbon materials for Li ion batteries." Carbon 38.2 (2000): 183-197.

[13] Jin, Bo, et al. "Effect of different carbon conductive additives on electrochemical properties of LiFePO 4-C/Li batteries." Journal of solid state electrochemistry 12 (2008): 1549-1554.

[14] Zhu, Yizhou, Xingfeng He, and Yifei Mo. "Strategies based on nitride materials chemistry to stabilize Li metal anode." Advanced Science 4.8 (2017): 1600517.

[15] Basile, Andrew, A. I. Bhatt, and A. P. O'mullane. "Stabilizing lithium metal using ionic liquids for long-lived batteries." Nature communications 7.1 (2016): ncomms11794.

[16] Ishikawa, Masashi, et al. "Pretreatment of Li metal anode with electrolyte additive for enhancing Li cyclability." Journal of power sources 146.1-2 (2005): 199-203.

[17] Younesi, Reza, et al. "Lithium salts for advanced lithium batteries: Li–metal, Li–O 2, and Li–S." Energy & Environmental Science 8.7 (2015): 1905-1922.

[18] Sakuda, Atsushi, Akitoshi Hayashi, and Masahiro Tatsumisago. "Sulfide solid electrolyte with favorable mechanical property for all-solid-state lithium battery." Scientific reports 3.1 (2013): 2261.

[19] Reddy, Thomas B., and David Linden. "Linden's handbook of batteries." (Chapter 14) (2011).

[20] Heiskanen, Satu Kristiina, Jongjung Kim, and Brett L. Lucht. "Generation and evolution of the solid electrolyte interphase of lithium-ion batteries." Joule 3.10 (2019): 2322-2333.

[21] Adenusi, Henry, et al. "Lithium batteries and the solid electrolyte interphase (SEI)—progress and outlook." Advanced Energy Materials 13.10 (2023): 2203307.

[22] Lin, Xianke, et al. "Lithium plating mechanism, detection, and mitigation in lithium-ion batteries." Progress in Energy and Combustion Science 87 (2021): 100953.

[23] Petzl, Mathias, Michael Kasper, and Michael A. Danzer. "Lithium plating in a commercial lithium-ion battery–A low-temperature aging study." Journal of power sources 275 (2015): 799-807.

[24] You, Heze, et al. "Charging strategy optimization at low temperatures for li-ion batteries based on multi-factor coupling aging model." IEEE Transactions on Vehicular Technology 70.11 (2021): 11433-11445.

[25] Nambisan, Praveen, Pankaj Saha, and Munmun Khanra. "Real-time optimal fast charging of Li-ion batteries with varying temperature and charging behaviour constraints." Journal of Energy Storage 41 (2021): 102918.

[26] Cope, Richard C., and Yury Podrazhansky. "The art of battery charging." In Battery Conference on Applications and Advances, 1999. The Fourteenth Annual, pp. 233-235.

[27] Notten, Peter HL, JHG Op het Veld, and J. R. G. Van Beek. "Boostcharging Li-ion batteries: A challenging new charging concept." Journal of Power Sources 145.1 (2005): 89-94.

[28] Keil, Peter, and Andreas Jossen. "Charging protocols for lithium-ion batteries and their impact on cycle life—An experimental study with different 18650 high-power cells." Journal of Energy Storage 6 (2016): 125-141.

[29] Waldmann, Thomas, Michael Kasper, and Margret Wohlfahrt-Mehrens. "Optimization of charging strategy by prevention of lithium deposition on anodes in high-energy lithium-ion batteries–electrochemical experiments." Electrochimica Acta 178 (2015): 525-532.

[30] Spingler, Franz B., et al. "Optimum fast charging of lithium-ion pouch cells based on local volume expansion criteria." Journal of Power Sources 393 (2018): 152-160.

[31] Huang, Xinrong. "The effects of pulsed charging current on the performance and lifetime of lithium-ion batteries." (2021).

[32] Dotoli, Matteo, et al. "Development of an Innovative Procedure for Lithium Plating Limitation and Characterization of 18650 Cycle Aged Cells for DCFC Automotive Applications." Batteries 8.8 (2022): 88.

[33] Anseán, David, et al. "Fast charging technique for high power lithium iron phosphate batteries: A cycle life analysis." Journal of Power Sources 239 (2013): 9-15.

[34] Abdel-Monem, Mohamed, et al. "Influence analysis of static and dynamic fast-charging current profiles on ageing performance of commercial lithium-ion batteries." Energy 120 (2017): 179-191.

[35] Zhang, Sheng Shui. "The effect of the charging protocol on the cycle life of a Li-ion battery." Journal of power sources 161.2 (2006): 1385-1391.

[36] Jiang, Li, et al. "Optimization of multi-stage constant current charging pattern based on Taguchi method for Li-Ion battery." Applied Energy 259 (2020): 114148.

[37] Lee, Chien-Hsing, et al. "Taguchi-based PSO for searching an optimal four-stage charge pattern of Li-ion batteries." Journal of Energy Storage 21 (2019): 301-309.

[38] Wu, Xiaogang, et al. "Multistage Constant Current Charging Strategy Based on Multiobjective Current Optimization." IEEE Transactions on Transportation Electrification 9.4 (2022): 4990-5001.

[39] Kannan, Dhevathi Rajan Rajagopalan, and Mark H. Weatherspoon. "The effect of pulse charging on commercial lithium nickel cobalt oxide (NMC) cathode lithium-ion batteries." Journal of Power Sources 479 (2020): 229085.

[40] Amanor-Boadu, J. M., Anthony Guiseppi-Elie, and E. Sánchez-Sinencio. "The impact of pulse charging parameters on the life cycle of lithium-ion polymer batteries." Energies 11.8 (2018): 2162.

[41] Huang, Xinrong, et al. "Effect of pulsed current on charging performance of lithium-ion batteries." IEEE Transactions on Industrial Electronics 69.10 (2021): 10144-10153.

[42] Li, Jun, et al. "The effects of pulse charging on cycling characteristics of commercial lithium-ion batteries." Journal of Power Sources 102.1-2 (2001): 302-309.

[43] Savoye, François, et al. "Impact of periodic current pulses on Li-ion battery performance." IEEE Transactions on Industrial Electronics 59.9 (2011): 3481-3488.

[44] Lee, Yong-Duk, and Sung-Yeul Park. "Electrochemical state-based sinusoidal ripple current charging control." IEEE Transactions on Power Electronics 30.8 (2014): 4232-4243.

[45] Wang, Fu-Ming, et al. "Differential pulse effects of solid electrolyte interface formation for improving performance on high-power lithium ion battery." Journal of Power Sources 196.23 (2011): 10395-10400.

[46] Brand, Martin Johannes, et al. "The influence of current ripples on the lifetime of lithium-ion batteries." IEEE Transactions on Vehicular Technology 67.11 (2018): 10438-10445.

[47] Lv, Haichao, Xiankun Huang, and Yongzhong Liu. "Analysis on pulse charging–discharging strategies for improving capacity retention rates of lithium-ion batteries." Ionics 26 (2020): 1749-1770.

[48] Uno, Masatoshi, and Koji Tanaka. "Influence of high-frequency charge–discharge cycling induced by cell voltage equalizers on the life performance of lithium-ion cells." IEEE Transactions on vehicular technology 60.4 (2011): 1505-1515.

[49] Huang, Xinrong, et al. "A review of pulsed current technique for lithium-ion batteries." Energies 13.10 (2020): 2458.

[50] Liu, Jiahao, and Xia Wang. "Investigating effects of pulse charging on performance of Li-ion batteries at low temperature." Journal of Power Sources 574 (2023): 233177.

[51] Zhu, Jiangong, et al. "Experimental investigations of an AC pulse heating method for vehicular high power lithium-ion batteries at subzero temperatures." Journal of power sources 367 (2017): 145-157.

[52] Wang, Chao-Yang, et al. "A fast rechargeable lithium-ion battery at subfreezing temperatures." Journal of The Electrochemical Society 163.9 (2016): A1944.

[53] Ji, Dengyue, et al. "Research on adaptability of charging strategy for electric vehicle power battery." Journal of Power Sources 437 (2019): 226911.

[54] Yang, Heng, et al. "Effects of pulse plating on lithium electrodeposition, morphology and cycling efficiency." Journal of Power Sources 272 (2014): 900-908.

[55] García, Grecia, et al. "Exceeding 6500 cycles for LiFePO 4/Li metal batteries through understanding pulsed charging protocols." Journal of Materials Chemistry A 6.11 (2018): 4746-4751.

[56] Wang, Fu-Ming, et al. "Differential pulse effects of solid electrolyte interface formation for improving performance on high-power lithium ion battery." Journal of Power Sources 196.23 (2011): 10395-10400.

[57] Zhu, Shaoqing, et al. "Performance improvement of lithium-ion battery by pulse current." Journal of Energy Chemistry 46 (2020): 208-214.

[58] Amanor-Boadu, Judy M., and Anthony Guiseppi-Elie. "Improved performance of Li-ion polymer batteries through improved pulse charging algorithm." Applied Sciences 10.3 (2020): 895.

[59] Monem, Mohamed Abdel, et al. "Lithium-ion batteries: Evaluation study of different charging methodologies based on aging process." Applied Energy 152 (2015): 143-155.

[60] Vermeer, Wiljan, et al. "A critical review on the effects of pulse charging of li-ion batteries." 2021 IEEE 19th International Power Electronics and Motion Control Conference (PEMC). IEEE (2021): 217-224.

[61] He, Hongwen, Rui Xiong, and Jinxin Fan. "Evaluation of lithium-ion battery equivalent circuit models for state of charge estimation by an experimental approach." energies 4.4 (2011): 582-598.

[62] Thele, Marc, et al. "Development of a voltage-behavior model for NiMH batteries using an impedance-based modeling concept." Journal of Power Sources 175.1 (2008): 635-643.

[63] Johnson, V. H. "Battery performance models in ADVISOR." Journal of power sources 110.2 (2002): 321-329.

[64] Park, Myounggu, et al. "A review of conduction phenomena in Li-ion batteries." Journal of power sources 195.24 (2010): 7904-7929.

[65] Plett, Gregory L. "Extended Kalman filtering for battery management systems of LiPB-based HEV battery packs: Part 3. State and parameter estimation." Journal of Power sources 134.2 (2004): 277-292.

[66] Gibson, Andrew, et al. "The potential and challenge of turboelectric propulsion for subsonic transport aircraft." 48th AIAA Aerospace Sciences Meeting Including the New Horizons Forum and Aerospace Exposition. 2010.

[67] Boston Consulting Group. "Batteries for Electric Cars. Challenges, Opportunities, and the Outlook to 2020." BCG Report (2010).

[68] EIA, US. "Annual Energy Review-Energy Information Administration." Annual Energy Review (2011).

[69] Hu, Yiran, et al. "Electro-thermal battery model identification for automotive applications." Journal of Power Sources 196.1 (2011): 449-457.

[70] Verbrugge, Mark, and Edward Tate. "Adaptive state of charge algorithm for nickel metal hydride batteries including hysteresis phenomena." Journal of Power Sources 126.1-2 (2004): 236-249.

[71] Andre, D., et al. "Characterization of high-power lithium-ion batteries by electrochemical impedance spectroscopy. I. Experimental investigation." Journal of Power Sources 196.12 (2011): 5334-5341.

[72] Dubarry, Matthieu, and Bor Yann Liaw. "Development of a universal modeling tool for rechargeable lithium batteries." Journal of Power Sources 174.2 (2007): 856-860.

[73] Hu, Xiaosong, Shengbo Li, and Huei Peng. "A comparative study of equivalent circuit models for Li-ion batteries." Journal of Power Sources 198 (2012): 359-367.

[74] Tang, Aihua, et al. "Research on pulse charging current of lithium-ion batteries for electric vehicles in low-temperature environment." Energy Reports 9 (2023): 1447-1457.

[75] Ramadesigan, Venkatasailanathan, et al. "Modeling and simulation of lithium-ion batteries from a systems engineering perspective." Journal of the electrochemical society 159.3 (2012): R31.

[76] Nagarajan, Gowri S., J. W. Van Zee, and R. M. Spotnitz. "A Mathematical Model for Intercalation Electrode Behavior: I. Effect of Particle-Size Distribution on Discharge Capacity." Journal of the Electrochemical Society 145.3 (1998): 771.

[77] Soetens, Jean-Christophe, Claude Millot, and Bernard Maigret. "Molecular dynamics simulation of Li+ BF4-in ethylene carbonate, propylene carbonate, and dimethyl carbonate solvents." The Journal of Physical Chemistry A 102.7 (1998): 1055-1061.

[78] Fuller, Thomas F., Marc Doyle, and John Newman. "Relaxation phenomena in lithium-ion-insertion cells." Journal of the Electrochemical Society 141.4 (1994): 982.

[79] West, Keld, Torben Jacobsen, and Sven Atlung. "Modeling of porous insertion electrodes with liquid electrolyte." Journal of The Electrochemical Society 129.7 (1982): 1480.

[80] Mao, Z., and Ralph E. White. "A model for the deliverable capacity of the TiS2 electrode in a Li/TiS2 cell." Journal of power sources 43.1-3 (1993): 181-191.

[81] Doyle, Marc, Thomas F. Fuller, and John Newman. "Modeling of galvanostatic charge and discharge of the lithium/polymer/insertion cell." Journal of the Electrochemical society 140.6 (1993): 1526.

[82] Doyle, Marc, and John Newman. "The use of mathematical modeling in the design of lithium/polymer battery systems." Electrochimica Acta 40.13-14 (1995): 2191-2196.

[83] Verbrugge, Mark W., and Brian J. Koch. "Lithium intercalation of carbon-fiber microelectrodes." Journal of the Electrochemical Society 143.1 (1996): 24.

[84] Doyle, Marc, et al. "Comparison of modeling predictions with experimental data from plastic lithium ion cells." Journal of the Electrochemical Society 143.6 (1996): 1890.

[85] Darling, Robert, and John Newman. "Modeling a porous intercalation electrode with two characteristic particle sizes." Journal of The Electrochemical Society 144.12 (1997): 4201.

[86] Darling, Robert, and John Newman. "Modeling side reactions in composite li y mn2 o 4 electrodes." Journal of The Electrochemical Society 145.3 (1998): 990.

[87] Arora, Pankaj, et al. "Comparison between computer simulations and experimental data for high-rate discharges of plastic lithium-ion batteries." Journal of power Sources 88.2 (2000): 219-231.

[88] Santhanagopalan, Shriram, et al. "Review of models for predicting the cycling performance of lithium ion batteries." Journal of power sources 156.2 (2006): 620-628.

[89] Fuller, Thomas F., Marc Doyle, and John Newman. "Simulation and optimization of the dual lithium ion insertion cell." Journal of the electrochemical society 141.1 (1994): 1.

[90] Jokar, Ali, et al. "An inverse method for estimating the electrochemical parameters of lithium-ion batteries." Journal of The Electrochemical Society 163.14 (2016): A2876.

[91] Pals, Carolyn R., and John Newman. "Thermal modeling of the lithium/polymer battery: I. Discharge behavior of a single cell." Journal of the Electrochemical Society 142.10 (1995): 3274.

[92] Pals, Carolyn R., and John Newman. "Thermal modeling of the lithium/polymer battery: II. Temperature profiles in a cell stack." Journal of the Electrochemical Society 142.10 (1995): 3282.

[93] Bernardi, D., E. Pawlikowski, and John Newman. "A general energy balance for battery systems." Journal of the electrochemical society 132.1 (1985): 5.

[94] Botte, Gerardine G., Bradley A. Johnson, and Ralph E. White. "Influence of some design variables on the thermal behavior of a lithium-ion cell." Journal of the Electrochemical Society 146.3 (1999): 914.

[95] Xu, Meng, et al. "A pseudo three-dimensional electrochemical–thermal model of a prismatic LiFePO4 battery during discharge process." Energy 80 (2015): 303-317.

[96] Xu, Meng, et al. "Two-dimensional electrochemical–thermal coupled modeling of cylindrical LiFePO4 batteries." Journal of power sources 256 (2014): 233-243.

[97] Wu, Billy, et al. "Coupled thermal–electrochemical modelling of uneven heat generation in lithium-ion battery packs." Journal of Power Sources 243 (2013): 544-554.

[98] Mao, Xinjian, Shaojing Song, and Feng Ding. "Optimal BP neural network algorithm for state of charge estimation of lithium-ion battery using PSO with Levy flight." Journal of Energy Storage 49 (2022): 104139.

[99] Sun, Jinlei, et al. "A novel multiobjective charging optimization method of power lithium-ion batteries based on charging time and temperature rise." International Journal of Energy Research 43.13 (2019): 7672-7681.

[100] Hlal, Mohamed Izdin, et al. "NSGA-II and MOPSO based optimization for sizing of hybrid PV/wind/battery energy storage system." International Journal of Power Electronics and Drive Systems 10.1 (2019): 463.

[101] Sun, Jinlei, et al. "A novel multiobjective charging optimization method of power lithium-ion batteries based on charging time and temperature rise." *International Journal of Energy Research* 43.13 (2019): 7672-7681.

[102] Deb, Kalyanmoy, et al. "A fast and elitist multiobjective genetic algorithm: NSGA-II." IEEE transactions on evolutionary computation 6.2 (2002): 182-197.

[103] Liu, Kailong, et al. "Multi-objective optimization of charging patterns for lithium-ion battery management." Energy Conversion and Management 159 (2018): 151-162.

[104] Amiri, Saeed Salimi, Shahram Jadid, and Hedayat Saboori. "Multi-objective optimum charging management of electric vehicles through battery swapping stations." Energy 165 (2018): 549-562.

[105] Gao, Ruibin, et al. "NSGA-III-SD based Fuzzy energy management system optimization for lithium battery/supercapacitor HEV." Applied Soft Computing 142 (2023): 110280.

[106] Minitab, Taguchi design.

[107] Liu, Yi-Hwa, and Yi-Feng Luo. "Search for an optimal rapid-charging pattern for Li-ion batteries using the Taguchi approach." IEEE transactions on industrial electronics 57.12 (2009): 3963-3971.

[108] Cho, Hyung-Man, et al. "A study on time-dependent low temperature power performance of a lithium-ion battery." Journal of Power Sources 198 (2012): 273-280.

[109] Takami, Norio, et al. "Structural and kinetic characterization of lithium intercalation into carbon anodes for secondary lithium batteries." Journal of The Electrochemical Society 142.2 (1995): 371.

[110] Jiang, Fangming, and Peng Peng. "Elucidating the performance limitations of lithium-ion batteries due to species and charge transport through five characteristic parameters." Scientific reports 6.1 (2016): 32639.

[111] Prada, Eric, et al. "Simplified electrochemical and thermal model of LiFePO4-graphite Li-ion batteries for fast charge applications." Journal of The Electrochemical Society 159.9 (2012): A1508.

[112] Fang, Weifeng, Ou Jung Kwon, and Chao‐Yang Wang. "Electrochemical‐thermal modeling of automotive Li‐ion batteries and experimental validation using a three‐electrode cell." International journal of energy research 34.2 (2010): 107-115.

[113] Farkhondeh, Mohammad, and Charles Delacourt. "Mathematical modeling of commercial LiFePO4 electrodes based on variable solid-state diffusivity." Journal of The Electrochemical Society 159.2 (2011): A177.